TECHNISCHE UNIVERSITÄT MÜNCHEN

Fakultät für Medizin

Institut für Medizinische Mikrobiologie, Immunologie und Hygiene

Isolation, Characterization and Functional Re-Expression of T Cell Receptors with Therapeutic Value for Adoptive T Cell Therapy

Manuel Effenberger

Vollständiger Abdruck der von der Fakultät für Medizin der Technischen Universität München zur Erlangung des akademischen Grades eines

Doktors der Naturwissenschaften

genehmigten Dissertation.

Vorsitzende:	Prof. Dr. Ulrike Protzer
Prüfer der Dissertation:	1. Prof. Dr. Dirk H. Busch
	2. Prof. Dr. Dirk Haller
	3. Prof. Dr. Vigo Heissmeyer

Die Dissertation wurde am 16.05.2019 bei der Technischen Universität München eingereicht und durch die Fakultät für Medizin am 31.12.2019 angenommen.

If you have an apple and I have an apple and we exchange these apples
then you and I will still each have one apple.
But if you have an idea and I have an idea and we exchange these ideas,
then each of us will have two ideas.

George Bernard Shaw

Parts of this thesis have already been published or are submitted for publication:

Manuel Effenberger*, Andreas Stengl*, Kilian Schober*, Maria Gerget, Maximilian Kampick, Thomas R. Müller, Dominik Schumacher, Jonas Helma, Heinrich Leonhardt, Dirk H. Busch: FLEXamer: A Double Tag for Universal Generation of Versatile Peptide-MHC Multimers. (*contributed equally). Journal of Immunology, 2019.

Kilian Schober*, Thomas R. Müller*, Füsun Gökmen, Simon Grassmann, **Manuel Effenberger**, Mateusz Poltorak, Christian Stemberger, Kathrin Schumann, Theodore L. Roth, Alexander Marson & Dirk H. Busch: Orthotopic replacement of T-cell receptor α and β chains with preservation of near-physiological T-cell function. (*contributed equally). Nature Biomedical Engineering, 2019.

Michaela Baldauf, Julia Gerke, Andreas Kirschner, Franziska Baeschke, **Manuel Effenberger**, Kilian Schober, Rebeca Alba Rubio, Takayuki Kanaseki, Merve Kiran, Merlene Dallmayer, Julian Musa, Nurset Akpolat, Ayse Akatli, Fernando Rosman, Özlem Özen, Shintaro Sugita, Tadashi Hasegawa, Haruhiko Sugimura, Daniel Baumhoer, Maximilian Knott, Giuseppina Sannino, Aruna Marchetto, Jing Li, Dirk H. Busch, Tobias Feuchtinger, Shunya Ohmura, Martin Orth, Uwe Thile, Thomas Kirchner, Thomas Grünewald: Systematic identification of cancer-specific MHC-binding peptides with RAVEN. Oncoimmunology, 2018

Stefan Audehm, Manuel Glaser, Matteo Pecoraro, Eva Bräunlein, Sabine Mall, Richard Klar, **Manuel Effenberger**, Julian Albers, Henrique de Oliveira Bianchi, Janet Peper, Nahid Yusufi, Dirk Busch, Stefan Stevanović, Matthias Mann, Iris Antes, Angela M Krackhardt: Key features relevant to select antigens and TCR from the MHC-mismatched repertoire to treat cancer. Frontiers in Immunology, 2019

Immanuel Andrä, Hanna Ulrich, Susi Duerr, Dominik Soll, Lynette Henkel, Corinne Angerpointner, Julia Ritter, Sabine Priszibila, Herbert Stadler, **Manuel Effenberger**, Dirk H. Busch and Matthias Schiemann: An Evaluation of T-Cell Functionality After Flow Cytometry Sorting Revealed p38 MAPK Activation. Cytometry Part A, 2020

Content

List of Figures

Abbreviations

2D	two dimensional
3D	three dimensional
Å	ångström
A488	Atto 488
aa	amino acid
ACT	adoptive cell therapy
ADC	antibody drug conjugate
AFM	atomic force microscopy
APC	antigen presenting cells
APC	allophycocyanin
ATP	adenosine-tri-phosphate
BCR	B cell receptor
bio	biotin
BV	brilliant violet
CAR	chimeric antigen receptor
CD	cluster of differentiation
CDR	complementary determining region
CDS	coding sequence
cfu	colony forming unit
CMV	cytomegalovirus
CTL	cytotoxic lymphocyte
D	diversity
d	day
DBCO	dibenzocyclooctyne
ddH_20	double distilled water
DLI	donor lymphocyte infusion
DMSO	dimethyl sulfoxide
DNA	deoxyribonucleic acid
dNTPs	nucleoside triphosphate

DTT	dithiothreitol
e.g.	exempli gratia
EC_{50}	peptide concentration mediating half-maximal effector function
ECD	energy-coupled dye (phycoerythrin-Texas Red)
EDTA	ethylenediaminetetraacetate
EMA	ethidium monoazide
FACS	fluorescence activated cell sorting
FCS	fetal calf serum
FDA	food and drug administration
FITC	fluorescein isothiocyanate
FPLC	fast protein liquid chromatography
g	gravity
g	gramm
GL	Glycyl-L-leucine
GM	Glycylmethionine
GMP	good manufacturing practice
Gy	Gray
h	hour
HC	heavy chain
Her2/neu	human epidermal growth factor receptor 2/ neu
HLA	human leucocyte antigen
HPV	human papilloma virus
i.e.	id est
IFNγ	interferon γ
Il	interleukine
Indel	insertion and deletion mutation
IPTG	Isopropyl-β-D-thiogalactopyranoside
J	joining
kb	kilo bases
K_D	dissociation constant
kDa	kilo Dalton
k_{off}-rate	dissociation rate
k_{on}-rate	association rate

l	liter
M	molar
mAb	monoclonal antibody
MART1	melanoma antigen recognized by T cells 1
MFI	mean fluorescence intensity
mg	milligram
MHC	major histocompatibility complex
min	minutes
ml	milliliter
mM	millimolar
MMAF	monomethylauristatin F
mRNA	messenger-RNA
mTrbc	murine T cell receptor beta constant
MWCO	molecular weight cut-off
n	natural number
N nucleotides	non-template nucleotides
neoORF	neo-open reading frames
NGS	next generation sequencing
Ni-NTA	Nickel nitrilotriacetic acid
nM	nanomolar
ns	not significant
o.n.	overnight
Oligo	oligonucleotide
PB	pacific blue
PBMC	peripheral blood mononuclear cell
PBS	phosphate-buffered saline
PC7	phycoerythrin- cyanine dye indotricarbocyanine
PCR	polymerase chain reaction
PD-1	programmed cell death protein 1
PDB	protein data base
PE	phycoerythrin
PEG	poly-ethylene glycol
PI	propidium Iodide
PMA	phorbol myristate acetate

pMHC	peptide loaded major histocompatibility complex
PO	pacific orange
RACE-PCR	rapid amplification of cDNA ends PCR
RNF43	ring finger protein 43
rpm	revolutions per minute
RT	room temperature
s	seconds
sCy5	sulfo cyanine5
SDS-PAGE	sodium dodecyl sulfate polyacrylamide gel electrophoresis
sec	second
SEC	size exclusion chromatography
SPR	surface Plasmon resonance
SrtA	Sortase A
$t_{1/2}$	half-live
TCR	T cell receptor
TEG	tetra-ethylene glycol
Th	T helper cells
TIL	tumor infiltrating lymphocyte
TNFα	tumor necrosis factor α alpha
TRAV	T cell receptor alpha variable
TRBV	T cell receptor beta variable
Treg	regulatory T cell
TTL	tubulin tyrosine ligase
U	international unit
UV	ultraviolet
V	variable
V	Volt
Y-N_3	3-azido-L-tyrosine
YFV	yellow fever
β2m	beta 2 microglobulin

1 Introduction

1.1 T cell immunity

The mammalian immune system developed various mechanism to protect the host against virtually any pathogenic entity. It is typically divided into two branches. The innate immune system, which utilizes a set of inherited, conserved mechanism that allows immediate defense by recognition of common pathogenic patterns. And the adaptive immune system, which conveys delayed but highly specific responses against defined molecular structures leading to efficient elimination (or sufficient surveillance) of pathogens and long-lived protection against reinfection with the same pathogen. The specificity of the adaptive immune system is mostly mediated by either B or T cells. Antibodies produced by B cells bind extracellular pathogens including their toxic products and pose the humoral part of the immune system, whereas T cells make up the cellular immune system. T cells recognize antigens of intracellular pathogens or mutated peptides of neoplastic cells loaded into major histocompatibility complex (MHC)[1]. T cells are further subdivided based on the surface expression of their co-receptors cluster of differentiation (CD) 4 and CD8 into T helper (Th) cells and cytotoxic T cells. $CD4^+$ T cells bind peptides presented on MHC class II molecules which are mainly expressed by professional antigen presenting cells (APCs) such as macrophages, B cells and dendritic cells. $CD4^+$ T cells are further categorized based on their secretion profile of growth and differentiation factors modulating immune responses. Th1 cells produce primarily interferon γ (IFNγ) and activate macrophages, Th2 cells secrete interleukine-4 (Il-4) and drive B cell activation. Th17 cell produce Il-17 and are associated with tissue inflammation, whereas regulatory T cells (Tregs) suppress inflammation[2]. In contrast to $CD4^+$ T cells, CD8+ T cells recognize antigens of intracellular pathogens presented on MHC class I molecules, which are expressed on almost every nucleated body cell. Binding of the T cell receptor (TCR) to its cognate pMHC leads to T cell activation and secretion of effector molecules inducing apoptosis of the target cell[3].

1.1.1 The T cell receptor

T cells recognize their cognate target epitope presented on MHC via their heterodimeric receptor. The structure of the TCR has considerable similarities to the immune globulin receptor of B cells (BCR) or its soluble form the antibody[45]. The two αß TCR chains are composed of a large extracellular domain containing the variable and constant region. Both chains are linked by a disulfide bound formed by opposing cysteine residues in the hinge region. The transmembrane domain anchors both chains in the cell membrane and is followed by a short intracellular domain. The transmembrane domain mediates interaction to the invariant chains of the CD3 complex via positively charged amino acid side chains, thus allowing TCR downstream signaling. Like for antibodies, the variable (V) regions of the TCR αß chains pair to form a region with high variability building the contact zone to the pMHC ligand (Fig 1.1).

Taking the vast variety of pathogen-derived peptide epitopes into account, the TCR repertoire must contain an immense TCR diversity to ensure reliable protection of the host. This diversity is mediated by somatic recombination of the TCR during T cell development. The first level of diversity is generated by rearrangement of the three TCR gene segments variable (V), diversity (D; TCR beta chain only) and joining (J). In detail, the complementary determining region (CDR)1α and CDR2α regions are coded by one of 47 germline-derived TCR-α variable (TRAV) genes, while the CDR1ß and CDR2ß regions are coded by one of the 57 germline-derived TCR- ß variable (TRBV) genes. The second level of diversity is generated by further editing of the CDR3 regions of both chains. Here, random deletion by DNA nuclease activity as well as random addition of N nucleotides at the V(D)J junctions results in the most variable region among individual TCRs[13]. The third level of diversity results from pairing of the two different TCR chains (αß or γ∂). Rearrangement of the three TCR gene segments, random deletion or addition of nucleotides as well as pairing of the heterodimeric TCR can theoretically yield as many as 10^{20} unique TCRs[1]. Each T cell is equipped with a unique TCR that allows to distinguish self- from non-self-peptide loaded MHCs.

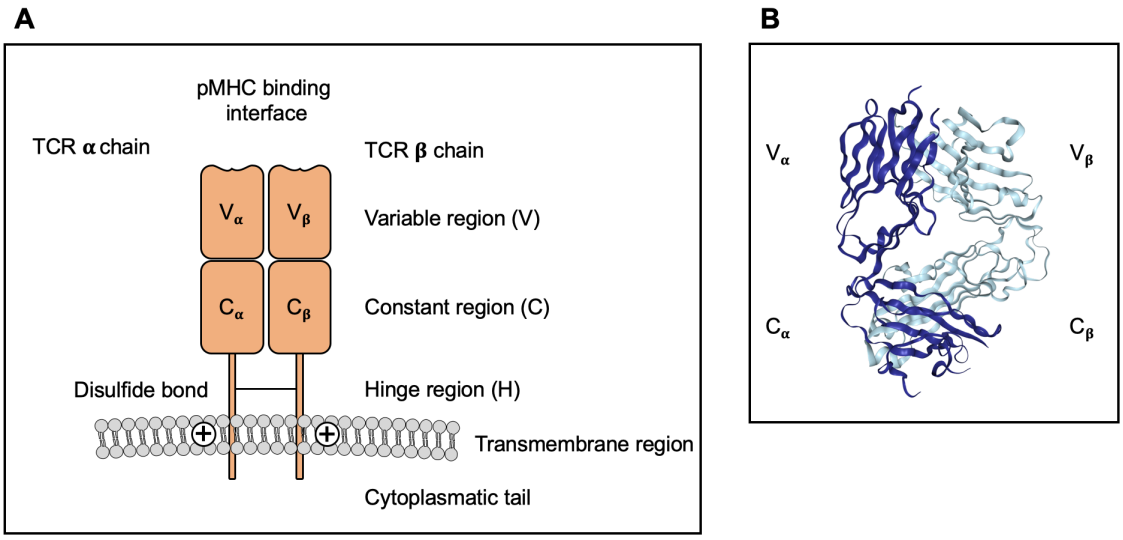

Figure 1.1 Schematic depiction of an *αß T cell receptor.* A) Illustration of a surface expressed heterodimeric αß TCR. Both chains consist of a Variable (V) and Constant (C) region. The V region harbors the complementary determining regions (CDRs) which represent the regions with highest variability among TCRs, mediating the contact to the ligand; the peptide loaded major histocompatibility complex (pMHC). Two opposing cysteine residues in the hinge region (H) form a disulfide bond, cross-linking both TCR chains. The transmembrane domain anchors both chains in the cell membrane. It contains positively charged side chains with which the TCR interacts with the CD3 complex, to allow TCR signaling into the cell. **B)** Crystal structure of the TCR 2B4 at a resolution of 2.4 Å, α chain in dark blue, ß chain in light blue (modified according to PDB: 3QJF).

1.1.2 TCR repertoire

VDJ rearrangement, random N nucleotide integration and deletion in the CDR3 region as well as differential paring of the TCR α and ß chain yields a theoretical number of 10^{20} unique TCRs[16]. However, there is an enormous gap between this number and the actual diversity, estimated to result in 10^8 individual TCRs in the periphery[7]. The difference between the theoretical and the actual TCR diversity may be explained by the combination of several biological factors. Somatic recombination is not a completely random process, because certain recombination events have a higher chance to occur than others[8]. Moreover, the redundancy of the triplet code allows that different DNA sequences lead to the very same sequence on amino acid level reducing the actual diversity[9]. Most significantly, theoretical TCR diversity is trimmed during thymic selection. During positive selection, T cells have to recognize peptides loaded on self-MHC with sufficient binding strength to ensure functionality in a given epitope-driven immune response[10]. This process is followed by a second step, called negative selection to delete T cells with self-reactive TCRs to prevent autoimmunity. These two control mechanisms of self-MHC restriction and self-tolerance allow only about 5% of the potential TCR combinations to leave the thymus and enter the

periphery as naïve T cell repertoire[11]. Current estimates of TCR diversity within humans suggest an average TCR repertoire size of approximately 10^8 individual TCRs and a total number of 10^{12} T cells per individual[7], which would set the absolute upper limit of diversity. However, homeostatic proliferation as well as the presence of large oligoclonal and monoclonal T cell populations resulting from (persisting) infections significantly reduce the space left for overall TCR diversity[12]. Spike in experiments using antigen-specific T cells hint at an average number of 20-200 $CD4^+$[13] and 80-1200 $CD8^+$[14,15] naïve precursor T cells recognizing the same epitope. These T cells build up the “protecton” scanning the periphery for non-self-epitopes[16].

1.2 The major histocompatibility complex

MHC molecules are polymorphic cell surface proteins which can be subdivided by their structure and tissue expression into two groups. MHC class II molecules are expressed mainly on professional APCs. They are heterodimers consisting of two similarly constructed non-identical peptides, the α and the β chain, which are non-covalently associated. Both have an intermembrane domain, anchoring the complex in the APC. Presented peptides show a length of 15 to 24 amino acids (aa) as peptides are allowed to protrude the peptide binding groove at the C- and N-terminus[17]. Only when binding a peptide, the MHC class II forms a stable complex[18]. In the periphery, MHC class II molecules are loaded with peptide fragments mostly derived from extracellular proteins and interact with $CD4^+$ T cells, which are important to orchestrate adaptive immunity[2].

In contrast, MHC class I molecules are expressed on nearly all nucleated body cells presenting peptides fragments derived from cytosolic proteins. Presentation of non-self-peptides (e.g. viruses or mutation derived non-synonymous peptides) to $CD8^+$ T cells induces direct target cell killing[3]. MHC class I molecules are also composed of two chains. The soluble globular light chain has a size of about 12 kilo Dalton (kDa) and is commonly referred to as β2 microglobulin (β2m). β2m is invariant within all MHC class I complexes. The heavy chain (HC), also called α chain, has a size of approximately 45 kDa and is a type I integral membrane glycoprotein[17]. The extracellular part of the heavy chain is subdivided into three domains. The α1 and α2 domains form the peptide binding groove presenting peptides of 8 to 12 aa length[19], whereas the α3 domain is located beneath the

peptide binding grove. It anchors the heavy chain into the cell via a transmembrane region[17]. β2m is associated in a non-covalent form with the heavy chain. Only the heterotrimeric complex, composed of one β2m bound to one heavy chain presenting a peptide, forms a stable MHC[18] (Figure 1.2).

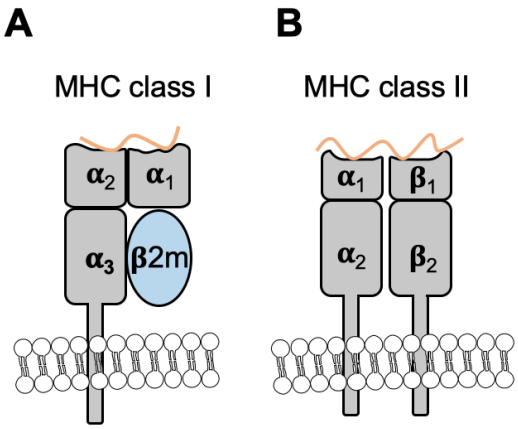

Figure 1.2 The class I and II major histocompatibility complexes. A) MHC class I molecules are expressed by almost all nucleated cells, loaded with cytosolic peptide fragments of 8-12 aa in length and recognized by $CD8^+$ T cells. B**)** MHC class II molecules are mainly expressed by antigen presenting cells (APCs), loaded with peptide fragments of extracellular origin with 15-24 aa length and recognized by $CD4^+$ T cells.

1.2.1 MHC diversity

MHC class I alleles are coded on the short arm of chromosome 6 (6p21) with about 3600 kilo bases (kb) of DNA and are known to be the most polymorphic genetic system in humans. This polymorphism is not evenly distributed throughout the whole MHC allele, but constrained to the sequences coding the α1 and α2 domains of the MHC heavy chain which together form the peptide binding groove [20]. The groove forms 6 pockets (A to F) which interact with the side chains of the loaded peptide fragment, thereby determining the peptide binding specificity of the MHC. The biochemical properties of these pockets (i.e. size, electrostatic charge and hydrophobicity) shape the peptide spectrum of the MHC molecule as they preferentially interact with defined side chains – so-called "anchor residues"– within the loaded peptide[21] . Therefore, peptides loaded on certain MHCs often share anchor motives, e.g. preferences of P and L at position 2 and 9 in peptides presented on B*07:02[20].

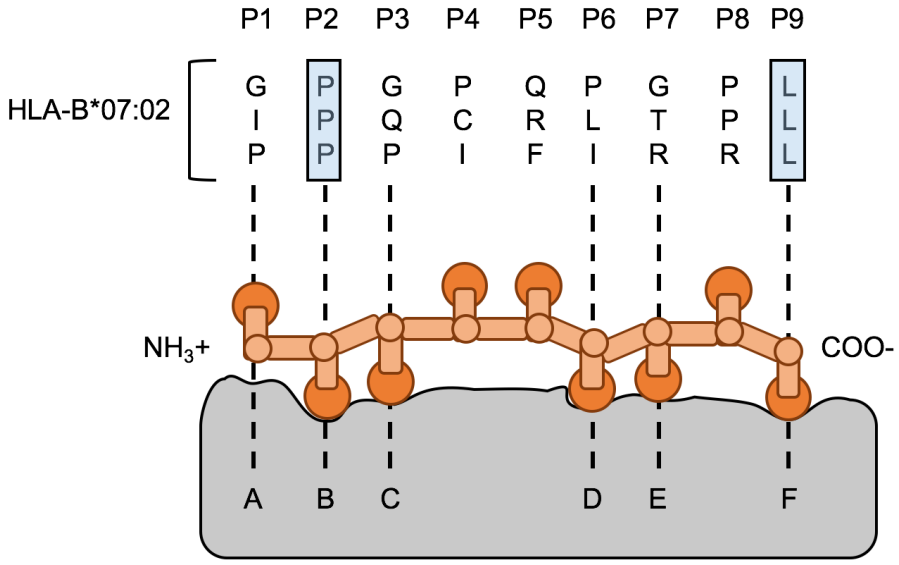

Figure 1.3 Longitudinal section through the peptide binding groove of a MHC class I molecule and its interaction with peptides. Panel of nonamers commonly found in complex with HLA-B*07:02. Anchor residues of the peptide are highlighted in blue. Schematic depiction of the peptide binding groove of the MHC class I molecule with the six binding pockets (A-F) indicated. The amino acid side chains of the nonamer are either facing down towards the pockets of the MHC or facing upwards. Modified from[20].

Based on their polymorphic diversity, the classical MHC class I complexes can be divided into three different subsets: human leucocyte antigen (HLA)-A, HLA-B and HLA-C. To date, HLA-A counts 633 different alleles, HLA-B 1911 and HLA-C 965 different alleles[22]. Furthermore, there are some non-classical MHC class I molecules with only limited polymorphism and lower cell surface expression: HLA-E, HLA-F and HLA-G[17,23].

Class I MHCs are polygenic, polymorphic and in addition co-dominantly expressed proteins. Given the high MHC diversity, it is theoretically highly probable that a given individual is heterozygous for HLA-A, B and C, thus presenting peptides using 6 different MHC molecules. HLA allele homozygosity is expected to be of a significant disadvantage, as these individuals are limited in the capacity to present diverse peptide repertoires compared to HLA allele heterozygote individuals[24]. However, high-resolution HLA allele sequencing revealed that the HLA frequency within human populations is not evenly distributed, but rather skewed towards a limited number of HLA alleles[22]. In addition to this, the HLA class I alleles show distinctive pattern of haplotype combinations, as some HLA alleles co-occur significantly more often than neutrally expenced[25,26]. Both, limited use as well as co-occurrence of HLA alleles

result in lower overall HLA diversity than theoretically possible, thereby increasing the chance of homozygosity on at least one of the three HLA class I alleles.

1.2.2. Peptide epitope diversity

Reliable protection by cellular immunity requires that the TCR repertoire is able to recognize the vast majority of unpredictable antigenic peptides derived from potentially invading pathogens. However, the question arises how diverse this MHC restricted pool of antigenic epitopes really is. MHC class II molecules present peptides with an average length of 11 aa. 20 natural aa implicate a maximal pool of $20^{11} = 2x10^{14}$ different peptides. MHC class I molecules present peptides with an average length of 9 aa resulting in $5.1x10^{11}$ possible different peptides[12]. Reversely, this theoretical number is lowered by several factors. Biochemical properties of side chains prohibit certain combinations of aa as they would result in hydrophobic insoluble peptides. Peptides presented on MHCs are generated by the proteasome, which in turn follows certain rules of peptide processing. It e.g. favors to cleave peptides after hydrophobic or basic residues to generate the carboxy-terminal anchor residue[27]. Interestingly, these are residues preferentially used as anchor residues in peptide-MHC interactions[28]. Only 1 % of processed peptides bind with sufficient stability to (one of 6 available) MHCs to trigger transport of the pMHC to the cell surface[28]. Finally, a significant part of the peptide sequence is buried by the presenting MHC complex, making only 5 residues directly accessible for TCR interaction. Based on this, Cohn and colleagues calculated that the epitope repertoire of these key residues has a size of $20^5 = 3.2x10^6$ different peptides[29]. However, conformational changes of the presenting MHC depending on the loaded peptide is not taken into this consideration, although the TCR has in fact more interaction interface with the MHC than with the peptide itself (Figure 1.4). Most considerations about the epitope diversity are theoretical and need to be further validated by experimental data. However, it seems certain that the TCR repertoire needs to cover a diverse but not infinite pool of peptide epitopes to ensure reliable protection of the host.

1.2.3 Interaction of TCRs with pMHC class I ligands

The molecular interaction of the TCR with its pMHC class I ligand is characterized by high specificity and allows TCRs to discriminate MHCs loaded with peptides that differ by a single amino acid[30,31]. Moreover, the interaction is incredibly sensitive as T cells are able to react on very few pMHCs by initiating transient calcium flux[32,33].

Numerous crystal structures of TCRs in complex with their pMHC ligand suggest that this interaction follows a rather conserved binding mode. TCRs dock in a diagonal fashion to the pMHC and bind with their α chain to the α2 domain and with the β chain to the α1 domain of MHC class I molecules. In this interaction, the CDR1 and CDR3 loops of the TCR α and β chain interact with the peptide as well as with the MHC surface. The CDR2 loops are positioned at the outer edge mainly contacting the MHC surface making limited or no contact with the peptide.

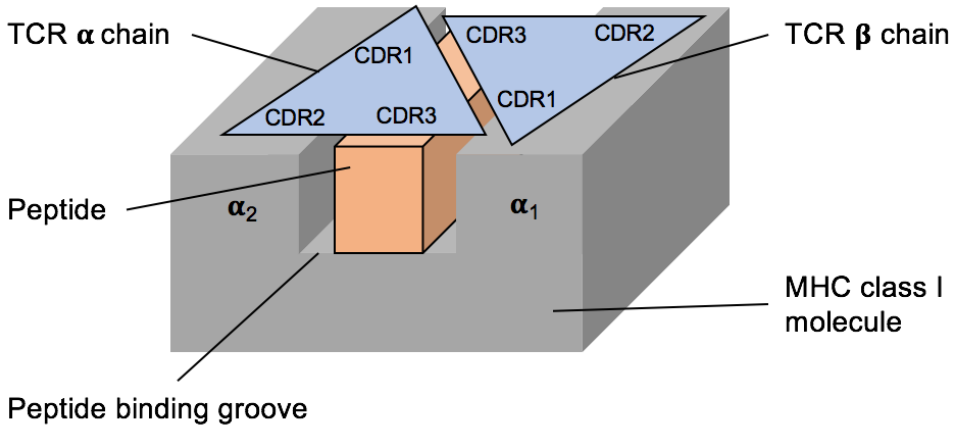

Figure 1.4 Interaction of the T cell receptor and its pMHC ligand. Diagonal orientation of the TCR on the interface of the pMHC. While both CDR3 regions mainly contact the presented peptide, the CDR1 region contacts the peptide and the MHC. The CRD2 regions make limited, or no contact to the peptide and interacts mainly with the MHC. Modified from[20].

This interaction is further stabilized by binding of the co-receptor CD8 contacting the conserved α3 domain of pMHCs. TCR and CD8 cooperate to increase the adhesion to pMHCs, which may increase the sensitivity of TCRs to discriminate peptide epitopes[34].

Although the TCR:pMHC interaction is highly specific, one TCR can cross-react with multiple targets. A single TCR could bind up to 10^6 different pMHCs[35]. This is a theoretical number and whether all these TCR:pMHC interactions result in T cell activation is unknown. In this framework, the binding strength of TCR:pMHC

complexes is thought to be a key parameter to determine if a T cell gets activated or not[36].

Thymic selection trims the TCR repertoire to contain TCRs within a certain affinity range specific for self-peptides. Binding to self-peptide loaded MHCs should occur only with low binding strength, insufficient to prime T cell activation, to prevent autoimmunity. Thymic selection is blind for foreign (e.g. viral) non-self-peptides, which should allow TCRs with high-avidity to non-self-peptides to exit the thymus. Interestingly, also the TCR interaction to non-self-peptides loaded MHCs occurs within a certain affinity window to ensure proper T cell activation[37]. T cell mediated distinction between self- and non-self is not only tightly regulated by TCR:pMHC binding strength but also by additional parameters such as presence or absence of certain adhesion molecules and (pro- or contra-inflammatory) cytokines[17].

1.2.4 TCR affinity and avidity

Affinity describes the bimolecular interaction of a receptor (e.g. the TCR) and its ligand (e.g. the pMHC). The term can be precisely quantified by measuring the dissociation constant K_D which describes the relation of the pMHC association (k_{on}-rate) and the pMHC dissociation (k_{off}-rate). Surface Plasmon resonance (SPR) assay is still thought to be the gold standard assay to determine this value. It allows to measure the specificity, k_{on}- as well as k_{off}-rate and thereby also delivers the K_D value[38]. However, SPR is tremendously time and labor intensive as both ligands need to be recombinantly expressed and extensively purified. Furthermore, the influence of co-receptors is not taken into account. It is described that the CD8 co-receptor binds to the conserved α3 domain of the pMHC heavy chain[39,40], which stabilizes the TCR:pMHC interaction 10-fold[41,42]. The additional binding of co-receptors (CD4 or CD8) makes the TCR:pMHC complex a multi-intermolecular interaction, which is rather described by the term avidity. Avidity encompasses not only the interaction of multiple TCR:pMHC complexes and co-receptor binding, but sometimes even receptor/ligand density and T cells phenotype. TCR avidity is measured by functional or structural assays. Functional avidity is a biological readout that assesses how well T cells sense their target antigen. T cells with a high functional avidity show effector functions already at low antigen doses[43]. Usually determined effector molecules

are the cytokines IL-2, IFNγ, tumor necrosis factor α (TNFα) as well as the effector molecules granzyme B and perforin. Simultaneous secretion of different molecules is commonly referred to as polyfunctionality, which is correlated with high proliferative capacity and superior control of infections and tumor *in vivo*[44,45,46,47]. The gold standard to estimate functional avidity is the stimulation of T cells using APCs loaded with limiting amounts of peptide. Lysis of APCs or cytokine production is measured as a functional readout[48]. A drawback of this method is that cell culture conditions might alter T cells´ phenotypes, e.g. by exhausting the cells or changing their TCR or co-receptor expression levels. Functional avidity values derived from different experiments or cell populations are therefore difficult to compare. In addition, cytokine production or cell lysis is routinely assessed by exposing T cells to peptide concentrations which drastically exceed physiologically relevant concentrations of epitopes present *in vivo*. This can mask the reduced peptide sensitivity of low-avidity T cells making it hard to discriminate them from true high-avidity T cells[48]. Nevertheless, cytokine release assays probe TCR quality as closely as possible to the *in vivo* situation, as many components relevant in physiological settings are obeyed.

Determining the singular contribution of e.g. the TCR/co-receptor remains difficult. Intensive work has been put in the establishment of assays that allow reliable and standardized characterization of TCR structural avidity. In SPR, TCR:pMHC interaction is measured isolated from their cellular context in a fluid phase in three dimensions (3D). In contrast, physiological TCR:pMHC interaction is restricted to two dimensions as both proteins are embedded in membranes on opposing cells. Assays to measure TCR avidity in its cellular context adopted biophysical methods using immobilized recombinantly expressed pMHCs on one side and TCRs expressed on T cells on the other side. Puech and colleagues described a method to monitor TCR:pMHC interaction at single bond level using atomic force microscopy (AFM). For this, a cantilever tip is functionalized with pMHC molecules and brought in close proximity to an antigen-specific T cell. Separating the biding partner allowed to measure the force needed to break up the TCR:pMHC complex[49]. Another technique to analyze TCR avidity *in situ* is the micropipette adhesion frequency assays[50]. Here, pMHC coated red blood cells and T cells are immobilized on micropipettes that are attached to a micromanipulator. The micromanipulator is subsequently used to break up the

TCR:pMHC interaction and allows to quantify the binding strength of the complex. This technique was recently used in combination with single cell sequencing, to directly isolate TCRs of T cells with favorable structural avidity[51]. However, through-put of single cell micromanipulator-based platforms is low, impeding their use for fast TCR characterization and identification.

By using fluorophore labeled reversible pMHC reagents, such as Streptamers or NTAmers, it is possible to exactly determine the k_{off}-rate of monomeric pMHC molecules from the surface of living T cells[52,53,54]. The microscope based k_{off}-rate assay allows k_{off}-rate determination in real-time on single cell level. However, the assay is also technically challenging and time-intensive to perform. Adopting the assay to the flow-cytometer allows k_{off}-rate measurement in an high-throughput compatible manner without losing accuracy[53]. TCR-ligand dissociation assays allow to calculate the half-life of TCR:pMHC complexes *in situ*, thus under consideration of any additional influence from co-receptors and surface molecules. k_{off}-rate assays cannot determine structural avidity per se, as k_{on}-rates are not measured. However, the k_{off}-rate has been suggested to be the main determinant to trigger T cell acivation[55] and has shown to be predictive of *in vivo* functionality[56].

1.2.5 TCR avidity in immune responses

The functional profile of a T cell is in large parts imprinted in the TCR, which determines the binding strength to cognate pMHC. The properties of the TCR:pMHC interaction guides the T cell literally from the cradle to the grave. It is the driving force in thymic selection[57], T cell differentiation[58] and consequently its response upon encountering pathogenic peptides[36].

The recruitment of naïve T cells into primary infection is characterized by clonal expansion of antigen-specific T cell clones with a broad avidity spectrum mounting a polyclonal immune response[59,60]. Low-avidity T cells expand in parallel to high-avidity T cells. However, they rapidly contract, whereas high-avidity clones are preferentially preserved during memory phase[61]. Hence, re-infection with the same pathogen triggers a T cell immune response composed of higher-avidity TCRs, resembling characteristics of affinity maturation or clonal focusing of the T cell repertoire[62,63,64]. High-avidity T cells get activated already in presence of lower antigen densities on target cells and execute effector

functions more rapidly than low-avidity T cells[65]. T cell transfer experiments demonstrated that high-avidity T cells confer better protection and pathogen clearance as low-avidity T cells specific for the same antigen[43,66]. These data indicate that high-avidity T cells may be necessary to effectively substitute lost or missing immunity by adoptive T cell transfer[67,68].

1.2.6 pMHC multimer reagents in T cell research

The hallmark of T cell immunity is its ability to scan the periphery for antigenic peptide. This immune surveillance is mediated by the specific binding of a T cell's TCR to its cognate pMHC ligand, which leads to execution of effector functions. Technologies that allow to monitor antigen-specific T cell responses are therefore of substantial interest for T cell research. One option to visualize antigen-specific T cells are functional readouts. Assays that detect cytokines, activation markers and target cell lysis haven given substantial insight into T cell biology. However, these assays fail to detect T cell populations that lack a particular functional property and change T cells´ phenotypes[48].

The first technique that allowed to detect T cells irrespective of their function and phenotype was described in 1996 by Altman and colleages[69]. T cells can be stained with fluorescently labeled multivalent pMHC reagents. To this end, recombinantly expressed, soluble pMHC molecules are biotinylated which allows non-reversible multimerization on a fluorescently labeled streptavidin backbone. These so called “tetramers” allow sensitive identification and isolation of antigen-specific T cells and have represented a breakthrough technology for in-depth T cell analysis and immune monitoring[69]. The adoptive transfer of T cells identified via pMHC labelling has subsequently also emerged as a promising treatment strategy against cancer and viral infections. However, stable binding of pMHC tetramers can also deteriorate T cell *in vivo* functionality through constant pMHC mediated TCR signaling inducing apoptosis[70,71]. In addition, safety concerns arise, as huge amounts of bacterially expressed proteins are co-transferred into the recipients.

Therefore, pMHC “Streptamers” have been developed by our laboratory[72], which enable stable pMHC binding through multimerization of Strep-tags[73,74] on a Strep-Tactin backbone. The multimeric complex can be disrupted, however, upon addition of D-biotin. Using Streptamers, a minimally manipulated cell product can

be isolated with no functional difference to cells that were never in contact with pMHC multimers[72]. Therapeutic effects of minimal cell numbers of Streptamer-sorted cytomegalovirus (CMV)-specific T cells in a phase I/II clinical trial have recently underlined the value of this technology for the generation of potent and safe clinical T cell products[75].

Furthermore, reversible pMHC multimer constructs have also been used to characterize T cells. When reversible pMHC monomers themselves are labeled with a fluorophore, their dissociation from TCRs on living T cells can be tracked over time[52,54,53]. Through this, absolute and reproducible measurements of TCR-ligand k_{off}-rates can be achieved in a relatively easy and high-throughput compatible manner. However, to allow fluorophore conjugation, an artificial solvent exposed cysteine residue has to be incorporated for maleimide dye conjugation[56].

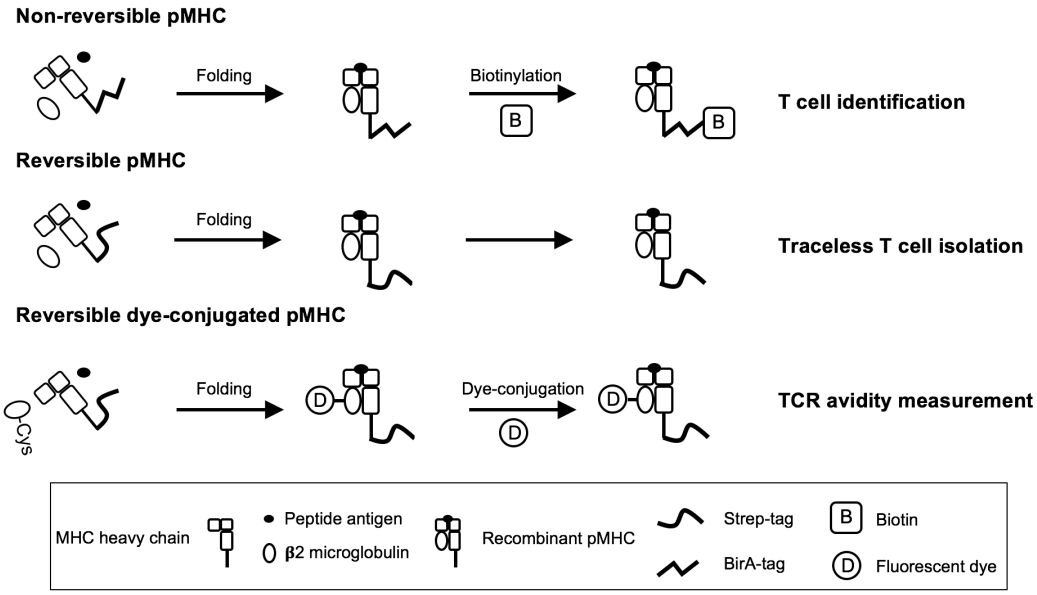

Figure 1.5 Generation of conventional pMHC reagents. Non-reversible pMHC reagents ("tetramers") are generated by refolding of pMHC molecules harboring an Avi-tag at the C-terminus of the heavy chain for biotinylation. Biotinylated pMHC monomers can be non-reversibly multimerized on streptavidin. Reversible pMHCs, e.g. "Streptamers", carry an affinity-tag (Strep-tag) at the C- terminus of the heavy chain, that allows stable multimerization on Strep-Tactin, which can be reversed upon addition of competitor molecules with higher affinity. Reversible dye-conjugated pMHC reagents can be generated through the introduction of an artificial solvent-exposed cysteine in the pMHC light chain, which allows dye coupling via maleimide chemistry after folding.

Comprehensive use of pMHC multimer technique is made difficult by biological complexity on different levels. First; the total epitope repertoire has been estimated to contain about $3x10^6$ different peptides[29]. Second, more than 3500 different HLA class I alleles are frequently found in human populations[22]. Third,

the different classes of pMHC multimer reagents allow sensitive identification, traceless cell isolation and TCR characterization. This versatilety, however, comes at the cost of distinct generation processes for each application including separate recombinant protein expression, *in vitro* refolding and pMHC purification processes. This makes the generation processes labor intensive and prone to batch-to-batch variability.

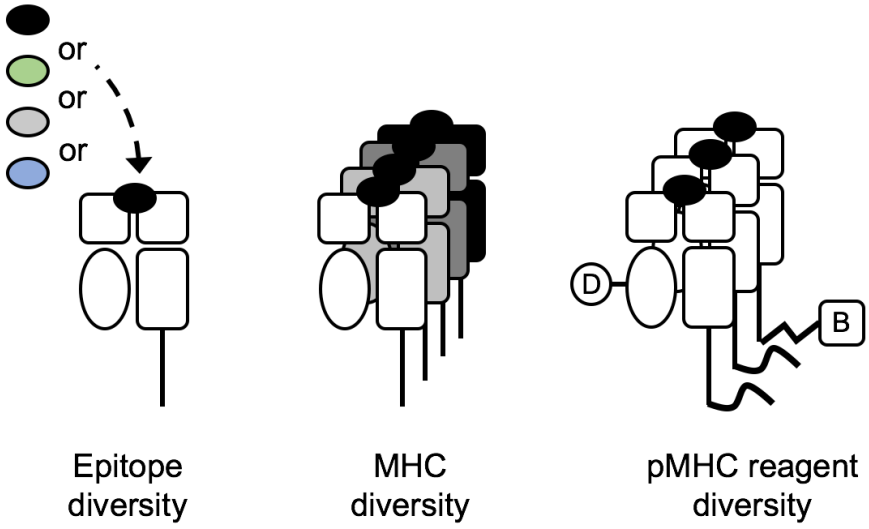

Figure 1.6 Epitope and MHC diversity complicate routine use of pMHC reagents. One MHC molecule can be loaded with a diverse set of peptide fragments. MHC molecules are heterogeneous proteins with several thousand allomorphs. At least three pMHC reagent classes are commonly used in basic T cell research and translational medicine.

In order to be compatible with the extreme diversity of epitopes, UV exchange[76] or di-peptide[77] technologies have been developed that can be used to load (a limited set of) HLA class I with any epitope of interest. In addition, combinatorial pMHC staining[78,79] and DNA barcoding[80] have massively enhanced throughput of screening antigen-specific T cell populations and their respective TCR repertoires.

Despite this progress, however, difficulties to generate distinct pMHC multimer reagents appropriate for each individual setting in a fast and reliable manner remain a significant challenge to personalized cell therapy and T cell-based diagnostics.

1.3 Adoptive T cell therapy

Equipping a T cell with a transgenic receptor allows to redirect the cell against new targets. Chimeric antigen receptor (CAR) transgenic T cells targeting CD19

have been successfully tested in several clinical trials for the treatment of B cell lymphomas resulting in cancer regression of previously incurable patients[81,82]. These advancements have culminated in the FDA approval of tisagenlecleucel (marketed as Kymriah) for the treatment of B cell lymphoma, the first ever approved transgenic cell product in medical history[83]. Adoptive transfer of unedited T cells in form of donor lymphocyte infusion (DLI)[84], tumor infiltrating lymphocytes (TILs)[85] or virus specific T cells[86], was brought into the clinic with outstanding therapeutic efficacy almost 30 years ago. All these studies mount evidence for the therapeutic value of antigen recognition through T cells and also the TCR itself.

The key role of TCR-mediated T cell function in tumor[87], infection[88] and autoimmunity[89] is underscored by several pre-clinical and clinical models. Nevertheless, the heterogeneity of infectious particles and malignancies highlights that TCR transgenic “living drugs” will most likely be highly personalized, costume made therapies.

Besides its outstanding clinical success, TIL therapy has several inherent biological and technical limitations. TILs are a heterogeneous cell mixture and consequently the therapeutic outcome is often unpredictable[90]. Furthermore, TILs are commonly generated from resected tumor tissue which implies that the tumor must be accessible. *In vitro* culture of TILs is very time and cost intensive as all steps need to be performed under good manufacturing practice (GMP) conditions. Finally, it is only for 50% of patients possible to generate tumor reactive TILs for treatment of multiple melanoma[91] and it is even more difficult to generate TILs for other cancer types. These drawbacks preclude TIL therapy as broad application for large patient cohorts.

TCR-engineered T cells could broaden the applicability of adoptive T cell therapy as it allows to redirect the cells with a TCR of in-depth characterized specificity and functionality. Furthermore, it is possible to select a cell product with defined phenotype for TCR engraftment[92]. It was shown that weakly differentiated cells such as naïve or central memory T cells have a prolonged peripheral persistence which is associated with better survival and are therefore best suited for immunotherapy[93,94,95,92,96,97]. However, adoptive cell therapy (ACT) using TCR transgenic T cells has so far been less effective than TIL therapy. Treatment of multiple myeloma using TCR transgenic T cells resulted in 30% objective

response rates[98]. In contrast, TIL therapy achieved up to 70 % objective response rates treating the same disease[99]. Still, direct comparison between clinical outcome of ACT trials performed with TCR-engineered T cells versus TILs is complicated as response rates are influenced many factors, such as the target epitope and used TCR.

The so far limited success of ACT using TCR-engineered T cells may be explained by several reasons. The TCR is a complex heterodimeric receptor, which is dynamically regulated. Upon antigen encounter, T cells downregulate TCR surface expression to prevent activation induced cell death[100,101]. Most studies conducted so far use viral gene-transfers[102], with at least semi-random genome integration[103]. This in turn requires that the TCR is transferred with a constitutively active promotor overwriting physiological TCR regulation. Recent progress in the field of targeted genome editing has enabled site specific TCR knock-in under the physiological TCR promotor. This allows tight control of transgene expression by the endogenous promotor, resulting in better sustained long-term functionallity[104]. Whether these advanced engineered cell products perform superior in clinical settings remains to be tested.

Furthermore, most studies conducted so far used TCR-transgenic T cells directed against self-antigens. However, targeting self-antigens provokes autoimmune side effects, as healthy tissue presenting the target antigen is targeted as well[105]. These on-target/off-tumor effects present a dose-limiting factor reducing the success-rate of TCR-transgenic T cells targeting self-antigens[67,106].

ACT directed against self-antigens can be acceptable, when destruction of collaterally damaged melanocytes is not life-threatening as in case of skin depigmentation (Vitiligo) in multiple myeloma[98,107] or anti-CD19 CAR therapy-mediated depletion of the B cell compartment[81,82]. However, targeting many other self-antigens would result in severe toxicity[108]. Targeting non-self-antigens, e.g. tumor-specific mutation-derived neoantigens, can broaden the applicability of ACT by circumventing on-target/off-tumor toxicity. Neoantigen-specific T cells can be detected in several cancer types[109,110]. Interestingly, they seem to be enriched in the programmed cell death protein 1 (PD-1) + compartment of TILs. PD-1 is an activation as well as exhaustion marker, thus indicating that neoantigen-specific T cells are a major contributor in tumor control[111].

Whether tumor patients are a reliable source for neoantigen-specific TCRs for use in ACT is still a matter of debate. Neoantigen-specific T cells accumulate in tumor tissue and tumor sites are frequently not accessible. Recently, neoantigen-specific T cells could be isolated form peripheral blood of melanoma patients, which could significantly facilitate isolation of neoantigen-specific T cells[112,113]. However, whether neoantigen-specific T cells also circulate in sufficient numbers in other tumor entities remains elusive. Besides limited accessibility to tumor sites and tumor patients as TCR donors in general, the spatiotemporal distribution of antigen-specific T cells in tumors is still unknown. T cells face high antigen loads in the tumor microenvironment which can induce anergy (i.e. functional deletion) or even activation induced cell death (i.e. physical deletion). In case of functional deletion, treatments using checkpoint inhibitors can unleash T cells from immunosuppression. In case of physical deletion, checkpoint inhibitors would prove ineffective. Current therapies using check point inhibitors are promising, leading to reduction in tumor burden in a variety of cancer types[114]. However, a significant proportion of patients do not respond, hinting towards a scenario where either T cell exhaustion is already irreversible[115,116] or optimal avidity T cell clones are physically depleted from the patient T cell repertoire[117]. Consequently, accessing a non-tolerized unbiased T cell repertoire could represent a more reliable resource for neoantigen-specific TCRs providing optimal functionality. The group of Ton Schumacher could generate proof of concept that antigen-unexperienced healthy donors can be an alternative resource for neoantigen-specific T cells[118]. Based on exome and RNA sequencing of tumor material about 250 non-synonymous mutations in protein coding sequences were identified. Less than 50% of peptides were predicted to bind MHC with sufficient affinity to form a potentially immunogenic T cell neoepitope. Of those, only 2 neoepitopes were detected by TILs derived from the patient. Surprisingly, T cells from healthy donors recognized up to five epitopes out of the 20 most promising neoepitope candidates. In contrast, these epitopes were not recognized by the T cell repertoire of the patient. Despite these significant advancements in the field, the number of so far identified TCRs for ACT is still very small.

1.3.1 Technical challenges to isolate tumor specific TCRs from antigen-unexperienced healthy donors

Focusing on antigen-unexperienced healthy donors as a resource for tumor (neo)antigen specific TCRs, two characteristics of the naïve T cell repertoire need to be considered. First, the number of T cells specific for a given antigen (i.e. precursor frequency) is extremely low[15]. Second, most of the few antigen-specific T cells are considered to be of low-avidity[51].

Alanio and colleagues combined pMHC multimer staining with magnetic bead enrichment to allow flow cytometric enumeration of extremely rare pMHC multimer-reactive T cell populations in the naïve repertoire. Interestingly, the number of pMHC-reactive $CD8^+$ T cells varied ~100 fold among the 6 screened epitopes ranging from $1x10^{-4}$ to $0.6x10^{-6}$. Surprisingly, the number of pMHC-reactive T cells per epitope seemed to be conserved among individuals[15]. Besides combination of pMHC multimer staining and bead based enrichments, antibodies cross-linking the TCR:pMHC multimer complex[119], use of protein kinase inhibitors to increase TCR surface expression[120] and higher-order multimer reagents ("dodecamers")[121] were described to lower the detection limit of pMHC multimer-based T cell identification. Furthermore, selective enrichment of the T cell subset which is expected to contain the majority of pMHC-reactive T cells could indirectly increase pMHC multimer sensitivity[122].

Selecting few T cell candidates with desirable functionality out of a majority of low functional T cells represents a second significant technical challenge. Although cell culture-independent protocols for isolation of functional TCRs have been published[123], most protocols rely on at least one *in vitro* cell culture propagation step. Commonly used functional avidity readouts could miss promising TCR candidates, because *in vitro* cultured T cells lose functionality over time. In contrast, structural avidity assays could present a more robust readout as they measure a physical value hardwired in the TCR itself[56,124,125].

A longstanding rate limiting step of TCR identification platforms was the technically highly challenging polymerase chain reaction (PCR)-based simultaneous isolation of both chains of the TCR heterodimer, concomitant with time and labor intensive cloning and Sanger sequencing. PCR based identification of both TCR chains from single-cell-level could be achieved by degenerate primers binding to consensus motives[126] or rapid amplification of

cDNA ends (RACE) PCR[127] and functionality of the isolated TCRs could be proven by transgenic reexpression[123].

Recent advancements in next generation sequencing (NGS) now allows high-throughput TCR identification, also from single cells[128]. However, (so far) a TCR primary sequence does not inform about antigen-specificity or functionality. Consequently, the bottleneck shifts within the TCR identification pipelines. The most cost- and labor-intensive step is currently the transgenic re-expression and characterization of dozens or hundreds of TCR candidates. Robust readouts that allow reliable ranking of TCR candidates could therefore dramatically improve the through-put of *de novo* identification of suitable TCRs for the use in ACT. These readouts should ideally predict functionality prior to TCR re-expression, allowing to select a limited set of TCRs to follow up for in-depth characterization in pre-clinical test systems. One powerful option are assays that measure structural avidity, which is hardwired in the TCR. In turn, the structure of a TCR is coded in its DNA sequence, defining the strength of non-covalent interactions such as Van der Waals forces, hydrogen bonds and electrostatic interactions between the receptor and its cognate pMHC ligand. TCR gene engineering allows to transfer TCR encoded characteristics from a native donor cell to a new T cell graft. Therefore, TCR structural avidity assays seem to be the ideal tool to screen the T cell repertoire for receptors providing preferable avidity for use in adoptive T cell therapy and specifically in adoptive T cell therapy using a TCR gene-engineered cell product.

2 Aim of this thesis

This thesis aimed at establishing a workflow that allows to identify promising TCR candidates' prior to TCR re-expression. In order to do so, we aimed to set up an antibody- and pMHC multimer-based staining panel that allowed flow cytometry-based detection and isolation of rare pMHC multimer-reactive T cell populations in the naïve T cell repertoire of antigen-unexperienced healthy donors. We wanted to establish a short-term feeder cell free expansion protocol that allows to propagate single cell-sorted T cells to clones of sufficient number to allow pMHC multimer staining to validate pMHC multimer reactivity before TCR isolation. Additionally, we aimed to implement the k_{off}-rate assay into the workflow to determine the structural TCR avidity of single cell expanded clones before TCR isolation. Both information, pMHC multimer reactivity and/or structural TCR avidity should be tested to predict TCRs functional avidity. To do so, we aimed to transgenically re-express a set of TCRs to characterize their functional avidity. Acquired data should be correlated with the two selection criteria, pMHC multimer MFI and k_{off}-rate.

Many TCR isolation and characterization platforms, also the one used in this thesis, are pMHC multimer-based. pMHC multimers allow T cell identification, traceless T cell isolation and TCR characterization. However, this versatility comes at the cost of 3 separate generation processes, including recombinant protein expression, purification and pMHC refolding. Epitope diversity adds even another level of complexity to the generation of pMHCs. This process is time, cost and labor intensive and prone to batch-to-batch variability. In order to reduce labor associated with pMHC multimer generation we aimed to test whether pMHC monomers can be equipped with a double tag to allow reversible multimerization and versatile functionalization of the pMHCs. Quality of these reagents should be tested against conventionally generated pMHC multimers. Furthermore, we aimed to test, whether the double-tagged pMHC multimers can be combined with a peptide exchange technique to allow rapid generation of a diverse pMHC library.

3 Material and methods

3.1 Materials

3.1.1 Commodities

Item	Supplier
3-way valve Discofix C 3SC	Braun, Melsungen, Germany
0.22 µm sterile filter	Millipore, Eschborn, Germany
1.0 ml Sub-Q	Franklin Lakes, USA
1.2 ml individual reaction tube	STARLAB, Hamburg, Germany
2.0 ml Cryo vial	Alpha Laboratories, Eastleigh, UK
1.0 ml, 1.5 ml, 2.0 ml reagent tubes	Zefa Laborservice, Grasbrunn, Germany
5 ml Polypropylen round-bottom tube	Greiner Corning, Durham, USA
15 ml, 50 ml Falcon Cell Star	Greiner bio-one, Heidelberg, Germany
1 l sterile filter cup (0.22 µm)	Millipore, Eschborn, Germany
10 kDa Amicon® Ultra-4, 15 centrifugal filters	Millipore, Eschborn, Germany
10 kDa membrane	Millipore, Eschborn, Germany
384 well plates medium binding	Greiner bio-one, Heidelberg, Germany
Culture flask 25 cm^2	VWR, Radnor, USA
Injection needle (20 G)	Braun, Melsungen, Germany
Leucosep™ centrifuge tubes	Greiner bio-one, Heidelberg, Germany

Safety-Multifly 21G	SARSTEDT, Nümbrecht, Germany
PCR reaction tubes	Brand, Werthelm, Germany
Pipette filter tips (1 µl, 10/20 µl, 200 µl, 1 ml)	STARLAB, Hamburg, Germany
Plastic cuvettes	Peske, Karlsruhe, Germany
Serological pipettes (5 ml, 10 ml, 25 ml)	Greiner bio-one, Heidelberg, Germany
Syringe (1 ml, 3 ml, 5 ml, 50 ml)	Braun, Melsungen, Germany
Tissue culture treated well plates (6-, 12-, 24-, 96-Well)	Greiner Corning, Durham, USA

3.1.2 Equipment

Equipment	Model	Supplier
Balance	ACS/ ACJ 320-4M	Kern & Sohn, Balingen, Germany
	EG 2200-2NM	Kern & Sohn, Balingen, Germany
Centrifuges	Biofuge fresco	Heraeus, Hanau, Germany
	Biofuge stratos	Heraeus, Hanau, Germany
	L8-70M Ultracentrifuge	Beckman, Krefeld, Germany
	Multifuge 3 S-R	Heraeus, Hanau, Germany
	Sorvall RC6+	Thermo Scientific, Ulm, Germany
	Varifuge 3.0RS	Heraeus, Hanau, Germany
Electrophoresis chamber	PerfectBlue™ Gel System Mini L	Peqlab, Erlangen, Germany
Electrophoresis power supply	EPS 600	Pharmacia Biotech, Uppsala, Sweden

Flow cytometer	Cyan ADP	Beackman Coulter, Fullerton, USA
	Cytoflex S	Beackman Coulter, Fullerton, USA
	MoFlo XDP Cell Sorter	Beackman Coulter, Fullerton, USA
	MoFlo Legacy Cell Sorter	Beackman Coulter, Fullerton, USA
FPLC	ÄKTApurifier™ 10	GE Healthcare, Chalfont St. Giles, UK
Gel filtration	Superdex200 increase	GE Healthcare, Chalfont St. Giles, UK
Gel imaging System	Molecular Imager® Gel Doc™ XR+	BioRad, München, Germany
	Amersham Imager 600 system	GE Healthcare, Chalfont St. Giles, UK
Heat block	Thermomixer compact	Eppendorf, Hamburg, Germany
Ice maker	ZBE 30-10	Ziegra Eismaschinen, Isernhagen, Germany
Incubator	HERAcell 240	Heraeus, Hanau, Germany
	Multititron	Infors, Bottmingen, Switzerland
	WB 300	Mytron, Heilbad Heiligenstadt, Germany
Laminar flow hood	HERAsafe	Heraeus, Hanau, Germany
Microscope	Axiovert S100	Carl Zeiss, Jena, Germany
Nanodrop device	ND-1000	Kisker, Steinfurt, Germany
Neubauer chamber	Neubauer Improved	Schubert, München, Germany

PCR cycler	T3000 Thermocycler	Biometra, Göttingen, Germany
pH-Meter	MultiCal pH 526	WTW, Weilheim, Germany
Spectrophotometer	NanoDrop ND-1000	Thermo Scientific, Ulm, Germany
Ultrasonic device	UW 2070	Bandelin, Berlin, Germany
Water bath	Type 1002	GFL, Burgwedel, Germany

3.1.3 Chemicals and reagents

Compound	**Supplier**
2-Propanol	Roth, Karlsruhe, Germany
Acetate	Roth, Karlsruhe, Germany
Acrylamide, Bis- solution (30 % / 2.6 %)	BioRad, München, Germany
Agarose	Roth, Karlsruhe, Germany
Ammonium persulfate	Sigma, Taufkirchen, Germany
Ampicillin	Roth, Karlsruhe, Germany
ATP	Roth, Karlsruhe, Germany
Azide-beads	JenaBioscience, Jena, Germany
Azido-Tyrosine	Watanabe Chemical
b-Mercaptoethanol	Sigma, Taufkirchen, Germany
Bicoll Seperating Solution	Merck, Darmstadt, Germany
Bovine Serum Albumine	Sigma, Taufkirchen, Germany
$CaCl_2$	Merck, Darmstadt, Germany
Carbenicillin	Sigma, Taufkirchen, Germany
Chloramphenicol	Roth, Karlsruhe, Germany
Coomassie blue	

D-Biotin	Sigma, Taufkirchen, Germany
D(+)-Saccharose	Roth, Karlsruhe, Germany
DBCO-beads	JenaBioscience, Jena, Germany
Dithiothreitol	Sigma, Taufkirchen, Germany
DMSO	Sigma, Taufkirchen, Germany
dNTPs	Roche, Penzberg, Germany
Ethanol	Roth, Karlsruhe, Germany
Ethidium Monoazide	Molecular Probes, Leiden, Netherlands
Fetal Calf Serum	GE Healthcare, Chalfont St. Giles, UK
Gentamicin	Life Technologies
GL	Bachem
Glutathione oxidized	Sigma, Taufkirchen, Germany
Glutathione reduced	Sigma, Taufkirchen, Germany
Glycerol	Sigma, Taufkirchen, Germany
GM	AG Springer, Jacobs University, Bremen, Germany
Golgi-Plug	BD Biosciences, Franklin Lakes, USA
Guanidine-HCl	Sigma, Taufkirchen, Germany
HEPES	Roth, Karlsruhe, Germany
Imidazole	Roth, Karlsruhe, Germany
Interleukin 2 (Il-2) (bulk culture)	PeproTech, Hamburg, Germany
Interleukin 2 Proleukin S (single cell culture)	Novaris, Basel, Switzerland
Ionomycin	Sigma, Taufkirchen, Germany

Isopropyl-β-D-thiogalactopyranoside	Applichem, Darmstadt, Germany
Kanamycin	Sigma, Taufkirchen, Germany
KCl	Merck, Darmstadt, Germany
KOH	Roth, Karlsruhe, Germany
L-Arginine-HCl	Roth, Karlsruhe, Germany
Leupeptin	Sigma, Taufkirchen, Germany
MES	Roth, Karlsruhe, Germany
Methanol	Roth, Karlsruhe, Germany
$MgCl_2$	Merck, Darmstadt, Germany
Na_2HPO_4	Roth, Karlsruhe, Germany
NaAcetate	Sigma, Taufkirchen, Germany
NaAzide	Sigma, Taufkirchen, Germany
NaCl	Roth, Karlsruhe, Germany
NaDesoxycholate	Sigma, Taufkirchen, Germany
NaEDTA	Roth, Karlsruhe, Germany
NaOH	Roth, Karlsruhe, Germany
Penicillin/Streptomycin	Life Technologies
Pepstatin	Sigma, Taufkirchen, Germany
Phenylmethylsulfonyl fluoride (PMSF)	Roche, Penzberg, Germany
Phorbol myristate acetate	Sigma, Taufkirchen, Germany
Phosphate Buffered Saline	Merck, Darmstadt, Germany
Propidium Iodide	Sigma, Taufkirchen, Germany
Rotisafe Gel Stain	Roth, Karlsruhe, Germany
Sodium dodecyl sulfate	Roth, Karlsruhe, Germany
TEMED	Roth, Karlsruhe, Germany
Tris-HCl	Roth, Karlsruhe, Germany

Triton-X 100	Roth, Karlsruhe, Germany
Trypan blue	Roth, Karlsruhe, Germany
Urea	Roth, Karlsruhe, Germany

3.1.4 Buffers and media

Solution	Composition
Complete freezing medium	1x FCS 10% (v/v) DMSO
Cryopreservation medium (bacteria)	1x LB-medium 10 % (v/v) Glycerol
CTL medium	500 ml RPMI 1640 50 ml HS 25 ml SC^+
D-biotin	100 mM stock solution
FACS buffer	1x PBS 0.5% (w/v) BSA pH 7,45
Guanidine solution	3 M Guanidine-HCl 10 mM NaAcetate 10 mM NaEDTA add 100 ml H2O, pH 4.2
IPTG	650 mg IPTG 6,5 ml LB-medium
LB-Ampicillin/Carbenicillin	1 l LB-medum 100 mg/l Ampicillin/Carbenicllin
LB-antibioticum plates	10 g/l Bacto-tryptone 5 g/l Yeast extract 20 g/l Agar 10 g/l e.g. Ampicillin

	pH 7.0
LB-Chloramphenicol	1 l LB-medium
	25 mg/l Chloramphenicol
Lysis buffer	50 mM Tris-HCl
	1 % Triton X-100
	0.1 % Na deoxycholate
	100 mM NaCl
	0.1 % NaN_3
	10 mM DTT
	add 500 ml H_2O, pH 8.0
Refolding buffer	100 mM Tris-HCl
	400 mM L-Arginin
	2 mM NaEDTA
	0.5 mM ox. Gluthathione
	5 mM red. Gluthathion
	add 1 L H_2O, pH 8,0
SC^+ (supplement complete, in 1 l medium)	1 ml β-mercaptoethanol
	20 ml Gentamicin
	23,83 g HEPES
	4g L-Glutamine
	200 ml Penicilin/Streptomycin
Solution buffer	50 mM Tris-HCl
	25 % Saccharose
	1 mM NaEDTA
	0.1 % NaN_3
	10 mM DTT
	add 500 ml H_2O, pH 8.0
Trypan blue solution	1 x PBS
	0,15% (v/v) trypan blue
Urea buffer 8 M	25 mM MES
	8 M urea
	10 mM NaEDTA

	0.1 mM DTT
	add 500 ml H_2O, pH 6.0
Washing buffer with Triton	50 mM Tris-HCl
	0.5 % Triton X-100
	100 mM NaCl
	1 mM NaEDTA
	0.1% NaN_3
	1 mM DTT
	add 500 ml H_2O, pH 8.0
Washing buffer without Triton	50 mM Tris-HCl
	100 mM NaCl
	1 mM NaEDTA
	0.1 % NaAzide
	1 mM DTT
	add 500 ml H_2O, pH 8.0

3.1.5 Peptides

Peptide	Sequence	MHC-allotype	Supplier
$pp50_{245-253}$	VTEHDTLLY	A*01:01	Peptides & elephants, Potsdam, Germany
$pp65_{363-373}$	YSEHPTFTSQY	A*01:01	Peptides & elephants, Potsdam, Germany
$Hexon_{886-894}$	LTDLGQNLLY	A*01:01	Peptides & elephants, Potsdam, Germany
$NS3_{1436-1444}$	ATDALMTGY	A*01:01	Peptides & elephants, Potsdam, Germany
$pp65_{495-503}$	NLVPMVATV	A*02:01	Peptides & elephants, Potsdam, Germany
HPV16 $E6_{29–38}$	TIHDIILECV	A*02:01	Peptides & elephants, Potsdam, Germany

HPV16 $E7_{11-19}$	YMLDLQPET	A*02:01	Peptides & elephants, Potsdam, Germany
PPI_{2-10}	ALWMRLLPL	A*02:01	Peptides & elephants, Potsdam, Germany
$FluMP1_{58-66}$	GILGFVFTL	A*02:01	Peptides & elephants, Potsdam, Germany
$NS3_{1073-1081}$	CVNGVCWTV	A*02:01	Peptides & elephants, Potsdam, Germany
$Her2/neu_{369-377}$	KIFGSLAFL	A*02:01	Peptides & elephants, Potsdam, Germany
$MART1_{(A27L)26-35}$	ELAGIGILTV	A*02:01	Peptides & elephants, Potsdam, Germany
NY $ESO_{157-165}$	SLLMWITQC	A*02:01	Peptides & elephants, Potsdam, Germany
RNF43_2	SLLPTCWAL	A*02:01	Peptides & elephants, Potsdam, Germany
YFV $NS4B_{212-222}$	LLWNGPMAV	A*02:01	Peptides & elephants, Potsdam, Germany
MMp25	KPILWRGLK	A*03:01	GeneScript, New Jersey, USA
KIF2C	RLFPGLAIK	A*03:01	GeneScript, New Jersey, USA
$IE1_{188-192}$	KLGGALQAK	A*03:01	Peptides & elephants, Potsdam, Germany
$pp65_{16-24}$	GPISGHVLK	A*11:01	Peptides & elephants, Potsdam, Germany
EBNA3b	AVFDRKSDAK	A*11:01	Peptides & elephants, Potsdam, Germany
$pp65_{341-350}$	QYDPVAALF	A*24:02	Peptides & elephants, Potsdam, Germany
$pp65_{417-426}$	TPRVTGGGAM	B*07:02	Peptides & elephants, Potsdam, Germany
$Core_{41-49}$	GPRLGVRAT	B*07:02	Peptides & elephants, Potsdam, Germany

$IE1_{199-207K}$	ELKRKMMYM	B*08:01	Peptides & elephants, Potsdam, Germany
$EBNA3a_{325-333}$	FLRGRAYGL	B*08:01	Peptides & elephants, Potsdam, Germany
$pp65_{123-131}$	IPSINVHHY	B*35:01	Peptides & elephants, Potsdam, Germany
$IE1_{309-317}$	CRVLCCYVL	C*07:02	Peptides & elephants, Potsdam, Germany
$OVA_{257-264}$	SIINFEKL	H2-Kb	Peptides & elephants, Potsdam, Germany

3.1.6 Antibodies

Epitope	Fluorophore	Clone	Supplier
CCR7	FITC	FAB197F	R&D Systems
CD19	ECD	J3-119	Beckman Coulter
CD3	FITC	UCHT1	Beckman Coulter
CD3	BV650	UCHT1	eBioscience
CD45	PB	PB986	DAKO
CD45	PECy7	2D1	eBioscience
CD45	PO	HI30	Exbio
CD45	ECD	J33	Beckman Coulter
CD45RA	PECy7	HI100	eBioscience
CD69	PE	FN50	BioLegend
CD8α	FITC	B9.11	Beckman Coulter
CD8α	PECy7	SFCI21ThyD3	Beckman Coulter
CD8α	PE	3B5	Invitrogen
CD8α	APC	RPA-T8	BioLegend
CD8α	eF450	OKT8	eBioscience

CD8α	PE	OKT8	eBioscience
HLA-A2	PE	BB7.2	BioLegend
Il-2	APC		BD Pharmingen
INFγ	FITC		BD Pharmingen
mTrbc	APC	H57-597	BioLegend
mTrbc	APCfire	H57-597	BioLegend
PD-1	APC	eBioJ105	Invitrogen
TNFα	PECy7	MAb11	eBioscience

3.1.7 Fluorescently labeled pMHC backbones

Backbone	Fluorophore	Supplier
Streptavidin	APC	eBioscience
Streptavidin	BV421	BioLegend
Streptavidin	FITC	BioLegend
Strep-Tactin	APC	IBA
Strep-Tactin	PE	IBA

3.1.8 Molecular kits and standards

Kit / Standard	Supplier
BD Cytofix/Cytoperm	BD Biosciences
CloneJET PCR Cloning Kit	Thermo Fisher
GeneRuler 1kb DNA ladder	Thermo Fisher
Pierce BCA Protein Assay	Thermo Fisher
PureLink Hi Pure Plasmid Filter Maxiprep Kit	Invitrogen (Thermo)
PureYield Plasmid Miniprep System	Promega

Q5 Site-Directed Mutagenesis Kit	New England Biolabs
SeeBlue protein marker	Invitrogen
SV Wizard Gel and PCR Clean-Up System	Promega

3.1.9 Vectors and organisms

Vectors and organism	Note	Supplier
pET3a	MHC LC+HC expression vector	
pET28-SUMO3	TTL Expression expression vector	AG Leonhardt
pASG-IBAwt1	HLA-C*07:02 expression vector	IBA
MP71	Retroviral TCR vector	
BL21-CodonPlus (DE3)-RIL	MHC LC+HC expression bacteria	Agilent Technologies
BL21(DE3)	TTL expression bacteria	Agilent Technologies
Stbl3	Bacteria for plasmid amplification	Thermo Scientific
RD114	Packaging cell line	
K562	Target cells	

3.1.10 Software

Software	Supplier	Version
Affinity Designer	Pantone	1.6.4.104
Excel 2016	Microsoft	
FlowJo 10	FlowJo	10.4.2

GraphPad PRISM	Graphpad Software	7.03
Power Point 2016	Microsoft	
Summit	Dako	4.4.00
Unicorn	GE Healthcare	7.1.0.378

3.2. Methods

3.2.1 *In vitro* cell culture of T cells

3.2.1.1 Isolation of peripheral blood mononuclear cells

For PBMC isolation, blood was obtained from whole blood of healthy donors or buffy coats. Written informed consent was obtained from the donors, and usage of the blood samples was approved according to national law by the local Institutional Review Board (Ethikkommission der Medizinischen Fakultät der Technischen Universität München). PBMCs were isolated by density gradient centrifugation using Ficoll (Biochrome). In brief, buffy coats were diluted 1:2 and whole blood 1:1 with sterile PBS. 15 ml Ficoll were overlaid with 35 ml diluted blood and centrifuged at 1000 g for 20 min at RT, brakes disabled. PBMCs were isolated, washed twice with sterile PBS and counted in a Neubauer Improved hemocytometer using trypan blue solution (0.15 % trypan blue in PBS) for live/dead discrimination.

3.2.1.2 Feeder-cell free single cell expansion

A short-term feeder-cell free expansion protocol for murine T cells using CD3/CD28 plate bound mAbs was previously established by Marten Plambeck (unpublished data). We adopted the protocol to naïve human $CD8^+$ T cells as following. PBMCs isolated from buffy coats or whole blood were stained with CD3-BV650, CD8-PE, CD19-ECD, CCR7-FITC, CD45RA-PECy7 and two pMHC multimers (identical pMHCs multimerized on streptavidin-BV421 and streptavidin-APC). Propidium iodide (PI) was used for live/dead discrimination. CD3+; CD8+; CD19- ; CCR7+; CD45RA+; pMHC multimer (double)+ T cells were flow-sorted as single cells directly into 384-well plates (medium binding Greiner bio-one) containing 25 µl CTL supplemented with 2 µl/ ml Expamer pre-mix (Juno Therapeutics GmbH) and 50 U/ml IL-2 (Proleukin S, Novartis). Plates were sealed with Parafilm (Sigma Aldrich) to reduce evaporation and incubated at 37°C, 5 % CO_2 and 95 % rel. humidity for 12-14 d or until single cell derived clones were considered large enough for analysis.

3.2.1.3 *In vitro* cell culture of bulk T cells

In vitro culture of bulk T cells was performed either with feeder cells using irradiated allogeneic PBMCs in combination with PHA or using CD3/CD28

Expamer. In brief, for feeder cell-based culture PBMCs were mitotically inactivated by irradiation (45 Gy) and washed twice in warm RPMI 1640. Subsequently, cell number and density were adjusted to yield a 1:5 ratio of target:feeder cells and transferred into into CTL medium containing 50 U/ml IL-2 and 1 µg/ml PHA (Oxoid). If the medium turned yellow, fresh CTL medium supplemented with 50 U/ml IL–2 (Peprotech) was added. Cells were passaged when reaching 90 % confluence.

In brief, for *in vitro* cell culture of bulk T cells using CD3/CD28 Expamer, cell density was adjusted to $1x10^6$ n/ml supplemented with 2 µl/ml CD3/CD28 Expamer and 180 U/ml Il-2 (Peprotech) in CTL medium. Cells were passaged when reaching 90 % confluence.

3.2.1.4 TCR transduction of peripheral blood mononuclear cells

For in-depth characterization of identified TCRs, we performed retroviral TCR transduction into PBMCs of HLA-A*02:01-negative donors, as all tested TCRs were HLA-A*02:01 restricted. $1.5x10^6$ RD114 cells were seeded in 3 ml of full DMEM medium (supplemented with 10 % FCS+ SC^+) and incubated o.n. at 37°C, 5 % CO_2. 18 µg plasmid DNA containing the respective TCR sequence were diluted in ddH_2O to a total volume of 135 µl. Afterwards, 15 µl of $CaCl_2$ solution (1.84 g in 5 ml ddH_2O, filtered sterile) were given to the DNA solution and added drop-wise to 150 µl transfection buffer under slow vortexing. DNA solution were incubated for 30 min on RT to allow formation of Ca^{2+}-DNA complexes. Subsequently, DNA solution was drop-wise added to plated RD114, changing medium after 6 h. Transfected RD114 were incubated for at 37°C, 5 % CO_2, 95 % rel. humidity to allow production of viral particles.

The next day, PBMCs were isolated from an HLA-A*02:01-negative donor, plated at a density of $1x10^6$ cells/ml and stimulated with 300 U/ml IL 2 and 2 µl/ml CD3/CD28 Expamer. PBMCs were incubated o.n. at 37°C, 5 % CO_2, 95 % rel. humidity.

After 48 h, the medium of RD114 cells was harvested, centrifuged at 1500 rpm for 3 min and the supernatant collected. Medium was replaced by addition of 3 ml full DMEM. 24 well flat bottom plate was coated with retronectin solution (TaKaRa) (300 µl /well) o.n. at 4°C.

1 ml of virus supernatant was coated on retronectin-treated plates by centrifuged for 2 h, 3000 g, 32°C. The medium of the RD114 cells was harvested, centrifuged at 1500 rpm for 3 min and the supernatant harvested. PBMCs were washed with 1 mM biotin for 20 min at RT, centrifuged and the conditioned medium collected. PBMCs were washed twice with sterile PBS, resuspended in full RPMI medium and counted. $0.8x10^6$ cells were resuspended in less than 0.3 ml full RPMI medium and added onto the virus- coated plate adding 1 ml of the second virus supernatant. The plate was centrifuged for 10 min, 1000 g, 32°C, supernatant removed and 1.5 ml full RPMI medium added together with 1.5 ml conditioned medium. The medium was supplemented with180 U/ml IL 2 (Peprotech) and cells were incubated at 37°C, 5 % CO_2. 4 d post transduction, the transduction efficacy was determined by co-staining of pMHC-multimer with mTrbc-APC and CD8-PE mAb.

3.2.2 Enzymes for pMHC monomer functionalization

3.2.2.1 Expression and purification of tubulin tyrosine ligase

The tubulin tyrosine ligase (TTL) enzyme was expressed and purified as described previously[129]. In brief, TTL coding sequence derived from *Canis lupus* was cloned into a pET28-SUMO3 vector (EMBL-Heidelberg, Protein Expression Facility) to allow expression as Sumo-TTL fusion protein with an N-terminal His-Tag. Sequence validated expression plasmids were transformed into *E. coli* BL21(DE3) (Agilent). Bacteria were grown to OD_{600}= 0.7 at 37°C, 180 rpm and induced with 0.5 mM IPTG. Recombinant enzyme expression is performed by incubation at 18°C, 180 rpm for 18 h. Bacteria lysis was performed by addition of 100 µg/ml lysozyme, 100 µg/ml DNAse in presence of 2 mM PMSF followed by sonication (5 cycles of 7x8 sec, 40 % amplitude). Debris was pelleted by 20000 g, for 30 min at 4°C. Supernatant containing the His-Sumo-TTL was purified using 5 ml His-Trap HP (GE Healthcare). Purified enzyme was desalted using PD10 column (GE Healthcare), buffer exchanged to MES/K pH 7.0 (20 mM MES, 100 mM KCl, 10 mM $MgCl_2$) supplemented with 50 mM L-glutamate, 50 mM L-arginine. TTL aliquots were snap-frozen and stored at -80°C.

3.2.2.2 Sortase A

Sortase A was kindly provided as purified enzyme derived from *S. aureus* by Dr. Hannelore Meyer, Technical University of Munich.

3.2.3 pMHC reagents

All pMHC monomers described in this report, including the double-tagged pMHC molecules, were generated as previously described[56,72,130]. All Tub- and SrtA-tagged Streptamers cloned in this work were generated based on the corresponding Streptamer within the pMHC expression plasmid library of the Busch laboratory.

3.2.3.1 Cloning of Tub- and Sortase-tag into Streptamer expression vectors

pET3a expression vectors containing the coding sequence of strep-tagged HLA allotypes, including murine H2-Kb, served as parental plasmid to insert the Tub-tag or Sortase A (SrtA)-His_6 tag sequence seamless downstream of strep-tag. All insertions were performed using the Q5 Site-Directed Mutagenesis Kit (New England BioLabs) following manufactures protocol. Insertion primers (Sigma Aldrich) contained 18 bp plasmid binding sequence flanking the integration site and encoded 1/2 of the Tub- or SrtA-tag sequence. Inserted sequences were codon optimized for protein expression in *E. coli*. The Mutagenesis PCR cycling steps were chosen as follows:

Step	Temperature [°C]	Time [s]	
Denaturation	95	30	
Denaturation	95	10	25 cycles
Annealing	65	20	
Elongation	72	60 / kb	
Final elongation	72	150	
Cool down	4	∞	

3.2.3.2 Transformation and plasmid purification

If bacterial transformation was not a step within the Q5 Site-Directed Mutagenesis Kit, we used following procedure for transformation. Stbl3 chemo competent *E. coli* were transformed with plasmid DNA, plated on LB-agar plates containing appropriate selection marker (100 µg/ml Ampicillin and/or 25 µg/ml Chloramphenicol) and incubated overnight (o.n.) at 37°C. 4 ml of LB medium (100 µg/ml Ampicillin and/or 25 µg/ml Chloramphenicol) were inoculated with a single colony forming unit (cfu) and incubated o.n. at 37°C, 180 rpm. Plasmid preparation was performed with the PureYield Plasmid Miniprep System (Promega) following manufactures protocol but using 3 ml of bacterial culture. Elution of plasmid DNA was performed with 30 µl ddH_2O.

3.2.3.4 Sanger sequencing

Sanger sequencing (Eurofins Scientific SE) using appropriate primers was performed for all cloned pMHC expression plasmid described in this work. Plasmids were checked for correct sequence integration by alignment against reference sequences (Tub-tag, Strep-tag, Sortase A-tag, His_6-tag) as well as HLA-allotype sequences using Basic Local Alignment Search Tool (BLAST) and Ensembl.

3.2.3.5 Transformation of expression bacteria and generation cryo-stocks

Sequence validated plasmids containing Tub-tagged Streptamers (“FLEXamer”) or SrtA-tagged Streptamers (“SrtA-FLEXamer”) were transformed into BL21 CodonPlus (DE3) RIL competent *E.coli* (Agilent), as recommended by the manufacturer’s protocol. To generate bacterial stocks for recombinant protein expression, a single CFU was picked and transferred into LB-medium containing 100 µg/ml Ampicillin and 25 µg/ml Chloramphenicol and grown to OD_{600}= 0.3 at 37°C, 250 rpm. Bacterial cultures were mixed 1:1 (v/v) with 20 % glycerol in cryopreservation vials and snap-frozen using liquid nitrogen. The ready-to-use stocks were stored at -80°C.

3.2.3.5 Recombinant protein expression of MHC heavy and light chains

We use BL21 (DE3) Codon+ RIL (Agilent) for recombinant protein expression of MHC heavy and light chains. Standard protein expressions are carried out using 6 l bacteria culture in 2 l baffled flasks. Per flask, 1 l LB-medium containing

25 µg/mL Chloramphenicol, 100 µg/mL Carbenicillin and 10 ml 40 % glucose were inoculated with 1 ml diluted expression bacteria (20 µl bacterial cyro-stock diluted in 7 ml LB-medium). Bacteria were incubated at 37°C at 180 rpm until OD_{600} = 0.7. Protein expression was induced by addition of IPTG to a final concentration of 0.5 mM, shaking for 3 h at 37°C, 180 rpm. Bacteria were harvested by centrifugation at 5000 g, 10 min, 4°C and pellets stored at -80°C until further processing.

3.2.3.6 Protein purification from inclusion bodies

Bacterial pellets were thawed on ice, resuspended in 13 ml solution buffer and homogenized by sonication (15 pulses, 70 %). For enzymatic lysis, 100 µl lysozyme (50 mg/ml), 250 µl DNase I (2 mg/ml) and 50 µl MgCl (0.5 M) were added and incubated for 1 h at RT, followed by freezing at -80°C for 20 min. Suspensions were thawed using a water bath, 30 min, 37°C and 50 µl MgCl (0.5 M) added. After 30 min, 350 µl NaEDTA (0.5 M) were added and the suspensions pelleted at 11000 g, 20 min. Supernatants were discarded and pellets re-suspended in 10 ml washing buffer with Triton X-100 and homogenized by sonication (15 pulses, 70 %). Centrifugation and resuspension were repeated with washing buffer without Triton X-100. Finally, suspensions were pelleted at 11000 g and 4°C, 20 min. The supernatant was discarded and pellet dissolved in small pieces in 2 to 4 ml of 8 M urea (size-dependent). The suspensions were placed on a slowly stirring at 4°C o.n. Insoluble aggregates were removed by ultracentrifugation at 45000 rpm, 20°C, 20 min in vacuum. The protein concentration of the supernatant was determined by standard BCA assay and aliquots stored at -80°C.

3.2.3.6 Determination of protein concentration

The protein concentrations are determined by standard BCA assay, following the protocol of the Pierce BCA Protein Assay Kit (Thermo Scientific). In brief, BSA standards are generated freshly in 8 M urea buffer (0, 1.5, 3, 6, 12.5, 25, 50, 100 mg/ml). 20 µl of standards and 20 µl of 1:10 diluted sample are added to 1 ml of the BCA solution (1:50 Pierce-B:Pierce-A solution). Samples are incubated for 5 min at RT and protein concentrations determined at OD_{562}.

3.2.4 Generation of pMHC multimers

3.2.4.1 Refolding of pMHC monomers

The following section describes refolding of pMHC monomers in the presence of full length peptides to form “conventional” pMHCs[130,131] and in the presence of di-peptides to form “peptide-exchange” pMHCs[77,132]. The protocols are very similar, only differing in the downstream purification of pMHC molecules. Here, buffers have to be supplemented with di-peptide to prevent aggregation of di-peptide loaded pMHCs as they are unstable below 10 mM di-peptide.

pMHC monomer refoldings are routinely performed in 200 ml volumes on 4°C. For small scale refolding, 60 ml volume was used and all components/reagents described in the following adjusted accordingly. Refolding buffer was supplemented with 100 µl of Pepstatin (2 mg/ml) and Leupeptin (2 mg/ml). For refolding of full-length peptide loaded pMHCs, 12 mg peptide were added to the refolding buffer. For refolding with di-peptide loaded pMHCs, refolding buffer with 40 mM di-peptide was used. In total, 18.6 mg of heavy chain and 13.2 mg of light chain were split into 3 equal aliquots and mixed 1:1 (v/v) with guanidine solution (3 M) prior to injection. Injections were performed in 3 h intervals, adding dropwise the light chain followed by the heahy chain to the refolding solution. Refolding solutions were incubated o.n. for full length peptide loaded pMHCs or 7 d for di-peptide loaded pMHCs, respectively.

Refolding solutions were centrifuged at 2000 g, 15 min, 4°C to remove aggregates and transferred into pressure chambers for buffer exchange over a 10 kDa membrane. Concentration was performed at 2,5 bar with compressed N_2 to a volume of 5-10 ml. The flow-through was reused for a second refolding following the steps described above. For buffer exchange, FPLC buffer (+/- 10 mM di-peptide) was added to a total volume of 200 ml and refolding solution again concentrated down to 10 ml. Solution was transferred to a 50 ml tube, aggregates removed by centrifugation at 2000 g, 10 min, 4°C and supernatant filtered through a 0.22 µm sterile filter. Final concentration down to 1 ml was performed by transferring the solution to 10 kDa molecular weight cut-off (MWCO) centrifugal filter (Amicon Ultra), centrifuging at 3000 g, 4°C. The solution was sterile filtered (0.22 µm) and applied onto a gel filtration column (Superdex 200 increase 10/300 GL) and purified at a flowrate of 0.5 ml/min using an ÄKTApurifier (FPLC buffer +/- 10 mM di-peptide). Eluate was collected in 0.5 ml

fractions, pooled according to the chromatography profile and concentrated with 10 kDa MWCO centrifugal filter to a volume of 500 µl. Protein concentration was determined by standard BCA assay. Further concentration was performed if the protein concentration was below 1.2 mg/ml. Per mL, 0. µl Pepstatin (2 mg/ml), 0.5 µl Leupeptin (2 mg/ml), 2 µl NaEDTA (0.5 M) and 1 µl of the appropriate full length peptide (10 mg/ml in DMSO) were added and stored at -80°C.

3.2.4.2 Conventional functionalization of pMHC monomers

Conventionally biotinylated pMHC monomers for generation for non-reversible multimers were generated as described[130]. In brief, up to 2 mg purified pMHC monomers are incubated with 30 µg Biotin-Protein Ligase BirA, 100 µl Solution A and100 µl solution B (both purchased by Avidity), 0.5 µl Pepstatin (2 mg/ml) and 0.5 µl Leupeptin (2 mg/ml) and incubated on RT o.n. Purification of biotinylated pMHC monomers was performed using size exclusion chromatography as described in 3.2.4.1.

Conventional dye-conjugated Streptamers were generated as described[56]. In brief, purified Streptamers carrying an additional solvent exposed cysteine residue were incubated with dithiotreithol (DTT) o.n.. After buffer exchange to degassed PBS pH 7.3, Streptamers were incubated with a 10-fold molar excess of Alexa Fluor 488 Maleimide C_5 (Thermo Fisher) under constant agitation on 4°C in dark o.n. Unconjugated fluorophore was separated from dye-conjugated Streptamer by NAP-25 gravidity flow desalting columns (GE Healthcare).

3.2.4.3 TTL mediated functionalization of Tub-tagged FLEXamers

TTL mediated functionalization of Tub-tagged Streptamers (“FLEXamers”) was performed as previously described[129], however the functionalization steps were optimized for pMHC monomers as following. TTL catalyzed ligation of 3-azido-L-tyrosine (Watanabe Chemical Industries LTD) to FLEXamers was performed in 25-100 µl consisting of 20 µM FLEXamers, 5 µM TTL and 1 mM 3-azido-L-tyrosine in TTL-reaction buffer (20 mM MES, 100 mM KCl, 10 mM $MgCl_2$, 2.5 mM ATP and 5 mM reduced glutathione) at 25°C for 3 h followed by buffer exchange to 20 mM Tris.HCl, 50 mM NaCl pH 8.0 by size exclusion chromatography using 7 kDa MWCO desalting spin columns (Thermo Scientific). Resulting purified azido-FLEXamers were directly used for click-functionalization by incubation of 20 µM Azido- FLEXamer with either 400 µM DBCO-PEG_4-Biotin, 400 µM DBCO-

sulfoCy5 or 200 µM DBCO-PEG_4-Atto488 (Jena Bioscience), 400 µM DBCO-PEG_4-MMAF or 80-160 µM DBCO-TEG-oligonucleotides (IDT DNA) for 18 h at 16°C followed by buffer exchange to 20 mM Tris, 50 mM NaCl pH 8.0. Functionalized FLEXamers were storage at -80°C. Conjugation was analyzed by reducing and Coomassie staining. In addition, biotinylated FLEXamers were plotted on a nitrocellulose membrane, stained with a streptavidin-Alexa Fluor 594 (Dianova) conjugate and detected on an Amersham Imager 600 system (GE Healthcare). In-gel fluorescence of fluorophore labeled FLEXamers was directly detected using the same instrumentation. Conjugation efficacy was evaluated using densitometry.

3.2.4.4 Sortase A mediated functionalization of SrtA-tagged FLEXamers

10 µM SrtA-tagged Flexamer was incubated with 1 mM Gly_5-FITC or 1 mM Gly_5-biotin peptide (JPT Technologies GmbH) and 30 µM SrtA in 20 mM HEPES, 5 mM $CaCl_2$, pH 7.5 at 25°C for 18 h. Ni-NTA sepharose bead-based pulldown in PBS, 20 mM imidazole, pH 8.0 at 4°C for 30 min was used to remove His-tagged SrtA and SrtA-tagged FLEXamer educts still carrying the His-tag. Purified functionalized SrtA-tagged FLEXamers were buffer exchange after functionalization to 20 mM Tris, 50 mM NaCl, pH 8.0. Conjugation and purification were analyzed by SDS-PAGE followed by detection of in-gel fluorescence and Coomassie staining as described above.

3.2.4.5 Sodium dodecyl sulfate polyacrylamide gel electrophoresis

Sodium dodecyl sulfate polyacrylamide gel electrophoresis (SDS PAGE) was performed to control successful recombinant protein expression and to determine the FLEXamer conjugation efficiency. We routinely used s 6 % stacking gel in conjunction with a 12,5 % separation gel. For expression controls, sample separation was performed as a one step process at 130 V for up to 2 h. To assess FLEXamer conjugation efficiency, this step was preceded by an additional step at 80 V for 10 min. Gels were either used for in-gel fluorescence measurements or stained by Coomassie Blue solution for 30 min at RT under agitation followed by destaining in ‘destaining solution’ for 2 h under agitation at RT.

3.2.4.6 Multimerization of pMHC monomers

All reversible pMHC monomers (with and w/o dye) were multimerized on Strep-Tacin APC or Strep-Tacin PE (IBA) by incubating 1 µg reversible pMHC monomer and 1 µl Strep-Tacin APC or PE in a total volume of 50 µl FACS buffer for 30 min on ice in dark. All biotin-functionalized pMHC monomers described in this work were multimerized by incubation of 0.4 µg biotinylated pMHC monomers with 0.1 µg Streptavidin BV421 (Biolegend), 0.1 µg Streptavidin APC (eBioscience) or 0.25 µg Streptavidin PE (Biolegend) in a total volume of 50 µl FACS buffer for 30 min on ice in dark.

3.2.4.7 Peptide exchange of di-peptide loaded pMHC monomers

Loading of di-peptide pMHCs with full length peptide was routinely performed in sample size of 5-10 µg of di-peptide loaded pMHC. Full length peptides were diluted in DMSO and added in 100x molar excess to di-peptide loaded pMHCs and incubated for 20 min on RT. Subsequently, pMHCs could be handled just as full-length peptide refolded pMHCs.

3.2.4.8 Validation of *in silico* predicted RNF43 peptide epitopes and their validation by *in vitro* proteasomal digest

In silico prediction of peptide epitopes derived from frame-shift mutations of the RNF43 gene was performed as previously described[133]. In brief, we generated all theoretically possible reading frames that can be derived by deletion of one ((n*3)-1) or two ((n*3)-2), DNA nucleotides. Resulting peptide candidates of 8-11 aa in length were fed into netMHC prediction algorithm, which ranks the binding probability of peptides to a limited set of HLA alleles[134]. Most promising peptide candidates were used to verify correct processing by *in vitro* proteasomal digest (AG Kloetzel, Charité, Berlin)[135].

3.2.5 Functional & structural assays and FACS analysis of T cells

3.2.5.1 Antibody and pMHC multimer staining

When solely performing pMHC multimer staining with a combination of non-reversible pMHC multimers, staining was incubated for 30 min on ice in dark. We routinely stain the pMHC multimer conjugated to the smaller dye first. After incubation, cells are washed and stained with the second pMHC multimer for 30 min. Antibody staining was added after 10 min and incubated for additional

20 min. For k_{off}-rate measurements, up to $5x10^6$ cells were incubated with dye-conjugated reversible pMHC multimers for 45 min on ice in dark. Antibody staining was added after 25 min and incubated for additional 20 min. If combinatorial staining with non-reversible pMHC multimers was performed, cells were washed and incubated for 10 min with non-reversible pMHC multimers on ice in dark. For live/dead discrimination, cells were washed in propidium iodide (PI) solution. When cells were stained with reversible pMHC multimers for traceless cell isolation, samples were incubated for 45 min with the multimer regent. After 25 min, antibody staining was added and incubated for additional 20 min. All FACS data were analyzed with FlowJo software (FlowJo, LLC).

3.2.5.2 CD45 multiplex color code

In order to process and analyze multiple samples in parallel, samples were color coded with CD45 mAbs carrying different fluorophores. We routinely used CD45 mAbs conjugated to Pacific Blue, Pacific Orange, PECy7 and ECD, as these fluorophores were easy to implement in standard flow cytometry panels. 4 differently labeled CD45 mAbs allow simultaneous processing and measurement of 16 samples. Depending on the experiment, CD45 mAbs were applied as first staining reagent (e.g. when color coding single cell derived clones for pMHC multimer restaining or k_{off}-rate measurement) or after pMHC multimer staining simultaneously with the mAb-master mix (e.g. to color code samples of different antigen-specific T cell populations for parallel acquisition on flow-cytometer).
For color coding, up to $5x10^6$ cells per sample were transferred into a 96 well V-bottom plate and washed twice and resuspended in 50 µl FACS buffer. CD45 mAbs were added as master-mix containing the different combinations of labeled CD45 mAbs and incubated for 20 min on ice in dark. Samples were washed 2.5 times with FACS buffer and transferred into a new well of a 96 well V-bottom plate to prevent mAbs carryover. Samples were centrifuged and subsequently pooled for further processing and analysis. Of note, use of V-bottom plates and prolonged centrifugation (5 min instead of routinely used 3 min) turned out to reduce cell lost considerably.

3.2.5.3 Intracellular cytokine staining

To assess functional avidity of the identified TCRs, we performed intracellular cytokine staining (ICCS) after co-culture of TCR-transduced T cells with peptide pulsed K562 target cells. To ensure that TCR-transgenic T cells are able to intrinsically produce Il-2, T cells were cultured at 50 U/ml Il-2 for two days after thawing and rested 24 h in medium without Il-2 prior to co-culture with peptide pulsed K562-HLA-A*02:01$^+$ target cells. One day prior to co-culture, K562 target cells were irradiated at 80 Gray (Gy), washed twice with complete RPMI (containing SC$^+$ and 10 % FCS) and resuspended at a cell density of 3x10^6 cells/ml. Subsequently, K562 target cells were pulsed with the respective cognate peptide epitope of the TCR to be analyzed at final concentrations ranging from 1 mM to 1 pM, as well as appropriate negative controls using an irrelevant peptide epitope. Pulsed K562 target cells were incubated o.n. at 37°C, 5 % CO_2, 95 % rel. humidity.

The next day, target cells were harvested and washed thrice in complete RPMI and resuspended at a density of 1x10^6 cells/ml. TCR-transgenic T cells were counted and resuspended at a density of 1x10^6 CD3$^+$ transgenic TCR$^+$ cells/ml. For co-culture, both 50.000 peptide pulsed K562 target cells and 50.000 CD3$^+$ transgenic TCR$^+$ cells (50 µl/well each) were co-cocultured and mixed with 100 µl complete RPMI medium containing 2 µl/ml GolgiPlug (BD Biosciences). As a positive control, 50.000 CD3$^+$ transgenic TCR$^+$ cells/well were incubated without K562-HLA- A0201$^+$ and stimulated with PMA (25 ng/ml) and Ionomycin (1 µg/ml) and 1 µg/ml GolgiPlug. All test conditions were performed in technical triplicates. Cells were co-incubated for 4 h at 37°C, 5 % CO^2. For live/dead staining, EMA was used. Cells were resuspeded in 50 µl FACS buffer containing a concentration of 2 µg/ml EMA and exposed to bright light on ice for 15 min. Cells were washed twice followed by surface staining of with mTrbc-APCfire and CD8-PE mAb for 20 min on ice in the dark. Samples were washed with FACS buffer and incubated for 20 min on ice in the dark in 100 µl Cytofix solution (BD Biosciences). Cells were washed twice in 1xPermwash (BD Biosciences). For intracellular staining, samples were stained with TNFα-PC7, IL2-APC, INFγ-FITC, CD8-PE and mTrbc-APCfire mAbs for 20 min on ice in the dark. Samples were washed twice in 1xPermwash and once in FACS. Finally, samples were filtered through a nylon mesh and analyzed on flow-cytometer.

3.2.5.4 Killing assay of peptide pulsed target cells

We analyzed the killing capacity of the isolated TCRs by co-culturing TCR transduced T cells with peptide pulsed HLA*0201-GFP$^+$ K562 target cells, where reduction of GPF+ target cells served as readout. For peptide pulsing, K562 target cells were washed twice in RPMI$^-$ (containing neither FCS nor SC$^+$) and incubated with 1 µM peptide for 2 h at RT under constant agitation. Cells were washed thrice in RPMI$^-$ and resuspended in full RPMI medium containing 50 U/ml Il-2 at a density of 1.5x10^6 cells/ml. Cells were plated at 75.000 cells (50 µl) per well into a 96-well flat bottom plate and rested for 1 h at 37°C, 5 % CO_2. Transgenic T cells were harvested and resuspended in complete RPMI medium containing 50 U/ml Il-2 at a density of 0.5x10^6 CD3$^+$ transgenic TCR$^+$ cells/ml. T cells were added in ratios of 1:5, 1:3 and 1:1 (30 µl, 50 µl and 150 µl respectively of T cell suspension) and wells filled up to 200 µl with full RPMI medium containing 50 U/ml IL2. All samples were measured in triplicates. Cells were co-cultured for 18 h at 37°C, 5 % CO_2. Afterwards, cells were transferred to a 96-well V-bottom plate, washed once in FACS buffer and stained with CD8-eF450, CD69-PE, PD1-APC and mTrbc-APCfire mAbs for 20 min on ice in the dark. Samples were washed twice; PI was used for live/dead discrimination. Samples were resuspended in 70 µl FACS buffer containing 1000 beads (123Count eBeads, Thermo Fisher) per sample, filtered through a nylon mesh and analyzed on flow-cytometer.

3.2.5.5 k_{off}-rate measurement

To determine structural avidity of identified TCRs as well as to compare the functionality of the newly generated FLEXamer, we performed the flow based k_{off}-rate assay as published[53]. In brief, appropriate numbers of TCR transduced T cells were harvested into 96 well V-bottom plates to acquire 1000 pMHC$^+$ cells/min in the final readout. Cells were stained with dye-conjugated reversible pMHC multimers (see 3.2.4.6) followed by staining with mTrbc and CD8 mAbs. For analysis of Ag-specific non-TCR transduced T cells, samples were incubated with non-reversible pMHC multimers for 10 min after mAb staining. PI was used for live/dead discrimination. Analysis was performed at medium flow-rate of 25000 (CyAn) or 140 µl/min (Cytoflex S) for 15 min under constant cooling using a Peltier cooling device set to 4.5°C. 30 s after start of acquisition, D-biotin was

injected into the ongoing measurement to a final concentration of 1 mM. All measurements were performed in technical triplicates.

3.2.5.6 FACS acquisition and analysis

Acquisition of FACS samples was performed on CyanADP (Beckman Coulter) or Cytoflex S flow cytometer (Beckman Coulter). Sort purifications were performed on MoFLo XDP (Beckman Coulter) and MoFLo legacy (Beckman Coulter). Data were analyzed with FlowJo software (Tree Star, Inc.).

3.2.5.7 TCR isolation of monoclonal expanded T cell clones

After positive pMHC multimer restaining and/or positive k_{off}-rate measurement of single cell derived clones, the TCR sequences were isolated via single clone PCR (performed by Thomas R. Müller) which is an optimized TCR gene specific RACE-PCR protocol based on a previous publication[123] (Thomas R. Müller, unpublished). Routine TCR identification was performed by in-house next generation sequencing (NGS). However, in exceptions TCRs were identified as described in the following steps. The PCR products were loaded onto an agarose gel (1 % agarose, 100 V) and the respective bands isolated and purified with the SV Wizard Gel and PCR Clean-Up System (Promega). Purified products were cloned into the pJET vector using the blunt end cloning protocol of the CloneJET PCR Cloning Kit (Thermo Fisher Scientific). Afterwards samples were sequenced and the TCRs assembled *in silico* according to sequence homology with known sequences the IMGT/HLA database. The TCR cassette for viral expression was routinely assembled as human Vß-chain-murine-constant-ß-chain-P2A-human-Vα-chain- murine-constant-α-chain fusion. TCR α- and β- chains are linked via self-cleaving porcine teschovirus 2A sequence (P2A)[136]. Accurate pairing and surface expression of the transgenic α- and β-TCR chains were optimized through a chimeric human/murine constant region[137].Fully reconstructed TCR sequences were synthesized and cloned into MP71 vector by Twist Bioscience.

4 Results

4.1 Establishment of a feeder cell-free single CD8$^+$ T cell expansion protocol allowing TCR characterization prior to TCR sequencing

The most critical drawback of feeder-cell based protocols is that they rely on a heterogeneous cell-mixture, which leads to variable expansion of T cells or even complete drop outs, since not all T cells can be cultured under the same conditions[138]. Furthermore, when feeder cell-based protocols are used in direct conjunction with PCR-based TCR isolation, TCR mRNA derived from the feeder cells can lead to contamination of the PCR product and thereby to incorrect sequencing result (data not shown). Cumbersome sort-based purification before TCR isolation drastically decreases throughput of TCR isolation workflows.

We focused on establishing a short-term feeder cell-free expansion protocol of pMHC multimer-guided single cell-sorted CD8$^+$ T cells. Testing a synthetic stimulation reagent-based expansion protocol could allow to overcome the inherent variability of feeder cell-based protocols and to streamline and standardize short term *in vitro* cell culture. Implementation of pre-screening steps appears absolutely mandatory, as most TCRs within the naïve T cell repertoire are expected to be of low functionality. Cost- and labor-intensive screening of dozens or hundreds of TCR candidates after isolation would prohibit fast identification of functional TCRs. Accepting a short propagation step before TCR sequencing could allow exclusion of false-positive sorted T cell clones by pMHC multimer re-staining, thereby enhancing the chance to isolate antigen-specific TCRs. Furthermore, T cell clones grown to sufficient size could be analyzed for their structural TCR avidity by k_{off}-rate assay, which could increase the chance to isolate functional TCRs as it was shown that structural avidity is predictive for functional avidity[53]. We set out to include the information about pMHC multimer reactivity and TCR structural avidity as ranking criteria to choose TCRs that are likely antigen-specific and functional when re-expressed in human PBMCs (Fig 4.1). T cells downregulate their T cell receptor and CD8 co-receptor upon

activation[100,101,139], which leads to reduced stainability of activated T cells with pMHC multimers. Therefore, we tested CD3/CD28 Expamers as stimulating agents, as this leads to a gentler expansion stimulus compared to CD3/CD28 mAbs since CD3/CD28 Expamers are made out of affinity-reduced antibody-fragments reversibly multimerized on a Strep-Tactin backbone (Juno Therapeutics GmbH). We chose a 384 well plate format out of biological and technical reasons; the small 25 µl volume can be easier conditioned by single T cells as larger volumes in 96 well format to support growth and 384 well plates allow sorting of sufficient single cells for high-throughput TCR repertoire analysis of pMHC multimer-reactive $CD8^+$ T cells.

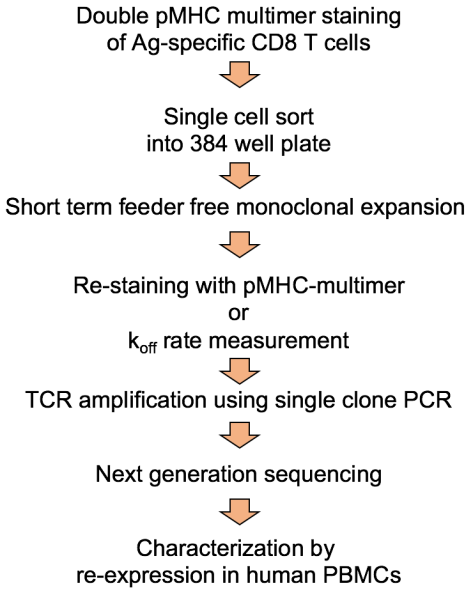

Figure 4. 1: Scheme of the TCR characterization and identification platform. pMHC multimer-reactive single **$CD8^+$**T cells are flow-sorted into a 384 well plate filled with medium containing CD3/CD28 Expamer and IL-2 as expansion stimulus. After 10-14 days, single cells grow clonally to sufficient cell number to validate pMHC multimer reactivity by pMHC multimer re-staining or measuring structural TCR avidity using k_{off}-rate assay. Both criteria are tested to rank TCR candidates that are identified via in-house NGS. In-depth characterization of candidate TCRs is performed by viral re-expression in human PBMCs.

pMHC multimer-based flow-sorting of rare T cell populations requires a well-balanced staining panel as certain cell types within PBMCs tend to bind pMHC multimer unspecifically, generating background noise and false-positive signal-artefacts[140,141]. Our sort-panel excluded B cells by dumping $CD19^+$ cells and identified naïve cytotoxic T cells using CD3, CD8, CCR7 and CD45RA mAbs. We routinely used double pMHC multimer staining to further reduce the probability of false-positive pMHC multimer binding (Fig 4.2 A). Double pMHC multimer-positive naïve $CD8^+$ T cells were single cell-sorted into a 384 well plate filled with

medium containing CD3/CD28 Expamer and IL-2 as expansion stimulus. After 10-14 d of expansion, single cells expanded clonally to sufficient numbers (Fig 4.2 B) to allow validation of pMHC multimer-reactivity by pMHC multimer re-staining. Irrelevant pMHC multimers and non-multimer-reactive T cell clones (sorted on pMHC multimer- naïve $CD8^+$ T cells during sort) served as negative controls (Fig 4.2 C). Furthermore, clones that expanded to sufficient size could be analyzed for structural TCR avidity by flow-based k_{off}-rate assay (Fig 4.2 D)[53].

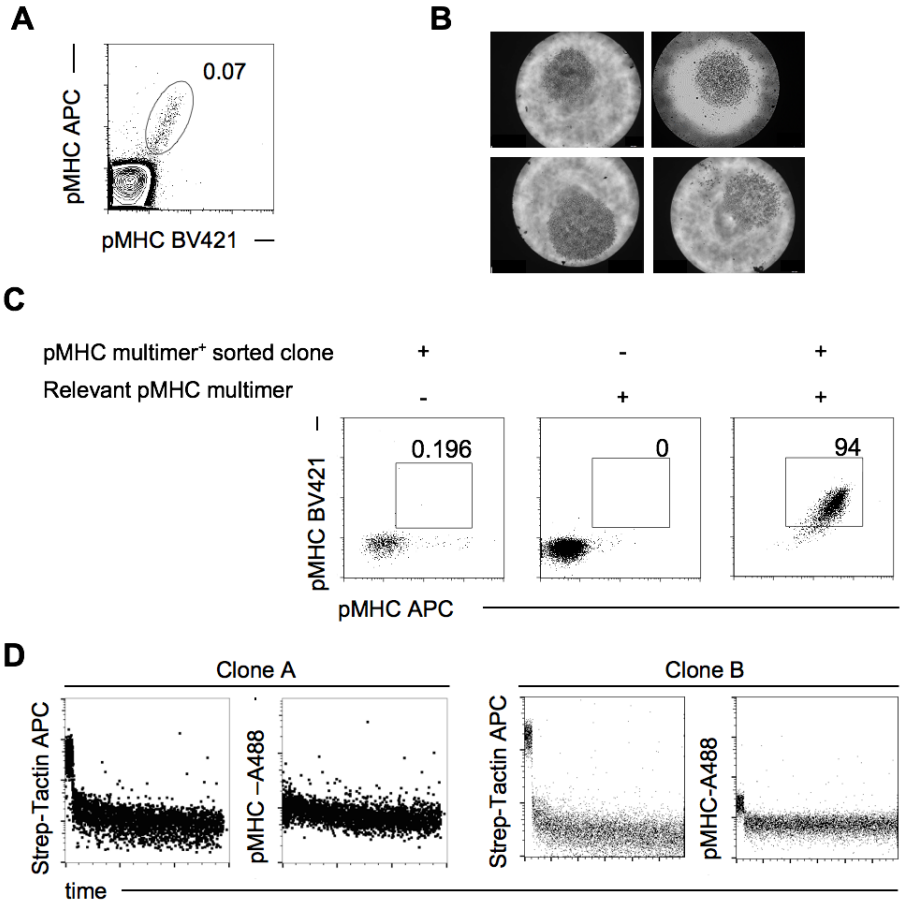

Figure 4. 2: Feeder-cell free short-term expansion of single-cell sorted pMHC multimer+ naïve $CD8^+$ T cells allows TCR characterization by pMHC multimer re-staining and k_{off}-rate measurement. A) Representative sort-gate of A2/MART1$_{(A27L)26-35}$ double pMHC-multimer+ naïve **$CD8^+$** T cells during single cell sort. **B**) Representative images of single cell derived clones after 10-12 d short term feeder free expansion. **C**) pMHC-multimer re-staining of feeder free single cell expanded clones. Irrelevant pMHC multimer A2/PR1$_{169-177}$; relevant pMHC multimer A2/MART1$_{(A27L)26-35}$; cells initially sorted on A2/MART1$_{(A27L)26-35}$ pMHC multimer reactivity. **D**) Flow-cytometer based k_{off}-rate measurement of feeder free single cell expanded clones sorted on A2/MART1$_{(A27L)26-35}$ pMHC multimer reactivity. Pre-gated on single, living, CD19-, CD3+, CD8+, CCR7+, CD45RA+ T cells in A). Pre-gated on single, living, CD8+ T cells in D) and E).

4.1.2 CD45 antibody-based multiplex color code for high-throughput T cell clone characterization

Feeder cell-free single cell expansion enabled us to validate pMHC multimer-reactivity by pMHC multimer re-staining and allowed estimation of structural TCR

avidity using flow based k_{off}-rate assay (Fig 4.2). However, processing and analyzing all clones as separate samples turned out to be extremely labor- and time-intensive. This issue was even more problematic when clones were analyzed by k_{off}-rate assay, as dissociation kinetics are measured over the time course of 15 min. Including washing steps in-between samples, analysis of 96 clones would take about 32 h for data acquisition on the flow-cytometer. However, analyzing several clones simultaneously could enable to reduce the time needed for data acquisition – pMHC multimer re-staining as well as k_{off}-rate measurement – drastically. Methods to multiplex T cell analysis based on intracellular dyes were published previously[118].

We decided to establish a color code based on fluorescently labeled CD45 mAbs to multiplex sample processing as well as sample acquisition on the flow-cytometer. CD45 is expressed on all T cells and actively recruited out of the TCR:pMHC binding site[142]. Staining for CD45 has therefore a minimal risk to interfere with pMHC multimer-based readouts. Incubating samples with combinations of 4 differentially labeled CD45 mAbs allows generation of 16 unique color codes. Pooled samples (e.g. single cell derived clones) are discriminated by gating on the respective fluorophore combination (Fig. 4.3 A). Further gating allows simultaneous analysis of pMHC multimer-reactivity when samples were stained with pMHC multimers (Fig. 4.3 B) or structural avidity measurement when samples were labeled with dye-conjugated Streptamers (Fig. 4.3 C).

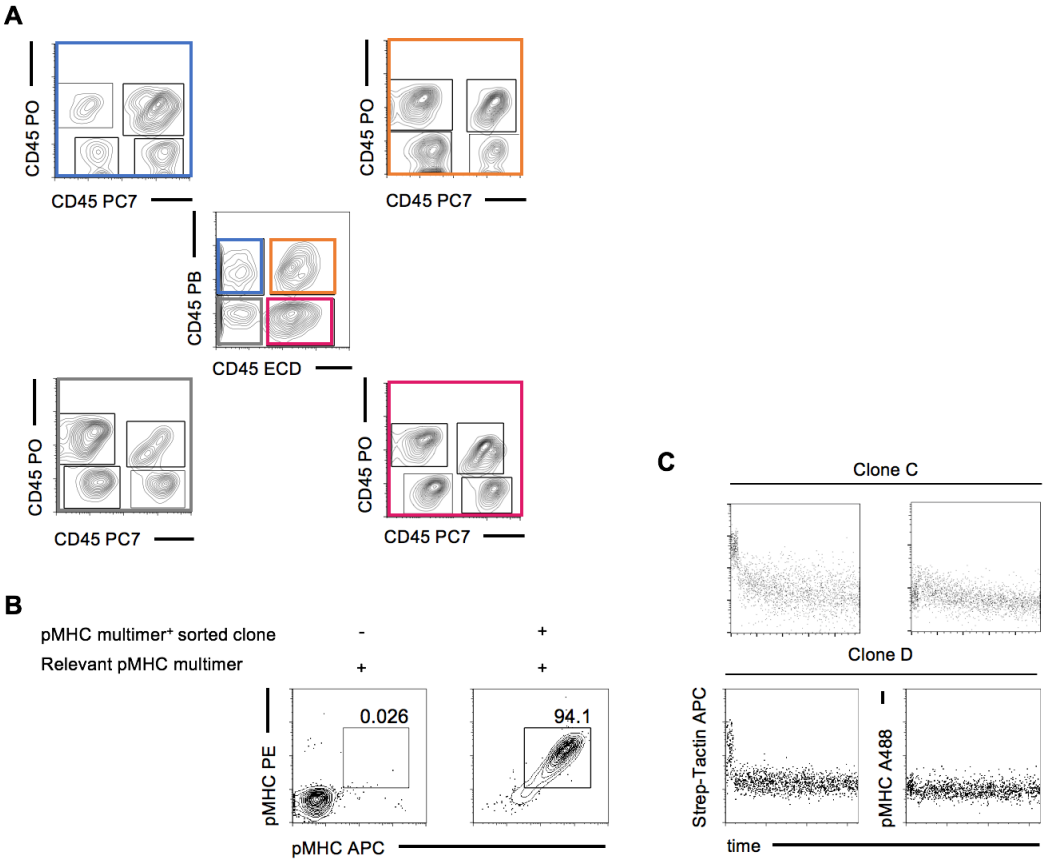

Figure 4. 3: CD45 mAb based color code allows multiplex analysis of up to 16 different samples in one acquisition. A) Exemplary gating on CD45 mAb color coded A2/YFV$_{212-222}$ pMHC multimer-reactive T cell clones. **B**) Sub-gating of CD45 mAb color coded samples allows analysis of pMHC multimer reactivity when samples are stained with pMHC multimers). **C**) Sub-gating of CD45 mAb color coded samples allows analysis of structural TCR avidity when samples were stained with dye-conjugated Streptamers (A2/YFV$_{212-222}$). Pre-gated on single living T cells in A), pre-gated on single living CD45+ CD8+ T cells in B), pre-gated on single living CD45+ CD8+ T cells in C)**.** Sort on A2/MART1$_{(A27L)26-35}$ pMHC multimer-reactive T cells or naïve **CD8$^+$** T cells. Relevant pMHC multimer: A2/MART1$_{(A27L)26-35}$ in B). k_{off}-rate measurement of A2/YFV NS4b$_{212-222}$ pMHC reactive T cell clones in C).

4.2 Feeder-cell free single cell expansion allows structural TCR avidity measurement of pMHC multimer-reactive T cell clones with subsequent TCR identification

We next set out to test the applicability of the TCR characterization and isolation platform to rank TCRs prior to PCR-based TCR identification. As a proof-of-concept epitope, we chose the HLA-A*02:01 restricted yellow fever (YFV) epitope A2/YFV-NS4b$_{212-22}$ and screened an HLA-A*02:01+ YFV vaccinated healthy donor for pMHC multimer-reactive CD8$^+$ T cells. YFV vaccination induces a readily detectable pMHC multimer-reactive CD8$^+$ T cell population in peripheral blood which consists mainly of phenotypically “naïve-like” T cells with proliferative capacity similar to naïve or stem cell-like T cells[143]. Additionally, A2/YFV-NS4b$_{(212-222)}$ pMHC multimer-reactive T cells are composed of medium to high

avidity T cell clones[143]. These two characteristics – naïve-like phenotype despite the decent precursor frequency and abundant medium to high-avidity T cell clones – made this population ideally suited to validate our TCR characterization and isolation workflow. Cells should be able to proliferate from single cells comparable to true naïve T cells and we should be able to detect a proportion of clones with a k_{off}-rate above detection limit of 30 sec[53]. Of note, we set the detection limit of the flow based k_{off}-rate assay to 30 sec, has a certain lag-phase to get completely released from cell surface. However, after 30 sec we can reliably assume true monomeric pMHC dissociation. Here, k_{off}-rates have to be seen in the light of measuring structural avidity from T cells taken directly from strongly activating expansion conditions. Therefore, measured values will not completely reflect the exact structural avidity as measured from unstimulated T cells, but should be used to group T cells clones into high and low structural avidity categories.

We performed single cell sorts of "naïve like" A2/YFV-NS4b$_{212-222}$ pMHC multimer-reactive CD8$^+$ T cells as described in Fig 4.2. After short-term feeder cell-free single cell expansion, multiplex k_{off}-rate measurement was performed as described in Fig 4.3 A+C). Fig 4.4 A) shows exemplary dissociation kinetics of 12 out of 57 analyzed single cell derived clones. All 12 clones showed Strep-Tactin APC signal during the first 30 sec of measurement before addition of D-biotin[53], indicating that all clones were pMHC multimer-reactive (Fig 4.4 A+C). The clones showed varying dissociation kinetics of pMHC-A488 over time. Immediate dissociation of all bound pMHC-A488 after D-biotin injection (e.g. clone #8, clone #46) as well as dye de-quenching[53] followed by slow decay of pMHC-A488 signal over time (e.g. clone #9, clone #49). Fitting one-phase exponential decay curves through the reduction of pMHC-A488 fluorescence intensity over time showed that the 12 clones cover a broad range of structural avidities, from avidities below the detection limit to medium avidities of about $t_{1/2}$= 150 sec (Fig 4.4 B). Plotting the initial pMHC multimer signal against the half-lives of the single cell derived clones showed no correlation, which indicated that pMHC multimer binding and structural TCR avidity were not directly related (Fig 4.4 D). These results confirmed previously published data about abundant medium to high-avidity T cell clones within the A2/YFV-NS4b$_{212-222}$ pMHC multimer-reactive CD8$^+$ T cell pool of YFV vaccinated healthy donors[143].

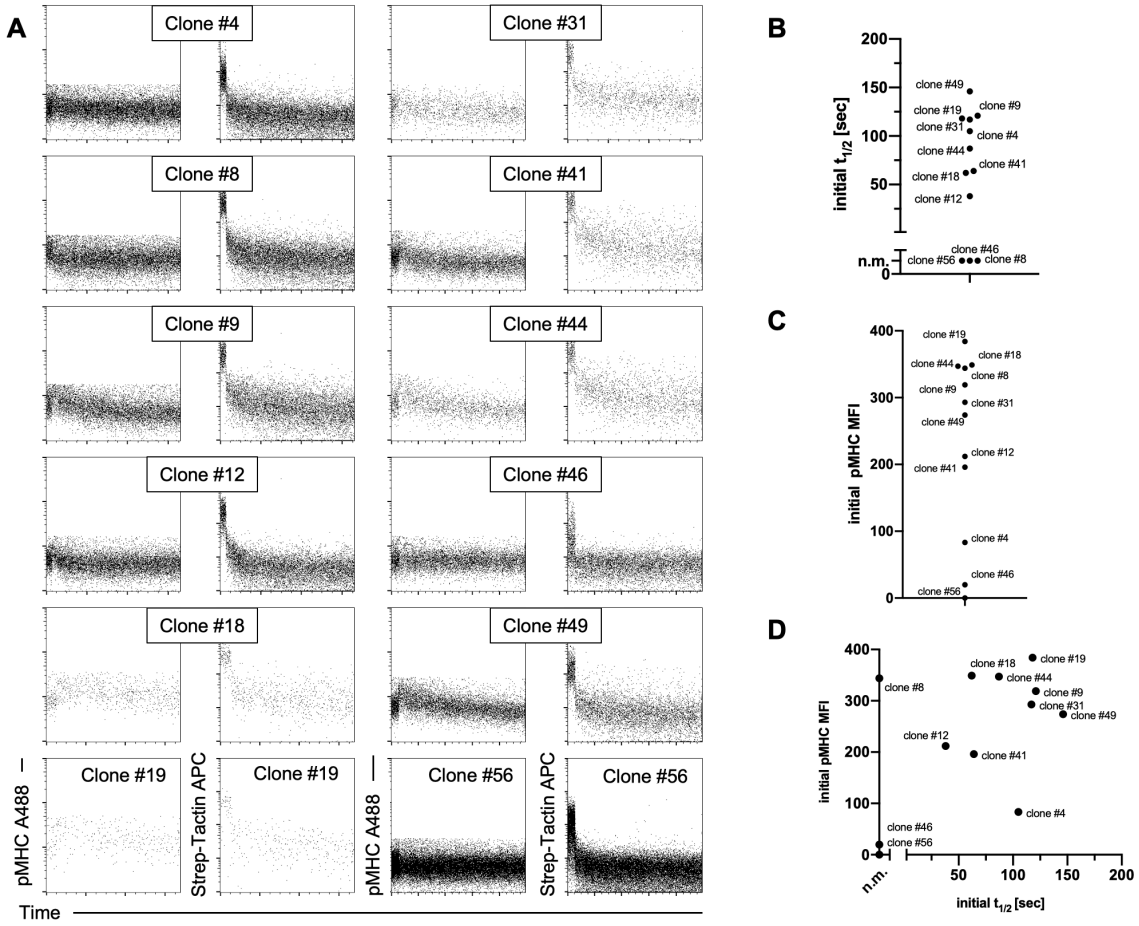

Figure 4. 4: Feeder-cell free short-term expansion of single-cell-sorted A2/YFV-NS4b$_{212-222}$ pMHC multimer-reactive CD8$^+$ T cell of a YFV vaccinated donor allow TCR characterization of clones by k_{off}-rate measurement. A) Dissociation kinetics of 12 out of 57 analyzed single cell derived clones**. B**) Quantification of dissociation kinetics of single cell derived clones sown in A) as half-lives. n.m.= not measurable ($t_{1/2}$ <30 sec). **C**) Quantification of initial Strep-Tactin APC signal of single cell derived clones shown in A) gating on first 30 sec before addition of D-biotin. **D**) Correlation of initial Strep-Tactin APC signal and half-lives of single cell derived clones shown in A). Pre-gated on single, living CD45+; CD8+ T cells in A).

4.2.1 Efficient TCR isolation of clonally expanded T cells

Accepting a short-term propagation step put us in the position to validate pMHC multimer reactivity and gain first insights about structural TCR avidity of the T cell clones (Fig 4.3+ Fig 4.4). A third advantage of clonal T cell expansion turned out to be the increased TCR mRNA amount in comparison to single cells when performing PCR based TCR isolation. In brief, performing single cell PCR is technically highly challenging and strongly dependent on mRNA quality of the cell material. Analyzing single cell derived clones (instead of single cells) diminishes the influence of naturally occurring fluctuation of mRNA content on single cell level leading to higher TCR identification efficacy (Thomas R. Müller, unpublished data). However, the TCR identification efficacy of the single clone PCR is per

definition limited by the recovery efficacy of the single cell expansion (i.e. percentage of single cell-sorted cells that start to expand to clones). We usually achieved 80 % recovery efficacy for naïve $CD8^+$ T cells (data not shown). We put 13 A2/YFV-NS4b$_{212-222}$ pMHC multimer-reactive T cell clones into our in-house NGS TCR isolation pipeline (established by Kilian Schober & Thomas R. Müller) and extracted 12 complete paired α:β TCR sequences (92 % TCR retrieval). 10/12 identified clones shared TRAV12-2 sequences, which was previously described to interact preferentially with the HLA-A*02:01 allotype[144,145].

Name	Variable	Joining	Diversity	CDR3	k_{off}-rate before TCR extraction [sec]	Initial APC MFI
Clone #4 TCR Y4	TRAV9-2*00	TRAJ36*00		CALNPPTGANNLFF	105	83.3
	TRBV11-2*00	TRBJ1-6*00	TRBD1*00	CASSPSGDSPLHF		
Clone #8 TCR Y8	TRAV38-1*00	TRAJ43*00		CAFRGGILDMRF	b.d.l	344
	TRBV29-1*00	TRBJ2-7*00	TRBD1*00	CSVQGLSYEQYF		
Clone #9 TCR Y9	TRAV12-2*00	TRAJ30*00		CAVIGDKIIF	121	319
	TRBV6-2*00	TRBJ2-7*00	TRBD1*00	CASSLGPVSYEQYF		
Clone #12 TCR Y12	TRAV12-2*00	TRAJ30*00		CAPGDDKIIF	38	212
	TRBV20-1*00	TRBJ2-3*00	TRBD1*00	CSATGGRGTDTQYF		
Clone #18 TCR Y18	TRAV12-2*00	TRAJ34*00		CAPEGDKLIF	62*	349
	TRBV9*00	TRBJ2-7*00	TRBD1*00	CASSPGTGAYEQYF		
Clone #19 TCR Y19	TRAV12-2*00	TRAJ34*00		CAVNDDKLIF	118*	384
	TRBV20-1*00	TRBJ2-3*00	TRBD1*00	CSARDQQRPADTQYF		
Clone #31 TCR Y31	TRAV12-2*00	TRAJ13*00		CAVVSGGYQKVTF	117	293
	TRBV7-2*00	TRBJ1-2*00	TRBD1*00	CASSPGASYGYTF		
Clone #41 TCR Y41	TRAV12-2*00	TRAJ34*00		CAVTNTDKLIF	64	196
	TRBV12-4*00	TRBJ1-2*00	TRBD1*00	CASSLGGGSYGYTF		
Clone #44 TCR Y44	TRAV12-1*00	TRAJ30*00		CVVGDDKIIF	87	347
	TRBV11-3*00	TRBJ2-7*00	TRBD1*00	CASSLQGAYEQYF		
Clone #46 TCR Y46	TRAV12-1*00	TRAJ31*00		CASNNARLMF	30	19.9
	TRBV20-1*00	TRBJ2-7*00	TRBD1*00	CSASQRGDGGEQYF		
Clone #49 TCR Y49	TRAV12-2*00	TRAJ30*00		CAGGDDKIIF	146	274
	TRBV29-1*00	TRBJ2-1*00	TRBD2*00	CSVATSGGSNEQFF		
Clone #56 TCR Y56	TRAV12-1*00	TRAJ41*00		CVVNLDGYALNF	30	75,5
	TRBV27*00	TRBJ2-7*00	TRBD2*00	CASSLSTAGGAYEQYF		

Figure 4. 5: TCR sequences of A2/YFV-NS4b$_{212-222}$ Streptamer-reactive T cell clones. T cell clones were analyzed for their structural TCR avidity (Fig 4.4) and subsequently put into in-house NGS TCR isolation pipeline (Kilian Schober & Thomas R. Müller). Complete paired TCR sequences could be retrieved for 92 % of the clones (12/13). Initial APC MFI was determined by gating on first 30 sec of k_{off}-rate measurement, before injection of D-biotin. * k_{off}-rate measurement was interrupted after 6 min.

4.2.2 Functional and structural characterization of A2/YFV-NS4b$_{212-222}$ pMHC multimer-reactive TCRs

4.2.2.1 Viral re-expression of A2/YFV-NS4b$_{212-222}$ pMHC multimer-reactive TCRs

To validate the pMHC multimer-reactivity of the extracted TCR sequences, we generated retro-viral TCR coding particles and re-expressed them in primary

human PBMCs. Successful TCR transduction was determined by mAb staining for the murine constant beta chain of the introduced TCR (mTrbc)[137]. pMHC multimer reactivity was determined by staining with A2/YFV-NS4b$_{212-222}$, specificity was assessed by staining with irrelevant pMHC multimer A2/MART1$_{(A27L)26-35}$ ((Fig 4.6 A), TCR Y46 representative for all shown TCRs, and B).

TCR transduction was routinely performed into primary human PBMCs isolated from fresh blood. Therefore, CD4$^+$ T cells alongside with CD8$^+$ T cells were transduced with CD8$^+$T cell-derived TCRs. TCR-transgenic CD4$^+$ T cells served to estimate CD8 dependence in pMHC multimer binding, as this characteristic can give a first hint about structural TCR avidity[146–148]. The overlay plots shown in Fig 4.6 B) indicate that 5/14 TCRs are CD8 independent (TCR V, 9, Y18, Y31, ,44, Y49,), while all other TCR-transgenic CD4$^+$ T cells are able to bind only weakly to pMHC multimer and were therefore considered to be CD8 dependent (Fig 4.6 B).

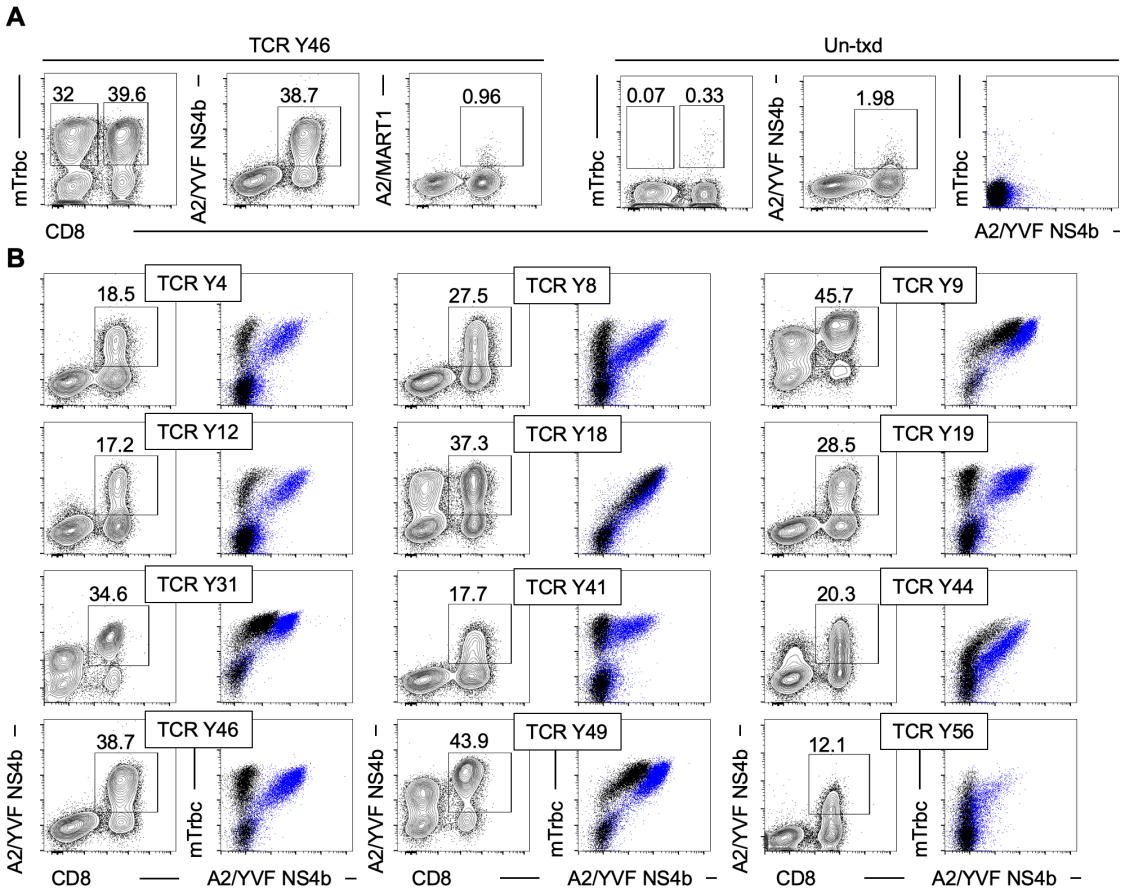

Figure 4. 6: Viral re-expression of A2/YFV-NS4b$_{212-222}$ pMHC multimer reative TCRs in primary human PBMCs. A) Exemplary flow cytometric analysis of pMHC multimer reactivity and specificity of TCR transduced PBMCs. Successful viral transduction was determined by mTrbc staining. pMHC-multimer reactivity and specificity was analyzed by staining with relevant (A2/YFV-NS4b$_{212-222}$) or irrelevant (A2/MART1$_{(A27L)26-35}$) pMHC multimer. Un-transduced PBMCs

(Un-txd) served as negative control. **B**) Validation of pMHC multimer reactivity and analysis of CD8 dependence in pMHC multimer binding. PBMCs transduced with indicated A2/YFV-NS4b$_{212-222}$-specific TCRs were stained with relevant pMHC multimer and mTrbc mAb. Pre-gated on single living lymphocytes in A) and B) for pMHC multimer staining, pre-gated on CD8+; mTrbc+ (blue) and CD8-; mTrbc+ (black) in B) for overlay plots.

4.2.2.2 Structural avidity measurement of A2/YFV-NS4b$_{212-222}$ pMHC multimer-reactive TCRs

Structural avidity measured by our k_{off}-rate assay allows to predict functional avidity in a simple and high-throughput compatible manner[52]. Therefore, after validating pMHC multimer reactivity and specificity, we measured the structural TCR avidity of the TCR transduced T cells (Fig 4.7 A). T cells transduced with the A2/YFV$_{212-222}$ pMHC multimer-reactive TCRs Y8, Y46 and Y56 showed a k_{off}-rate below the detection limit of the flow based k_{off}-rate assay (30 sec). Still those TCR-transduced T cells showed a distinctive Strep-Tactin APC signal before addition of D-biotin (Fig 4.7 A). T cells expressing TCR Y12, Y19, Y31, Y41 and Y44 showed medium half-lives around 100 sec, while TCR Y4, Y9, Y18 and Y49 showed long half-lives above 200 sec (Fig 4.7 B). Interestingly, TCRs that were extracted from T cell clones with a k_{off}-rate ≥ 60 sec could also be measured for structural avidity when transgenically re-expressed (Fig 4.7 C).

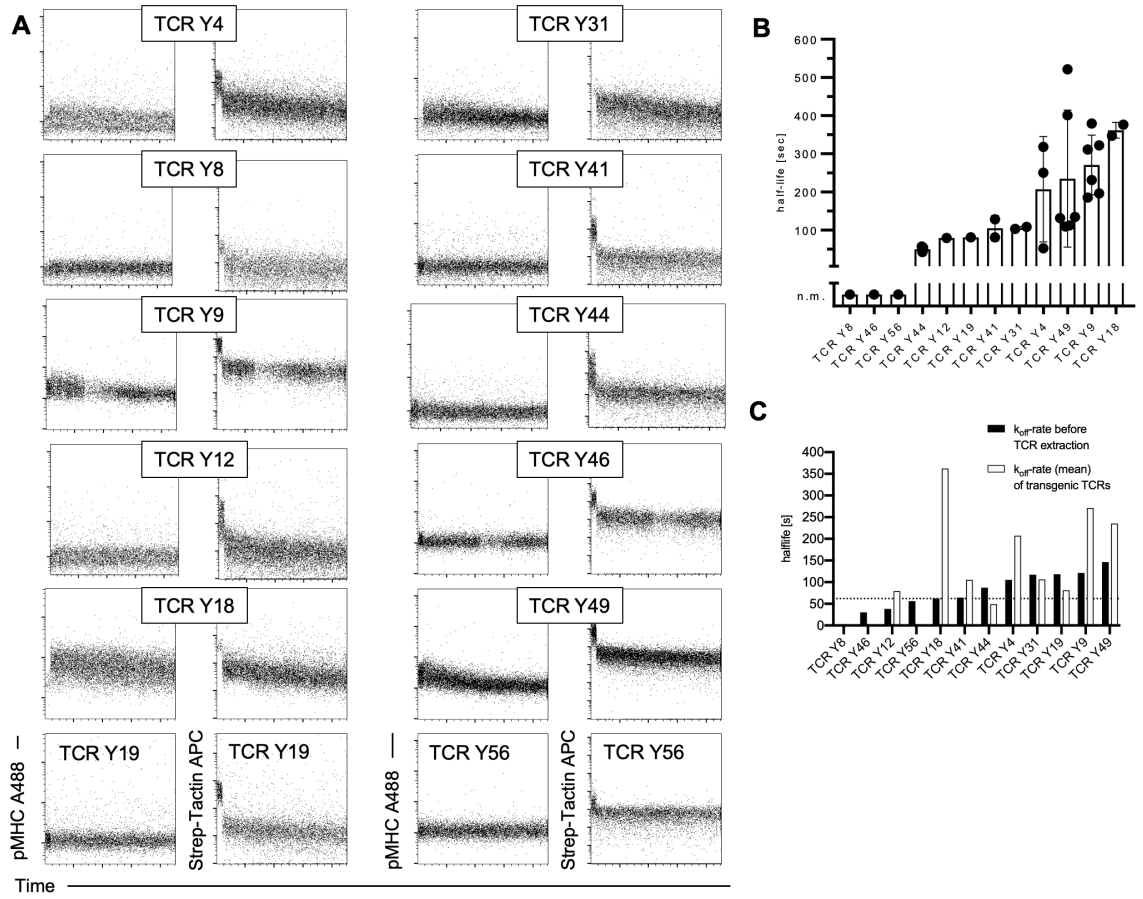

Figure 4. 7: Structural avidity measurement of T cells transduced with A2/YFV$_{212-222}$-specific TCRs. A) Flow-cytometry based k_{off}-rate assay of **CD8$^+$** T cells transduced with the indicated A2/MART1$_{(A27L)26-35}$-specific TCRs. **B**) Quantification of pMHC monomer dissociations shown in A). Representative experiment with technical replicates, one symbol represents one dissociation. Pre-gated on single, living mTrbc+ CD8+ T cells. n.m.: not measurable (<30 sec). **C**) Comparison of $t_{1/2}$ measured from T cell clones after feeder-cell free single-cell expansion and after retro-viral TCR re-expression in primary human PBMCs. T cell clones with $t_{1/2} \geq 60$ sec (dotted line) harbored a TCR that showed a measurable structural avidity also after transgenic re-expression in primary human PBMCs.

4.2.2.3 Functional avidity measurements A2/YFV-NS4b$_{212-222}$ pMHC multimer-reactive TCRs

pMHC multimer reactivity has been reported to not directly correlate with functional avidity[149], although until now a large-scale, systematic investigation of this assumption has not been performed. Consequently, we further validated specificity and sensitivity of the A2/YFV$_{212-222}$ pMHC multimer-reactive TCRs in ICCS as well as cytotoxicity assays. We measured IFNγ, Il-2 and TNFα secretion after A2/YFV$_{212-222}$ TCR-transgenic T cells were co-cultured with peptide-pulsed K562 target cells. K562 target cells pulsed with irrelevant peptide (pp65$_{495-503}$) served as negative controls. PMA/Iono-stimulated cells served as positive controls. All TCR-transgenic T cells showed peptide concentration-dependent IFNγ release and no cross-reactivity when co-cultured with K562 target cells

presenting an irrelevant peptide epitope (Fig 4.8 A). Interestingly, the 12 A2/YFV$_{212-222}$-specific TCRs displayed a broad range of peptide sensitivity. TCR Y44 reacts to the highest peptide amount of 10^{-4} M only with minor cytokine production while TCR Y8, Y19, Y46 and Y56 trigger cytokine production already between 10^{-6}-10^{-9} M. T cells transduced with TCR Y4, Y9, Y12, Y18, Y31, Y41 and Y49 react already at the lowest peptide amount of 10^{-12} M with cytokine secretion epitope (Fig 4.8 A). This broad spectrum of peptide sensitivity is summarized in the half-maximal cytokine production (EC_{50}) values in Fig 4.8 B) ranging from ~10^{-5} (Y44, Y46) to 10^{-9} (Y9, Y49). We additionally checked the cytotoxicity of the 12 A2/YFV$_{212-222}$-specific TCRs when co-cultured with peptide pulsed K562 target cells. Again, the TCRs mediated a broad range of cytotoxicity at the different E:T ratios (Fig 4.8 C).

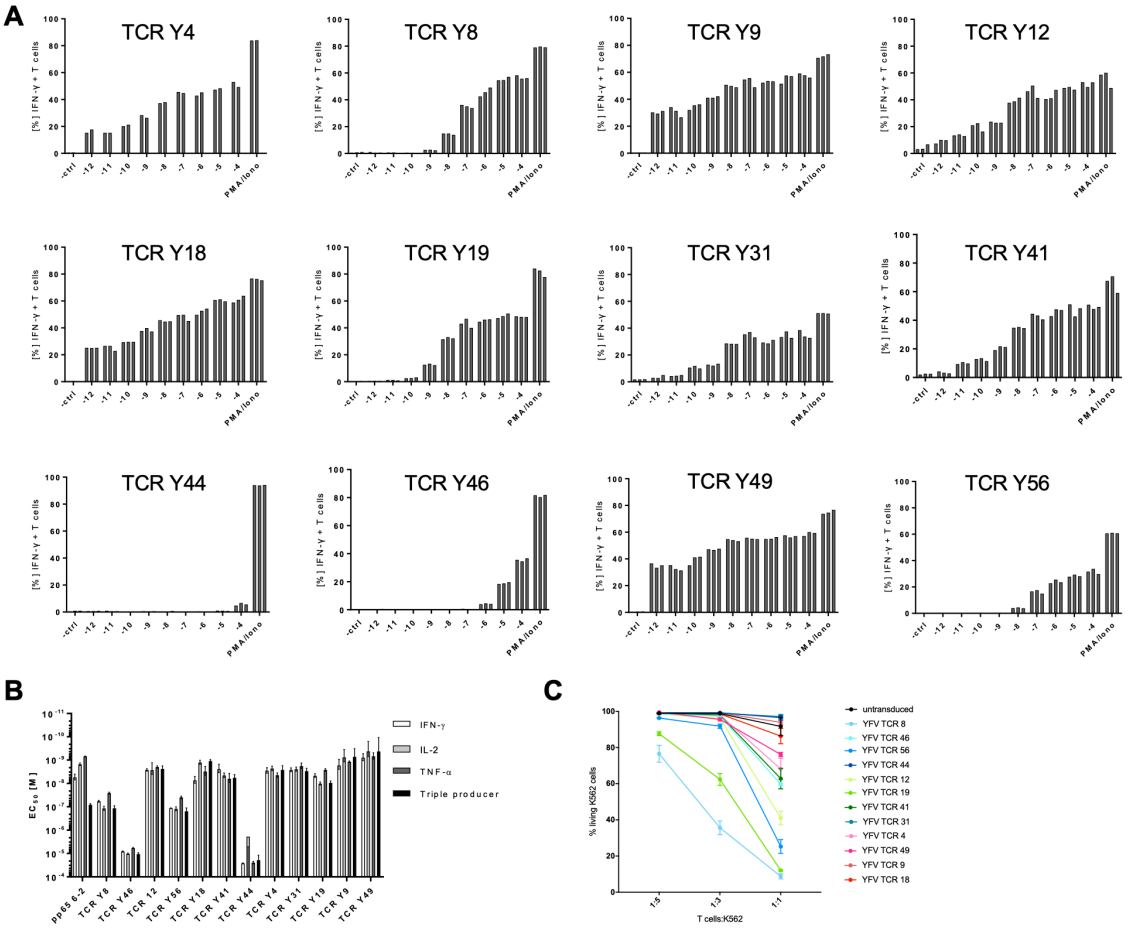

Figure 4. 8: Intracellular cytokine staining and killing capacity of T cells transduced with A2/YFV$_{212-222}$ pMHC multimer-reactive TCRs. A) Peptide concentration dependent IFNg production of T cells transduced with indicated A2/YFV$_{212-222}$ pMHC multimer-reactive TCRs. T cells were co-cultured with K562 target cells presenting increasing amounts of peptide (10^{-12}-10^{-4} M) or 10^{-4} M irrelevant peptide (pp65$_{495-503}$; ctrl). PMA/Iono-stimulated T cells served as positive controls. **B**) Half-maximal IFNg, TNFa and IL-2 production (EC_{50}) of T cells transduced with the A2/YFV$_{212-222}$ pMHC multimer-reactive TCRs. **C**) Killing capacity of T cells transduced with the indicated A2/YFV$_{212-222}$ pMHC multimer-reactive TCRs. T cells were co-cultured for 18h with

A*02:01+ K562 target cells pulsed with 10^{-6} M $YFV_{212-222}$ peptide in the effector: target ratio (E:T) 1:5, 1:3, 1:1. Untransduced T cells (Un-txd) served as negative controls.

4.2.2.4 Correlating structural and functional avidity of A2/$YFV_{212-222}$ pMHC multimer-reactive TCRs

To further investigate the relation between functional and structural avidity, we plotted the data gathered after feeder cell-free single cell expansion (before TCR isolation) against the data collected after the TCRs were virally transduced into primary human PBMCs. We did not detect a correlation between the pMHC multimer binding of naturally or transgenically expressed TCRs with their functional or structural avidity measured by flow-based k_{off}-rate assay or ICCS and cytotoxicity assay (Fig 4.9 A+B).

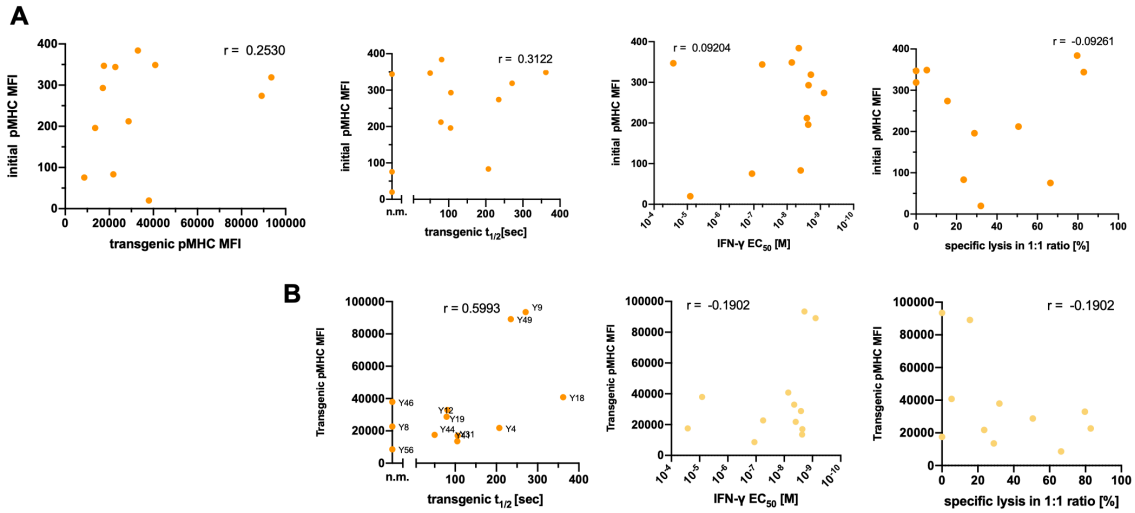

Figure 4. 9: Correlation of initial and transgenic pMHC multimer MFI with functional and structural avidity of A2/$YFV_{212-222}$ pMHC multimer-reactive TCRs. A) Correlation of pMHC multimer MFI after feeder-cell free single cell expansion (initial pMHC MFI) versus k_{off}-rate of transgenically re-expressed TCRs, their IFNg EC_{50} and cytotoxicity against K562 target cells. **B**) Correlation of pMHC multimer MFI after TCR gene-transfer into primary human PBMCs versus their k_{off}-rate, their IFNg EC_{50} and cytotoxicity against K562 target cells. Each dot represents the mean of technical replicates, except for pMHC multimer MFI.

We also did not detect a direct correlation between the structural avidity of naturally or transgenically expressed TCRs with pMHC multimer binding or their functional avidity. However, a k_{off}-rate of ~60 sec after feeder cell-free single cell expansion or of ~80 sec after transgenic re-expression seem to coincide with a

certain degree of functional avidity measured by IFNγ EC_{50} (Fig 4.10 A+B, dotted lines).

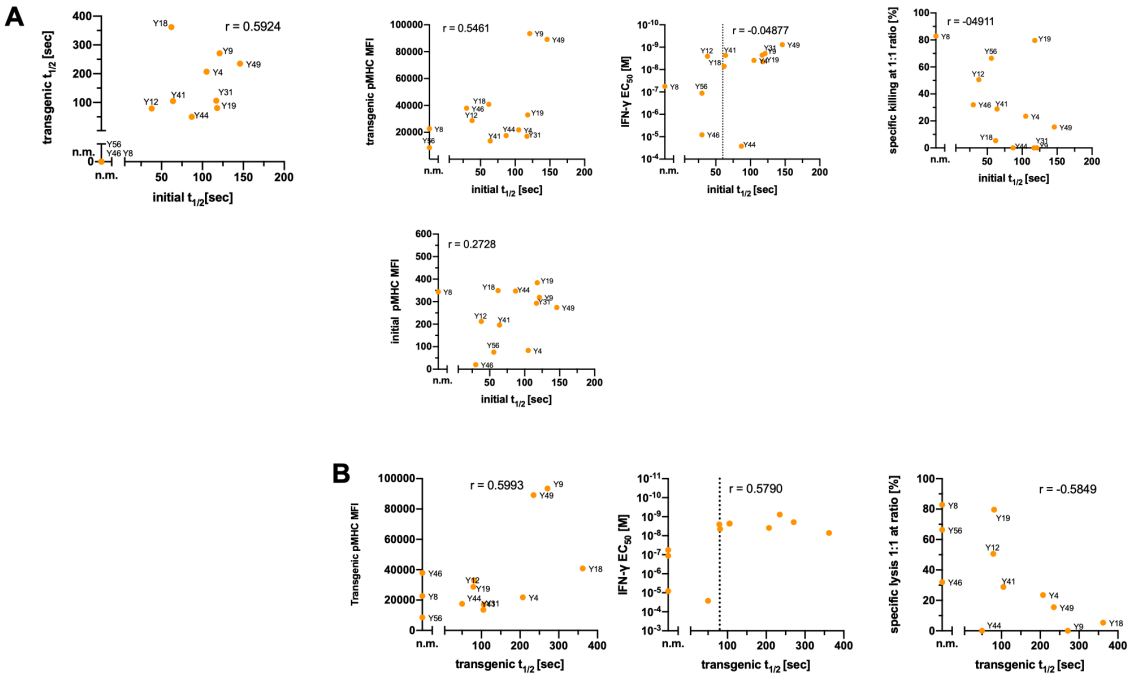

Figure 4. 10: Correlation of structural TCR avidity after feeder-cell free single cell expansion and after transgenic re-expression versus pMHC multimer MFI and functional avidity of A2/YFV$_{212-222}$ pMHC multimer-reactive TCRs. A) Correlation of k_{off}-rate after feeder-cell free single cell expansion (initial k_{off}-rate) versus k_{off}-rate of transgenically re-expressed TCRs, their pMHC multimer MFI, thei IFNg EC_{50} and cytotoxicity against K562 target cells. **B**) Correlation of k_{off}-rate after TCR gene-transfer into primary human PBMCs versus their pMHC multimer MFI, their IFNg EC_{50}, maximal cytokine secretion and cytotoxicity against K562 target cells. Each dot represents the mean of technical replicates, except for pMHC multimer MFI. Dotted line at 60 sec in A) and 80 sec in B).

4.2.3 Isolation of A2/MART1$_{(A27L)26-35}$ pMHC multimer-reactive TCRs from the naïve T cell repertoire

After validating the TCR characterization and isolation platform with the model epitope A2/YFV-NS4b$_{212-222}$ in a YFV vaccination setting (Fig 4.4-Fig 4.8), we set out to further test our platform, now focusing on the naïve T cell repertoire of antigen-inexperienced healthy donors. We chose A2/MART1$_{(A27L)26-35}$ as a proof-of-concept epitope taking advantage of the described unusually high precursor frequency within the naïve CD8$^+$ T cell compartment[15].

After feeder free expansion of single cell-sorted pMHC multimer-reactive naïve CD8$^+$ T cells, clones were analyzed for structural TCR avidity using multiplex k_{off}-rate assay as describe above (Fig 4.2 and Fig 4.3). Fig 4.11 shows representative 6 out of 176 analyzed clones from two independent experiments. pMHC multimer reactivity of the analyzed clones were 85,9 % and 77,4 %. Interestingly, only two clones showed structural avidity above detection limit (Fig. 411 B). Initial Streptamer APC MFI varied about five-fold in signal intensity. Of note, T cell clones having a measurable k_{off}-rate showed also highest Streptamer APC signal (Fig 4.11 C). TCRs of all six pMHC multimer-reactive clones could be extracted by TCR sequencing (Fig 4.11 C).

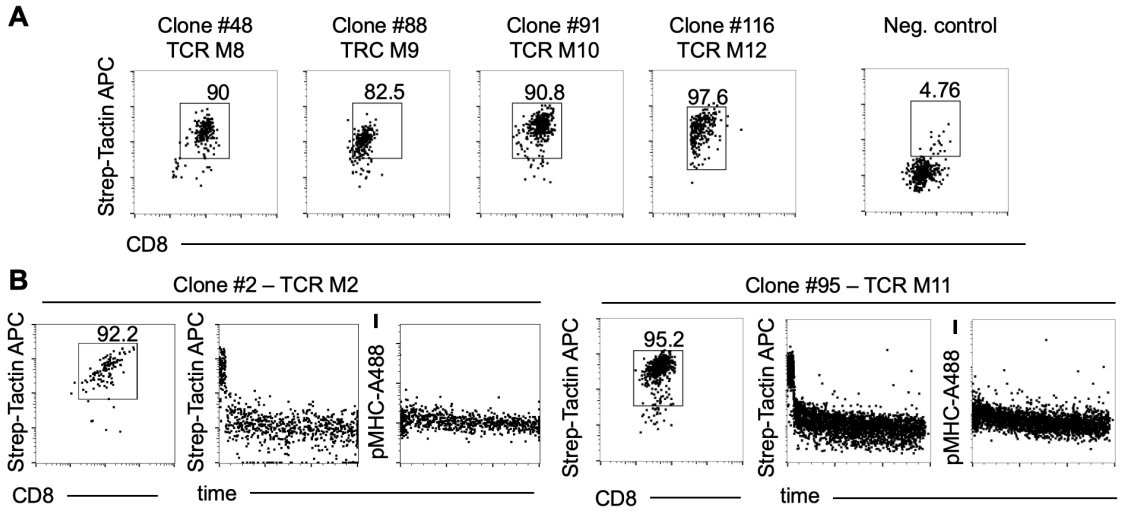

C

Name	Variable	Joining	Diversity	CDR3	k_{off}-rate before TCR extraction [sec]	Initial APC MFI
Clone #2 TCR M2	TRAV12-2*00	TRAJ45*00		CAPDSGGGADGLTF	277	503*
	TRBV19*00	TRBJ2-1*00	TRBD1*00	CASSIYGTALLSVEQFF		
Clone #48 TCR M8	TRAV12-2*00	TRAJ45*00		CAAYSGGGADGLTF	n.m.	186
	TRBV6-5*00	TRBJ2-2*00	TRBD1*00	CASSRVSGELFF		
Clone #88 TCR M9	TRAV12-2*00	TRAJ45*00		CAVDDSGGGADGLTF	n.m.	108
	TRBV6-5*00	TRBJ1-3*00	TRBD1*00	CASQNGQGVNTIYF		
Clone #91 TCR M10	TRAV12-2*00	TRAJ23*00		CAVGGGKLIF	n.m.	257
	TRBV4-3*00	TRBJ2-7*00	TRBD1*00	CASSQARLSGEQYF		
Clone #95 TCR M11	TRAV12-2*00	TRAJ22*00		CAVEGLTF	84	370
	TRBV6-1*00	TRBJ2-1*00	TRBD1*00	CASFPVGTTYNEQFF		
Clone #116 TCR M12	TRAV12-2*00	TRAJ30*00		CAVDDKIIF	n.m.	198
	TRBV27*00	TRBJ2-7*00	TRBD1*00	CASKVGQGLVGEQYF		

Figure 4. 11: Isolation of A2/MART1$_{(A27L)26-35}$ pMHC multimer-reactive TCRs from the naïve T cell repertoire. A) Streptamer reactivity of feeder-cell free single cell expanded clones. **B**) k_{off}-rate measurement of feeder-cell free single cell expanded T cell clone. StrepTactin APC signal in A) and B) was determined by gating on first 30 sec of k_{off}-rate measurement, before injection of D-biotin. Pre-gated on single, living CD45+ T cells in A) and B). **C**) TCR sequences of A2/MART1$_{(A27L)26-35}$-Streptamer-reactive T cell clones shown in A) and B) isolated via in-house NGS TCR isolation pipeline. Complete paired TCR sequences could be retrieved for all clones (6/6; 100% TCR retrieval, Thomas R. Müller). *Data from TCR M2 were acquired in an independent experiment.

4.2.3.1 Functional and structural characterization of A2/MART1$_{(A27L)26-35}$ pMHC multimer-reactive TCRs

4.2.3.2 Viral re-expression of A2/MART1$_{(A27L)26-35}$ pMHC multimer-reactive TCRs

Again, we validated the pMHC multimer reactivity and specificity of the identified TCR sequences by retro-viral re-expression in primary human PBMCs. All TCRs could be successfully transduced, judged by mTrbc staining (Fig 4.12 A, TCR M11 representative for all shown TCRs). All TCRs – except for TCR M12 – showed a clear pMHC multimer reactivity when stained with A2/MART1$_{(A27L)26-35}$, and no cross-reactivity when stained with irrelevant pMHC multimer control (A2/Her2/neu$_{369-377}$). The overlay plots indicated that a considerable proportion of

$CD4^+$ T cells transduced with TCR M11 could bind pMHC multimer. TCR M8 was mostly CD8 dependent, while TCR M2; M9 and M10 bound weakly pMHC multimer in an CD8 independent manner (Fig 4.12 B). No conclusion can be drawn for TCR M12. Here TRC-transgenic $CD8^+$ T cells show pMHC multimer reactivity above background. However, the overall pMHC multimer signal intensity was too low in 2 independent transductions (Fig 4.12 B and data now shown).

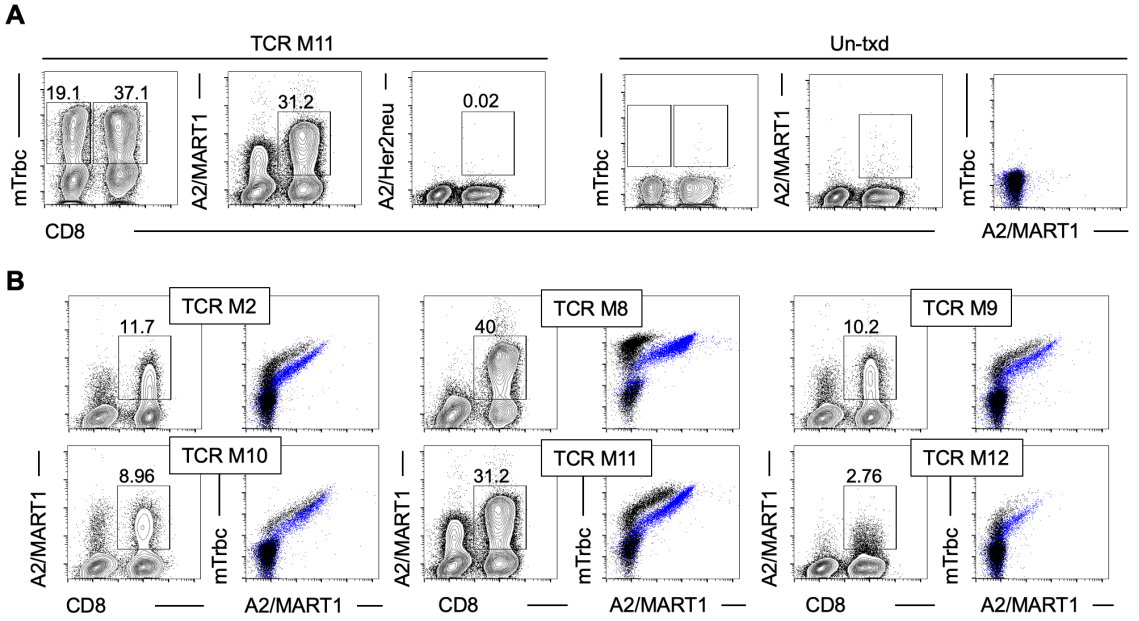

Figure 4. 12: Viral re-expression of A2/MART1$_{(A27L)26-35}$ pMHC multimer-reactive TCRs in primary human PBMCs. A) Exemplary flow cytometric analysis of pMHC multimer reactivity and specificity of TCR transduced PBMCs. Successful viral transduction was determined by mTrbc staining. pMHC-multimer reactivity and specificity was analyzed by staining with relevant (A2/MART1$_{(A27L)26-35}$) or irrelevant (A2/Her2/neu$_{369-377}$) pMHC multimer. Un-transduced PBMCs (Un-txd) served as negative control. **B**) Validation of pMHC multimer reactivity and analysis of CD8 dependence in pMHC multimer binding. PBMCs transduced with indicated A2/MART1$_{(A27L)26-35}$–specific TCRs were stained with relevant pMHC multimer and mTrbc mAb. Pre-gated on single living lymphocytes in A) and B) for pMHC multimer staining, pre-gated on CD8+; mTrbc+ (blue) and CD8-; mTrbc+ (black) in B) for overlay plots.

4.2.3.2 Structural avidity measurement of A2/MART1$_{(A27L)26-35}$ pMHC multimer-reactive TCRs

Subsequently, we set out to analyze the structural avidity of the A2/MART1$_{(A27L)26-35}$-specific TCRs (Fig 4.13 A). k_{off}-rate measurements revealed that TCR M8 has a k_{off}-rate below detection limit (30 sec). TCR M9 shows only weak pMHC-A488 binding (Fig 4.13 A) and was therefore hard to analyze ($t_{1/2}$= 58 sec). TCR M10, M11 and M12 had comparable k_{off}-rates varying around $t_{1/2}$= 120 sec, while TCR M2 showed the slowest pMHC-A488 kinetic with an $t_{1/2}$ of 230 sec (Fig 4.13 B). k_{off}-rate values measured prior to TCR isolation (after feeder-cell free single cell expansion) were in the range to the values measured for the transgenically re-

expressed TCRs M2 (clon #2= 277 sec; TCR M2= 230 sec) and M11 (clone #11= 84 sec; TCR M11= 106 sec) (Fig 4.11 C+ 4.13 B).

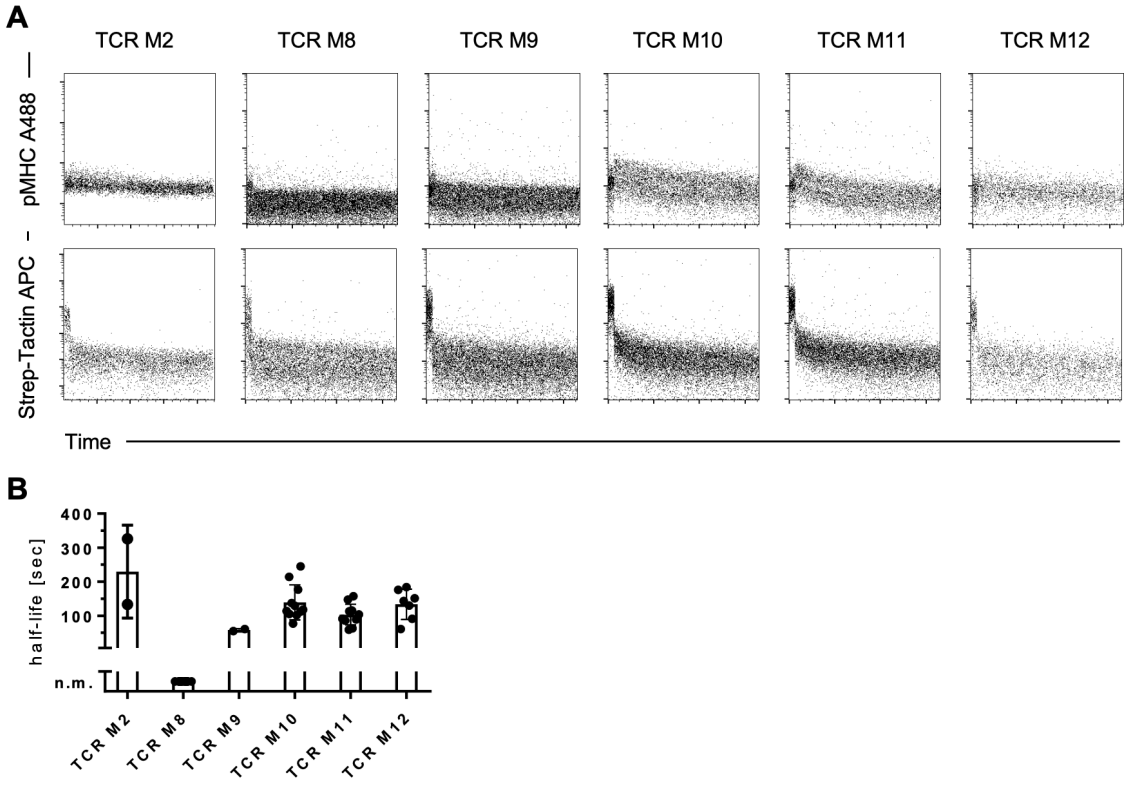

Figure 4. 13: Structural avidity measurement of T cells transduced with A2/MART1$_{(A27L)26-35}$-specific TCRs. A) Flow-cytometry based k_{off}-rate assay of **CD8$^+$** T cells transduced with the indicated A2/MART1$_{(A27L)26-35}$ pMHC multimer-reactive TCRs. **B**) Quantification of pMHC monomer dissociations shown in A). Representative experiment with technical triplicates, one symbol represents one dissociation. Pre-gated on single, living mTrbc+ CD8+ T cells. n.m.: not measurable (<30 sec). **C**) Comparison of $t_{1/2}$ measured from T cell clones after feeder-cell free single cell expansion and after retro-viral TCR re-expression in primary human PBMCs.

4.2.3.3 Functional avidity of A2/MART1$_{(A27L)26-35}$ pMHC multimer-reactive TCRs

We performed ICCS as well as a killing assay of T cells transduced with A2/MART1$_{(A27L)26-35}$ pMHC multimer-reactive TCRs by co-culture with peptide pulsed K562 target cells. Except for TCR M12, all TCRs mediated IFNγ secretion in a peptide concentration dependent manner (Fig 4.14 A). Of note, all TCR-transduced T cells showed background activation when co-cultured with 10^{-4} M irrelevant peptide pulsed K562 target cells (Fig 4.14 A). Quantification of the cytokine secretion reflected a broad spectrum of peptide sensitivity ranging from EC_{50} values of 10^{-5} M (TCR M8) to 10^{-9} M (TCR M2) (Fig 4.14 B). Measuring the killing capacity of the TCR transduced T cells after co-cultured with peptide pulsed K562 target cells indicated that all TCRs mediate cytotoxicity, again with the exception of TCR M8 (Fig 4.14 C).

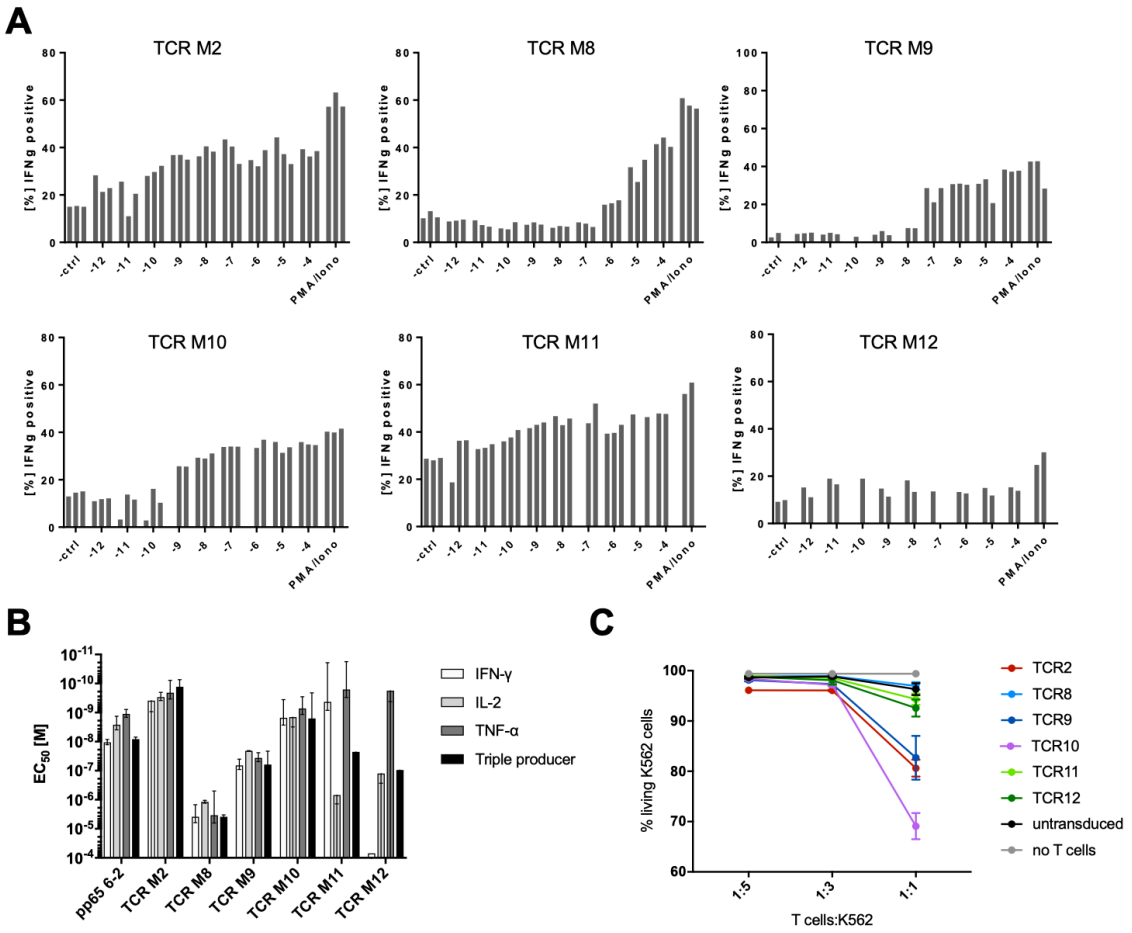

Figure 4. 14: Intracellular cytokine staining and killing capacity of T cells transduced with A2/MART1$_{(A27L)26-35}$ pMHC multimer-reactive TCRs. A) Peptide concentration dependent IFNg production of T cells transduced with indicated A2/MART1$_{(A27L)26-35}$ pMHC multimer-reactive TCRs. T cells were co-cultured with K562 target cells presenting increasing amounts of relevant peptide (10^{-12}- 10^{-4} M) or 10^{-4} M irrelevant peptide (pp65$_{495-503}$). **B**) Half-maximal IFNg, TNFa and IL-2 production (EC_{50}) of T cells transduced with the A2/MART1$_{(A27L)26-35}$ pMHC multimer-reactive TCRs. **C**) Killing capacity of T cells transduced with the indicated A2/MART1$_{(A27L)26-35}$ pMHC multimer-reactive TCRs. T cells were co-cultured for 18h with A*02:01+ K562 target cells pulsed with 10^{-6} M MART1$_{(A27L)26-35}$ peptide in the effector: target ratio (E:T) 1:5, 1:3, 1:1. Untransduced T cells (Un-txd) served as negative control.

4.2.3.4 Correlating structural and functional avidity of A2/MART1$_{(A27L)26-35}$ pMHC multimer-reactive TCRs

Again, we analyzed whether the data that we gathered after feeder-cell free single cell expansion (before TCR isolation) and the information collected after the TCRs were virally transduced into primary human PBMCs could help to further understand the relation of structural and functional avidity. However, we did not detect a correlation between the pMHC multimer binding of naturally or transgenically expressed TCRs with their functional or structural avidity measured by flow based k_{off}-rate assay or ICCS and cytotoxicity assay (Fig 4.15 A+B). Still, this might be explained due to the limited data points of 6 TCRs.

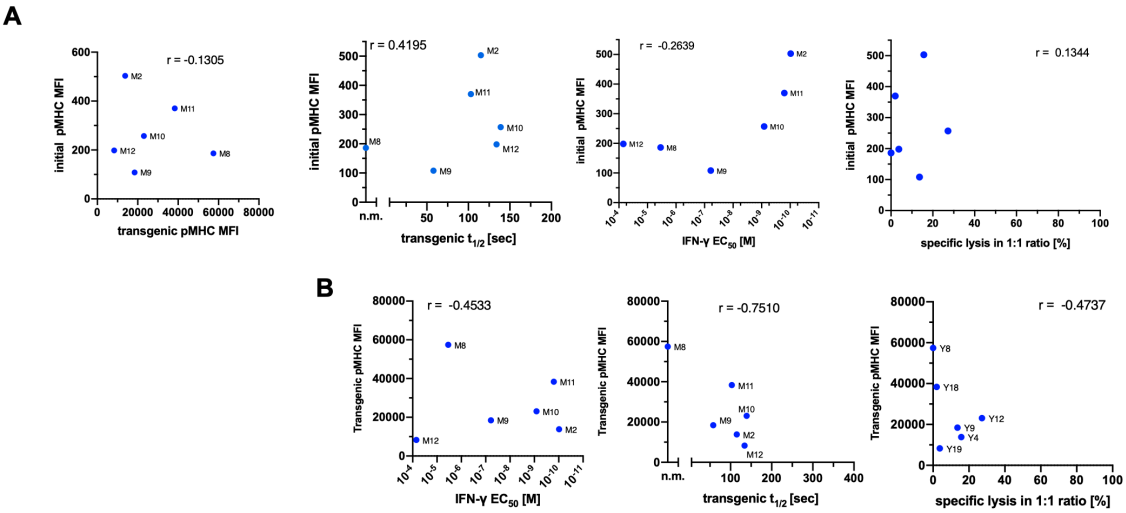

Figure 4. 15: Correlation of initial and transgenic pMHC multimer MFI with functional and structural avidity of A2/MART1$_{(A27L)26-35}$ pMHC multimer-reactive TCRs. A) Correlation of pMHC multimer MFI after feeder-cell free single cell expansion (initial pMHC MFI) versus k_{off}-rate of transgenically re-expressed TCRs, their IFNg EC_{50} and cytotoxicity against K562 target cells. **B**) Correlation of pMHC multimer MFI after TCR gene-transfer into primary human PBMCs versus their k_{off}-rate, their IFNg EC_{50} and cytotoxicity against K562 target cells. Each dot represents the mean of technical replicates, except for pMHC multimer MFI.

Subsequently, we checked, whether the data derived from the MART1 TCRs hint towards a direct correlation between structural avidity of naturally or transgenically expressed TCRs with pMHC multimer binding or their functional avidity (Fig 4.16). As observed for the A2/YFV$_{212-222}$ pMHC multimer-reactive TCRs, again a measurable k_{off}-rate after feeder-cell free single cell expansion coincided with functionality upon TCR transfer (Fig 4.16 A). This relation hold also true for k_{off}-rates measured for TCR transduced T cells (Fig 4.16 B). $t_{1/2}$ of ~60 sec (prior and post TCR isolation and transduction) seem to set a cut-off value for functional A2/MART1$_{(A27L)26-35}$ pMHC multimer-reactive TCRs in the shown panel (Fig 4.16 A+B).

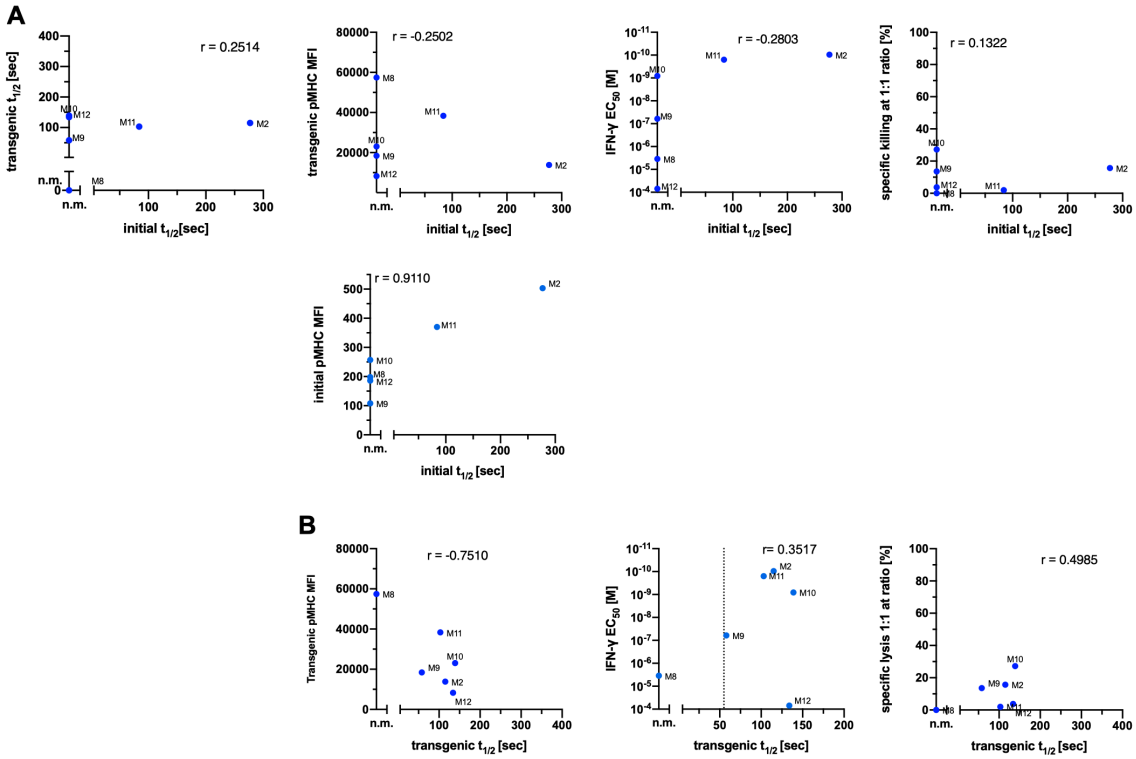

Figure 4. 16: Correlation of structural TCR avidity after feeder-cell free single cell expansion and after transgenic re-expression versus pMHC multimer MFI and functional avidity of A2/MART1$_{(A27L)26-35}$ pMHC multimer-reactive TCRs. A) Correlation of k_{off}-rate after feeder-cell free single cell expansion (initial k_{off}-rate) versus k_{off}-rate of transgenically re-expressed TCRs, their pMHC multimer MFI, thei IFNg EC_{50} and cytotoxicity against K562 target cells. **B**) Correlation of k_{off}-rate after TCR gene-transfer into primary human PBMCs versus their pMHC multimer MFI, their IFNg EC_{50}, maximal cytokine secretion and cytotoxicity against K562 target cells. Each dot represents the mean of technical replicates, except for pMHC multimer MFI. Dotted line at 60 sec in A) and 80 sec in B).

4.2.4 Isolation of A2/Her2neu$_{369-377}$ pMHC multimer-reactive TCRs from the naïve T cell repertoire

We next set out to use our TCR characterization and isolation platform to probe the naïve T cell repertoire for antigen-specific T cells of lower precursor frequency than A2/MART1$_{(A27L)26-35}$. Of note, we used the heteroclitic epitope of MART1, which is maybe rather seen as non-self-epitope by the immune system as is contains an aa exchange (A27L)[150,151]. However, it allowed easy access to antigen-specific CD8$^+$ T cells out of the naïve repertoire. Therefore, we next focused on A2/Her2neu$_{369-377}$ as an exemplary epitope, with a precursor frequency of approx. 0.6x10^{-6} ([152] and data not shown). pMHC multimer-guided single cell-sort of naïve CD8$^+$ T cells followed by feeder cell-free single cell expansion allowed successful validation of pMHC multimer reactivity by Streptamer re-staining (Fig 4.17 A). Noteworthily, clone #9 showed in comparison to all other clones a low initial Streptamer APC signal (Fig 4.17 A+B). We observed an up to 8-fold inter-clonal variation of the initial Streptamer APC signal (Fig 4.17 A+B). None of the analyzed clones showed a k_{off}-rate above detection limit (Fig 4.17 B). Fully paired TCRs could be extracted from all seven pMHC multimer-reactive T cell clones passed into the NGS TCR isolation platform (Fig 4.17 B) (Thomas R. Müller).

A

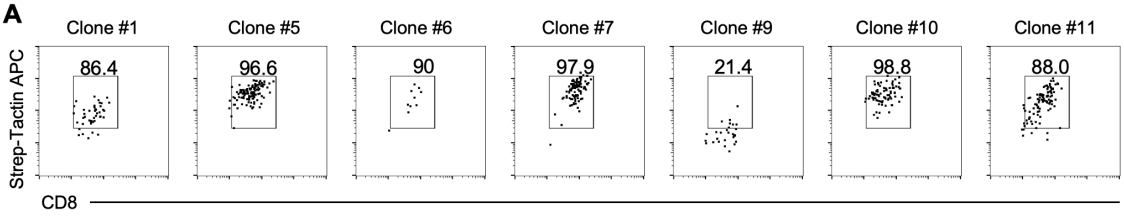

B

Name	Variable	Joining	Diversity	CDR3	k_{off}-rate before TCR extraction [sec]	Initial APC MFI
Clone #1 TCR H1	TRAV12-2*00	TRAJ16*00		CAAWFSDGQKLLF	b.d.l	86.5
	TRBV20-1*00	TRBJ1-2*00	TRBD1*00	CSAADRGYGYGYTF		
Clone #5 TCR H5	TRAV12-2*00	TRAJ20*00		CAVNPNDYKLSF	b.d.l	358
	TRBV20-1*00	TRBJ2-3*00	TRBD2*00	CSAPGTSGGGSTDTQYF		
Clone #6 TCR H6	TRAV12-2*00	TRAJ20*00		CAVNANDYKLSF	b.d.l	240
	TRBV29-1*00	TRBJ2-1*00	TRBD2*00	CSGILAVVWGNEQFF		
Clone #7 TCR H7	TRAV8-2*00	TRAJ40*00		CVVSEPDEGTYKYIF	b.d.l	419
	TRBV10-2*00	TRBJ1-1*00	TRBD1*00	CAISPMQGTNTEAFF		
Clone #9 TCR H9	TRAV19*00	TRAJ6*00		CALYSSGGSYIPTF	b.d.l	50.6
	TRBV3-1*00	TRBJ2-6*00	TRBD2*00	CASSPLGETGANVLTF		
Clone #10 TCR H19	TRAV12-2*00	TRAJ20*00		CAVNINDYKLSF	b.d.l	311
	TRBV12-3*00	TRBJ2-2*00	TRBD2*00	CASEGQGAVNTGELFF		
Clone #11 TCR H11	TRAV12-3*00	TRAJ34*00		CAMSEGTADKLIF	b.d.l	215
	TRBV7-9*01	TRBJ1-1*01	TRBD2*01	CASSLVRGGTTEAFF		

Figure 4. 17: Isolation of A2/Her2neu$_{369-377}$ -specific TCRs from the naïve T cell repertoire. A) Streptamer reactivity of feeder free single cell expanded clones. StrepTactin APC signal was

determined by gating on first 30 sec of k_{off}-rate measurement, before injection of D-biotin. Pre-gated on single, living CD45+ T cells. **B**) TCR sequences of A2/Her2neu$_{369-377}$-Streptamer-reactive T cell clones shown in A) isolated via in-house NGS TCR isolation pipeline. Completely paired TCR sequences could be retrieved for all clones (7/7; 100% TCR retrieval, Thomas R. Müller).

4.2.4.1 Functional and structural characterization of A2/Her2neu$_{369-377}$ pMHC multimer-reactive TCRs

4.2.4.2 Viral re-expression of A2/Her2neu$_{369-377}$ pMHC multimer-reactive TCRs

For in-depth characterization of the extracted putative A2/Her2neu$_{369-377}$ pMHC multimer-reactive TCRs, we again generated viral particles and re-expressed the TCRs in primary human PBMCs. All seven TCRs could be successfully re-expressed as judged by staining with mTrbc mAb (Fig 4.18 A; TCR H5 representative for all shown TCRs). However, staining the TCR-transduced PBMCs with A2/Her2neu$_{369-377}$ pMHC multimer revealed that only TCR H5 is clearly pMHC multimer-reactive (in a CD8-dependent manner). PBMCs transduced with TCR H6, H7, H10 and H11 bind pMHC multimer above background, although the signal intensity was very low. TCR H1 and H9 showed no pMHC multimer reactivity at all (Fig 4.18 B).

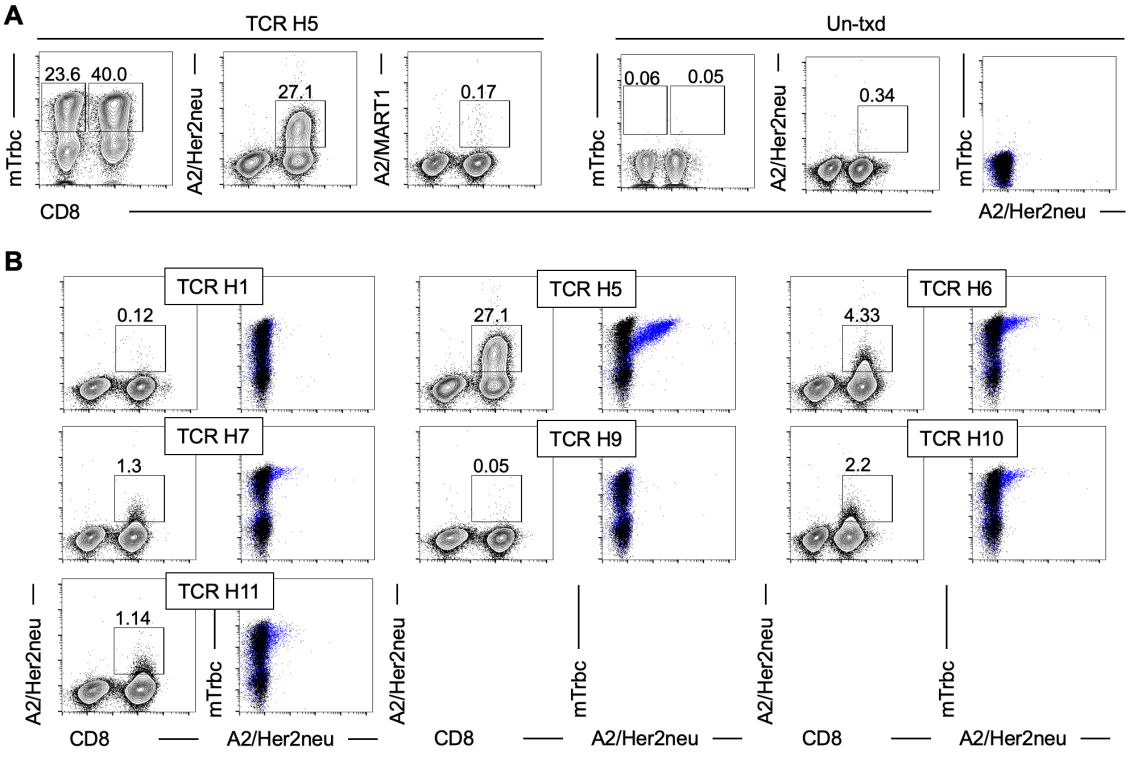

Figure 4. 18: Viral re-expression of A2/Her2neu$_{369-377}$ pMHC multimer-reactive TCRs in primary human PBMCs. A) Exemplary flow cytometric analysis of pMHC multimer reactivity and specificity of TCR transduced PBMCs. Successful viral transduction was determined by mTrbc

staining. pMHC multimer reactivity and specificity was analyzed by staining with relevant (A2/Her2/neu$_{369-377}$) or irrelevant (A2/MART1$_{(A27L)26-35}$) pMHC multimer. Un-transduced PBMCs (Un-txd) served as negative control. **B**) Validation of pMHC multimer reactivity and analysis of CD8 dependence in pMHC multimer binding. PBMCs transduced with indicated A2/Her2/neu$_{369-377}$-specific TCRs were stained with relevant pMHC multimer and mTrbc mAb. Pre-gated on single living lymphocytes in A) and B) for pMHC multimer staining, pre-gated on CD8+; mTrbc+ (blue) and CD8-; mTrbc+ (black) in B) for overlay plots.

4.2.4.2 Structural avidity measurement of A2/Her2neu$_{369-377}$ pMHC multimer-reactive TCRs

After determining pMHC multimer reactivity, we measured the structural avidity of the TCR transduced PBMCs by flow-based k_{off}-rate assay (Fig 4.19 A). TCR H5 possesses a k_{off}-rate of $t_{1/2}$= 79 sec while all other A2/Her2neu$_{369-377}$-candidate TCRs have an k_{off}-rate below detection limit (Fig 4.19 B). All TCR transduced T cells (including TCR H1) showed an initial Strep-Tactin APC signal before addition of D-biotin with exception of T cells transduced with TCR H9 (Fig 4.19 A).

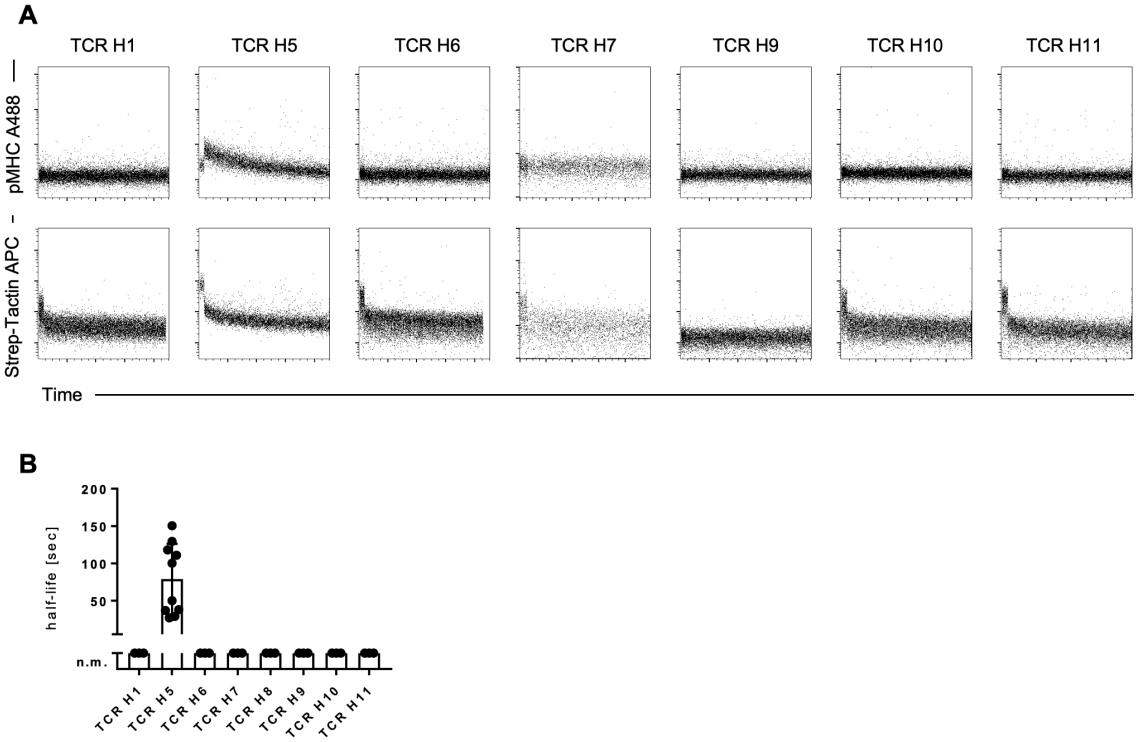

Figure 4. 19: Structural avidity measurement of T cells transduced with A2/Her2neu$_{369-377}$-specific TCRs. A) Flow-cytometry based k_{off}-rate assay of **CD8$^+$** T cells transduced with the indicated A2/Her2neu$_{369-377}$ pMHC multimer-reactive TCRs. **B**) Quantification of pMHC monomer dissociations shown in A). Two independent experiments in technical triplicates, one symbol represents one dissociation. Pre-gated on single, living mTrbc+ CD8+ T cells. n.m.: not measurable (< 30 sec).

4.2.4.3 Functional avidity of A2/Her2neu$_{369-377}$ pMHC multimer-reactive TCRs

Next, we tested the functional avidity of T cells transduced with the A2/Her2neu$_{369-377}$ pMHC multimer-reactive TCR performing ICCS and killing assay using peptide pulsed K562 target cells. TCR H9 did not respond to any of the rested peptide concentrations, while TCR H1, H5, H6, H7 and H11 showed IFNγ secretion at high peptide concentrations (Fig. 4.20 A). Here, TCR H5 showed the highest peptide sensitivity, which was also reflected in the EC50 values (Fig. 4.20 B). Performing a killing assay using peptide-pulsed K562 target cells indicated that TCR H5 and H1 also mediate cytotoxicity when co- cultured at an E:T ratio of 1:1 (Fig 4.20 C).

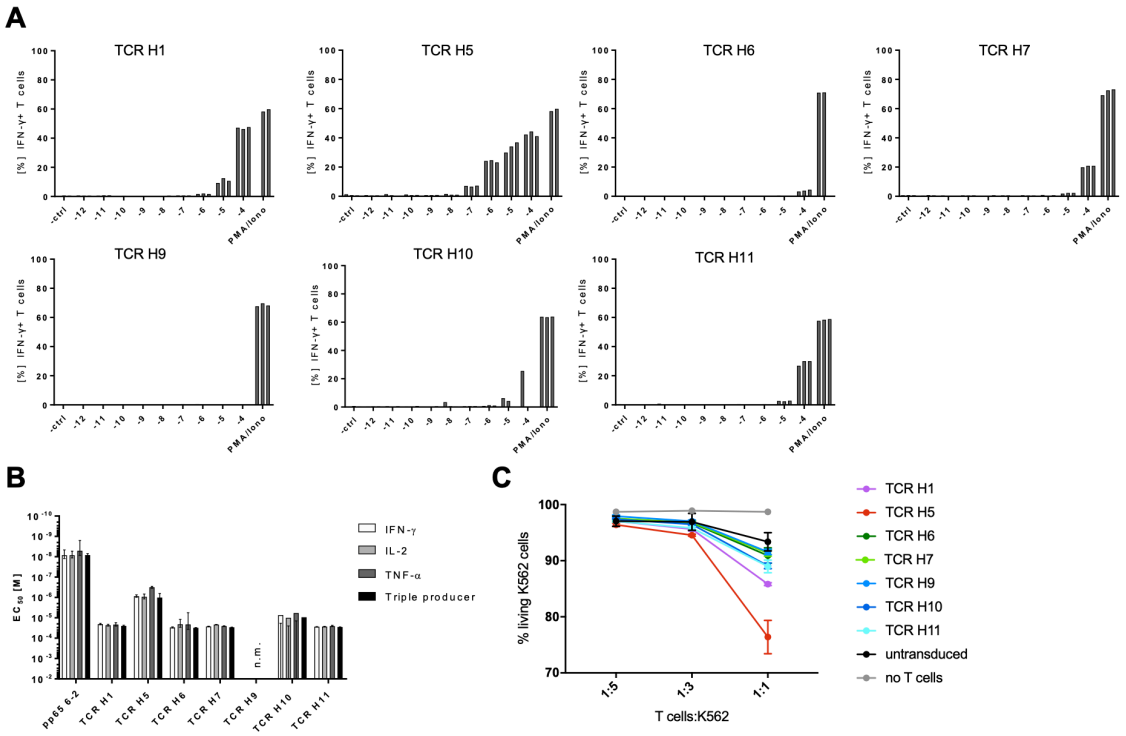

Figure 4. 20: Intracellular cytokine staining and killing capacity of T cells transduced with A2/Her2neu$_{369-377}$ pMHC multimer-reactive TCRs. A) Peptide concentration dependent IFNg production of T cells transduced with indicated A2/Her2neu$_{369-377}$ pMHC multimer-reactive TCRs. T cells were co-cultured with K562 target cells presenting increasing amounts of relevant peptide (10^{-12}- 10^{-4} M) or 10^{-4} M irrelevant peptide (pp65$_{495-503}$). **B**) Half-maximal IFNg, TNFa and IL-2 production (EC_{50}) of T cells transduced with indicated A2/Her2neu$_{369-377}$ pMHC multimer-reactive TCRs. **C**) Killing capacity of T cells transduced with indicated A2/Her2neu$_{369-377}$ pMHC multimer reactive TCRs. T cells were co-cultured for 18h with A*02:01+ K562 target cells pulsed with 10^{-6} M A2/Her2neu$_{369-377}$- peptide in the effector: target ratio (E:T) 1:5, 1:3, 1:1. Untransduced T cells (Un-txd) served as negative control.

4.2.4.5 Correlating structural and functional avidity of A2/Her2neu$_{369-377}$ pMHC multimer-reactive TCRs

We subsequently plotted the collected data of the identified A2/Her2neu$_{369-377}$ pMHC multimer-reactive TCRs against each other. The data might show a beneficial effect of high initial pMHC MFI (i.e. strong multimer binding after feeder-cell free single cell expansion) (Fig 4.21 A). This tendency holds true for the transgenically re-expressed TCR H5 (Fig 4.21 B). However, because of the very limited data set of 7 TCRS, observed tendencies have to be validated with further data.

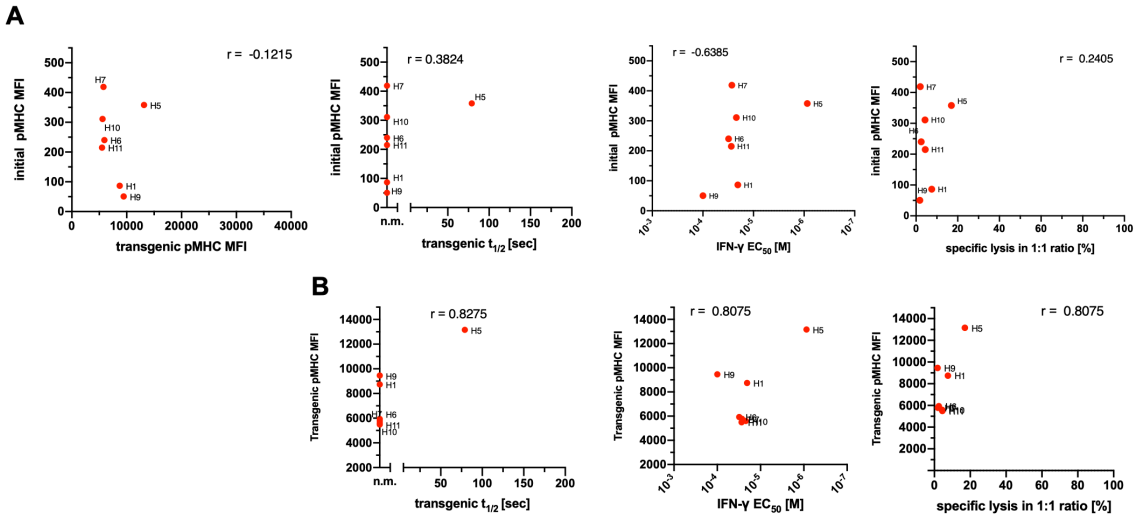

Figure 4. 21: Correlation of initial and transgenic pMHC multimer MFI with functional and structural avidity of A2/Her2neu$_{369-377}$ pMHC multimer-reactive TCRs. A) Correlation of pMHC multimer MFI after feeder-cell free single cell expansion (initial pMHC MFI) versus k_{off}-rate of transgenically re-expressed TCRs, their IFNg EC_{50} and cytotoxicity against K562 target cells. **B**) Correlation of pMHC multimer MFI after TCR gene-transfer into primary human PBMCs versus their k_{off}-rate, their IFNg EC_{50} and cytotoxicity against K562 target cells. Each dot represents the mean of technical replicates, except for pMHC multimer MFI.

No conclusion could be drawn by analyzing the data concerning a relation between structural and functional avidity, as all TCRs did not show a measurable k_{off}-rate after feeder-cell free single cell expansion and only one out of seven TCRs showed a measurable koff rate upon transgenic re-expression in primary human PBMCs (Fig 4.22 A+).

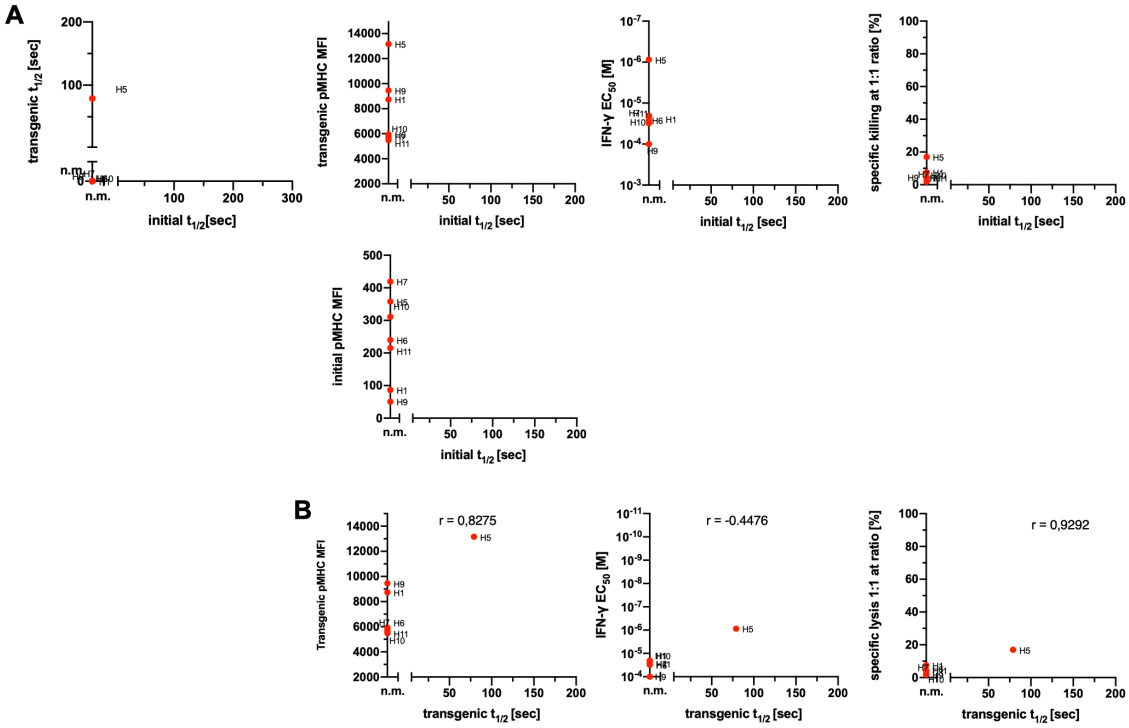

Figure 4. 22: Correlation of structural TCR avidity after feeder cell-free single cell expansion and after transgenic re-expression versus pMHC multimer MFI and functional avidity of A2/Her2neu$_{369-377}$ pMHC multimer-reactive TCRs. A) Correlation of k_{off}-rate after feeder-cell free single cell expansion (initial k_{off}-rate) versus k_{off}-rate of transgenically re-expressed TCRs, their pMHC multimer MFI, thei IFNg EC_{50} and cytotoxicity against K562 target cells. **B**) Correlation of k_{off}-rate after TCR gene-transfer into primary human PBMCs versus their pMHC multimer MFI, their IFNg EC_{50}, maximal cytokine secretion and cytotoxicity against K562 target cells. Each dot represents the mean of technical replicates, except for pMHC multimer MFI. Dotted line at 60 sec in A) and 80 sec in B).

4.2.5. Isolation of A2/RNF43 pMHC-multimer-reactive TCRs from the naïve T cell repertoire

Choosing the right target epitope for adoptive T cell therapy is of tremendous importance. On one side “self-similarity” of the epitope influences the quantity and quality of epitope reactive high-avidity TCRs that are allowed to exit the thymus. On the other side, tissue-restricted expression of the epitope determines the risk of on-target/off-tumor toxicity[153]. Mutation-derived neoantigens are considered to be prime target epitopes for adoptive T cell therapy as they should be seen by the immune system as non-self-antigen eliciting high-avidity T cell responses. Additionally, this target epitope group should possess a high safety profile, as only mutated cancer cells are able to present mutated peptide[154].
However, most mutation-derived neoantigens are patient-specific epitopes. Generating one (or a set) of neoantigen-specific TCRs in such an individualized setting is (so far) not feasible in a reasonable time and cost frame. Frame shift-derived neoepitopes at least pose the chance to find the very same neoantigen in a larger patient cohort which would allow to treat several patients with one and the same TCR. Among others, colon cancer patients show high frequency of insertion or deletion mutations (InDels). Consequently, within these patient cohorts, different frame-shift mutations in various patients can lead to the generation of the very same neoantigen[155]. We focused on frame-shift-derived neoantigens resulting from the ring finger protein (RNF) 43 gene. RNF43 is mutated in 20 % of colorectal adenocarcinomas and endometrial carcinomas. Of those, more than 70% of non-silent mutations are generated by InDels[156]. Looking at all theoretically possible neo-open reading frames (neoORFs) of RNF 43, we predicted *in silico* about 4500 MHC class I binding peptides (8-11 mers), with a predicted binding affinity to the MHC (netMHC) ranging from 4 nM-50000 nM (Kilian Schober, unpublished data). 35 epitopes were predicted to have a peptide binding affinity below 20 nM, which is within the range of affinities described to trigger durable tumor rejection[157,158]. Of those, 7 epitopes were verified for correct processing by *in vitro* proteasomal digest (Peter Kloetzel, Charité, Berlin).

Peptide	Length	neoORF (n+)	HLA type	Predicted affinity Kd [nM]	Published mutations leading to neoORF with epitope	*In vitro* processed
HPRSQAWAL	9	1	B*07:02	5	R27fs, K145fs, R40fs, S41fs, E43fs, L65fs, A115fs, R117fs, C119fs, P192fs, R225fs, Q254fs, S264fs, C275fs	11mer, 12mer, 14mer
VPSVWRSSL	9	1	B*07:02	6	R27fs, K145fs, R40fs, S41fs, E43fs, L65fs, A115fs, R117fs, C119fs, P192fs, P195fs, R225fs, Q254fs, S264fs	epitope, 10mer, 11mer
IPAMPTTTSL	10	1	B*07:02	6,5	R27fs, K145fs, R40fs, S41fs, E43fs, L65fs, A115fs, R117fs, C119fs, P192fs, P195fs, R225fs, Q254fs, S264fs, C275fs	13mer, 14mer
SLLPTCWAL	**9**	**1**	**A*02:01**	**6,8**	**R27fs, K145fs, R40fs, S41fs, E43fs, L65fs, A115fs, R117fs, C119fs, P192fs, P195fs, R225fs, Q254fs, S264fs, C275fs**	**epitope**
RPAAGRPGV	9	1	B*07:02	13,2	R27fs, K145fs, R40fs, S41fs, E43fs, L65fs, A115fs, R117fs, C119fs, P195fs, R225fs,	12mer, 14mer
APGRSPAPL	9	2	B*07:02	15	A33fs, K54fs, L88fs, R117fs, R119fs, L311fs, R363fs, K45fs, L61fs, F69fs, P195fs,	epitope
HPRSQAWAL	9	1	B*08:01	17,7	see above	see above

Figure 4. 23: *In vitro* proteasomal digest of RNF43 peptide epitope candidates. Correct processing of RNF43 peptide epitope candidates (sequence and length) was validated by digesting overlapping peptide strings in presence of proteasomal enzyme mix. Resulting peptide fragments were identified by mass spectrometry. Predicated peptide binding affinity to corresponding HLA allotype was determined using netMHC. Published frameshift mutations leading to neo-open reading frames (noeORFs) that could result in translation of the neo-epitope candidate are indicated. “epitope”: exact peptide sequence resulted from *in vitro* digest, longer epitope variants are indicated by “n-mer”. In bold: A*02:01 restricted RNF43 neo-epitope used to generate pMHC monomers to isolated reactive TCRs from the naïve **CD8$^+$** T cell repertoire.

We decided for the RNF43 neoantigen candidate “SLLPTCWAL”, as exactly this peptide was generated by *in vitro* proteasomal digest (Fig.4 23). Furthermore, this peptide had the highest predicted binding affinity to A*02:01, which is the most common HLA allotype in Caucasian population. We successfully refolded A*02:01/SLLPTCWAL (A2/RNF43) pMHC monomers (Fig 4. 24), thereby verifying the *in silico* predicted high peptide binding affinity to A*02:01.

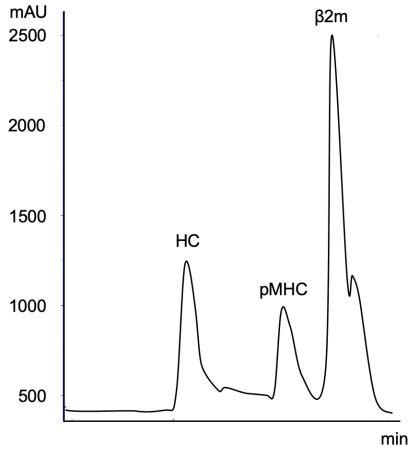

Figure 4. 24: RNF43 candidate epitope forms stable pMHC monomer with in A*02:01. *In silico* predicted and through *in vitro* proteasomal digest verified RNF43 derived neoantigen peptide candidate SLLPTCWAL was refolded in presence of A*02:01 and β2m. Purification via size exclusion chromatography indicated stable refolding into heterotrimeric pMHC monomers.

Fraction of 2nd peak was collected and pooled. HC: soluble heavy chain aggregates, pMHC: peptide loaded major histocompatibility complex, LC: light chain, β2m: beta 2 microglobulin.

We subsequently used the generated pMHC monomers to screen the naïve T cell repertoire of antigen-inexperienced, healthy HLA-A*02:01$^+$ donors for A2/RNF43 pMHC multimer-reactive CD8$^+$ T cells. Neoantigen-reactive CD8$^+$ T cells in antigen-inexperienced donors are rare events[118,159]. We therefore focused on CD8$^+$ T cell-enriched apheresis as staring material to maximally increase the size of our target population (naïve CD8$^+$ T cells). Double pMHC multimer-guided single cell sort followed by short-term feeder cell-free expansion allowed validation of pMHC multimer reactivity in two independent experiments (Fig 4.25 A; Donor A#1: 2/5 analyzed clones; Donor #2: 2/4 analyzed clones pMHC multimer-reactive). Of note, all 4 pMHC multimer-reactive clones differed considerably in their pMHC APC MFI (Fig 4.25 B). However, experiments were performed independently which makes direct comparison of MFI values problematic. CD8$^+$ T cell clones resulting from pMHC multimer-negative T cells during sort served as negative control (Fig 4.25 A). pMHC multimer-reactive T cell clones were identified via Sanger sequencing. 3 out of 4 full paired TCR chains could be extracted (Fig 4.25 B).

A

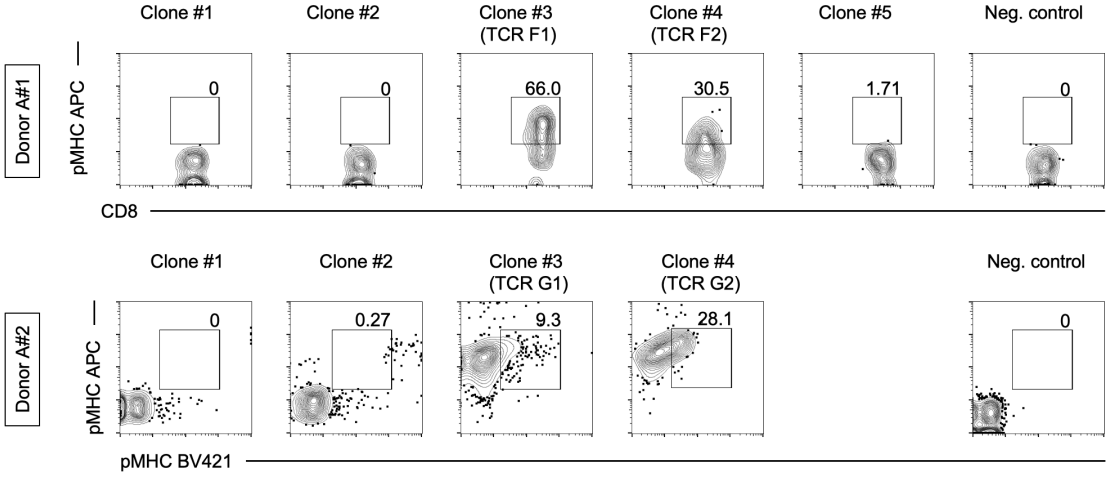

B

Name	Variable	Joining	Diversity	CDR3	pMHC APC MFI
Clone #3 D1 TCR F1	TRAV38-1*01	TRAJ42*01		CAFSYGGSQGNLIF	49.9
	TRBV20-1*00	TRBJ2-7*01	TRBD2*02	CSAIGSGSYEQYF	
Clone #4 D1 TCR F2	TRAV12-2*02	TRAJ48*01		CAVNVANFGNEKLTF	39.9
	TRBV9*01	TRBJ2-7*01	TRBD1*01	CASSGTGNEQYF	
Clone #3 D2 TCR G1	TRAV38-2/DV8*01	TRAJ43*01		CALNDMRF	283
	TRBV11-2*01	TRBJ2-1*01	TRBD2*01	CASSLFFGTNKYNEQFF	
Clone #4 D2 TCR G2	-	-	-	Not identified	460
	-	-	-	Not identified	

Figure 4. 25: Identification of A2/RNF43 neoantigen-reactive CD8$^+$ T cells from the naïve T cell repertoire of antigen-inexperienced healthy donors. A) Validation of A2/RNF43 pMHC multimer reactivity of feeder-cell free expanded single cell derived clones. Double pMHC multimer positive naïve **CD8$^+$** T cells were sorted as single cells for feeder-cell free expansion. Clones were stained with pMHC multimer to validate pMHC reactivity. **B**) TCR sequences of indicated pMHC multimer-reactive **CD8$^+$** T cell clones. 3/4 fully paired TCR sequences; 75 % TCR recovery rate (Thomas R. Müller). Mean fluorescence intensity (MFI) of pMHC multimer APC of corresponding clone indicated. A) Pre-gated on single, living CD45+ lymphocytes.

4.2.5.1 Functional and structural characterization of A2/RNF43 pMHC multimer-reactive TCRs

4.2.5.2 Viral re-expression of A2/RNF43 pMHC multimer reactive TCRs

We generated retro-viral particles of the isolated RNF43 pMHC multimer-reactive TCRs and re-expressed them in primary human PBMCs for in-depth characterization. All three TCRs could be transgenically re-expressed as determined by mTrbc mAb staining. pMHC multimer reactivity could be validated for all three TCRs by pMHC multimer staining, while none of the RNF43 pMHC-reactive TCRs showed cross reactivity when stained with irrelevant pMHC multimer (A2/pp65$_{495\text{-}503}$) (Fig 4.26 A; TCRG1 representative for all shown TCRs). The overlay plots indicated that T cells transduced with TCR G1 bound A2/RNF43 pMHC multimer in an CD8 independent manner, while pMHC

multimer binding for TCR F1 and TCR F2 was strictly CD8 dependent. (Fig 4.26 B).

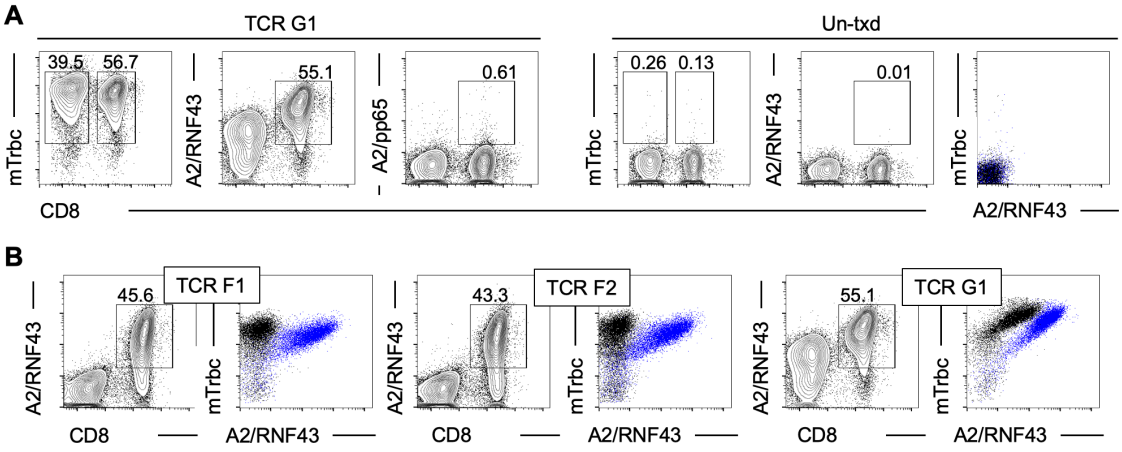

Figure 4. 26: Viral re-expression of A2/RNF43 pMHC multimer-reactive TCRs in primary human PBMCs. A) Exemplary flow cytometric analysis of pMHC multimer-reactivity and specificity of TCR transduced PBMCs. Successful viral transduction was determined by mTrbc staining. pMHC multimer-reactivity and specificity was analyzed by staining with relevant (A2/RNF43) or irrelevant ($A2/pp65_{495\text{-}503}$) pMHC multimer. Un-transduced PBMCs (Un-txd) served as negative control. **B**) Validation of pMHC multimer-reactivity and analysis of CD8 dependence in pMHC multimer binding. PBMCs transduced with indicated A2/RNF43-specific TCRs were stained with relevant pMHC multimer and mTrbc mAb. Pre-gated on single living lymphocytes in A) and B) for pMHC multimer staining, pre-gated on CD8+; mTrbc+ (blue) and CD8-; mTrbc+ (black) in B) for overlay plots.

4.2.5.2 Structural avidity measurement of A2/RNF43 pMHC multimer-reactive TCRs

After analyzing the pMHC multimer reactivity and specificity, we set out to measure the structural avidity of the TCR-transduced T cells by flow cytometry-based k_{off}-rate assay (Fig 4.27 A). $CD8^+$ T cells transduced with TCR G1 possessed a k_{off}-rate assay of $t_{1/2}$= 160 sec while the k_{off}-rate for $CD8^+$T cells transduced with TCR F1 and TCR F2 was below the limit of detection (30 sec) (Fig 4.27 B).

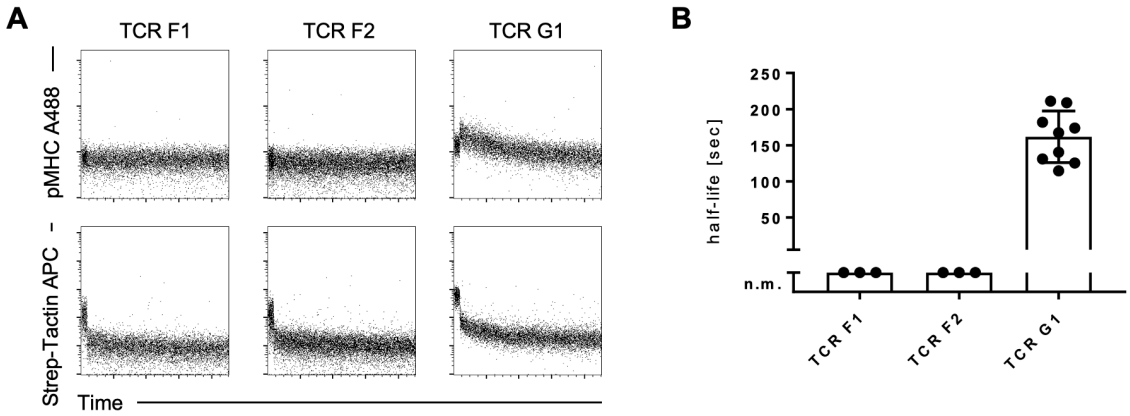

Figure 4. 27: Structural avidity measurement of T cells transduced with A2/RNF43 pMHC multimer-reactive TCRs. A) Flow-cytometry based k_{off}-rate assay of **CD8$^+$** T cells transduced with the indicated A2/RNF43-specific TCRs. **B**) Quantification of pMHC monomer dissociations shown in A). One symbol represents one dissociation, 3 independent experiments with technical triplicates. Pre-gated on single, living mTrbc+ CD8+ T cells. n.m.: not measurable (<30 sec).

4.2.5.3 ICCS of T cells transduced with A2/RNF43 pMHC multimer-reactive TCRs

To further validate specificity and sensitivity of the A2/RNF43 pMHC multimer-reactive TCRs, we performed ICCS of RNF43 TCR-transgenic T cells after co-culture with peptide pulsed K562 target cells. T cells transduced with TCR G1 showed cytokine secretion upon stimulation with 10^{-4} M target epitope, while T cells transduced with TCR F1 and TCR F2 were non-responsive (4.28 A). We observed for TCR G1 a basal cytokine secretion upon co-culture with K562 target cells pulsed with RNF43 peptide between 10^{-12} - 10^{-8} M, which turned into peptide concentration-dependent cytokine secretion from 10^{-9} - 10^{-4} M (Fig 4.28 B+C). Additionally, T cells transduced with TCR G1 secreted cytokine in response to K562 target cells pulsed with 10^{-4} M irrelevant peptide ($pp65_{495\text{-}503}$) (Fig 4.28 A+C). Further experiments included A*02:01$^+$ K562 pulsed with 10^{-12} and 10^{-3} M irrelevant peptide, unpulsed A*02:01$^+$ K562 target cells as well as unpulsed B*08:01$^+$ K562 target cells and T cells only as additional negative controls (Fig 4.28 D). Here, T cells transduced with TCR G1 reacted with IFNγ secretion to peptide pulsed as well as unpulsed A*02:01$^+$ K562 target cells, while unpulsed B*08:01$^+$ K562 target cells did not trigger cytokine production. This A*02:01 restricted cross-reactivity induced cytokine production on a similar level as co-culture with A*02:01$^+$ K562 target cells pulsed with 10^{-12}-10^{-8} M relevant RNF43 peptide (Fig 4.28 B+C+D). T cells transduced with TCR G1 showed an EC_{50} value of 10^{-7} and were thereby about 1 log less peptide sensitive than an in-depth characterized A2/$pp65_{495\text{-}503}$-specific TCR (TCR6-2, Thomas R. Müller

unpublished). EC_{50} values calculated for IFNγ$^+$ IL 2$^+$ TNFα$^+$ triple producers (i.e. T cells with highest functionality) indicated the same distance between TCR G1 and TCR 6-2. Values for TCR F1 and TCR F2 reflected peptide unresponsiveness (Fig 4.28 E).

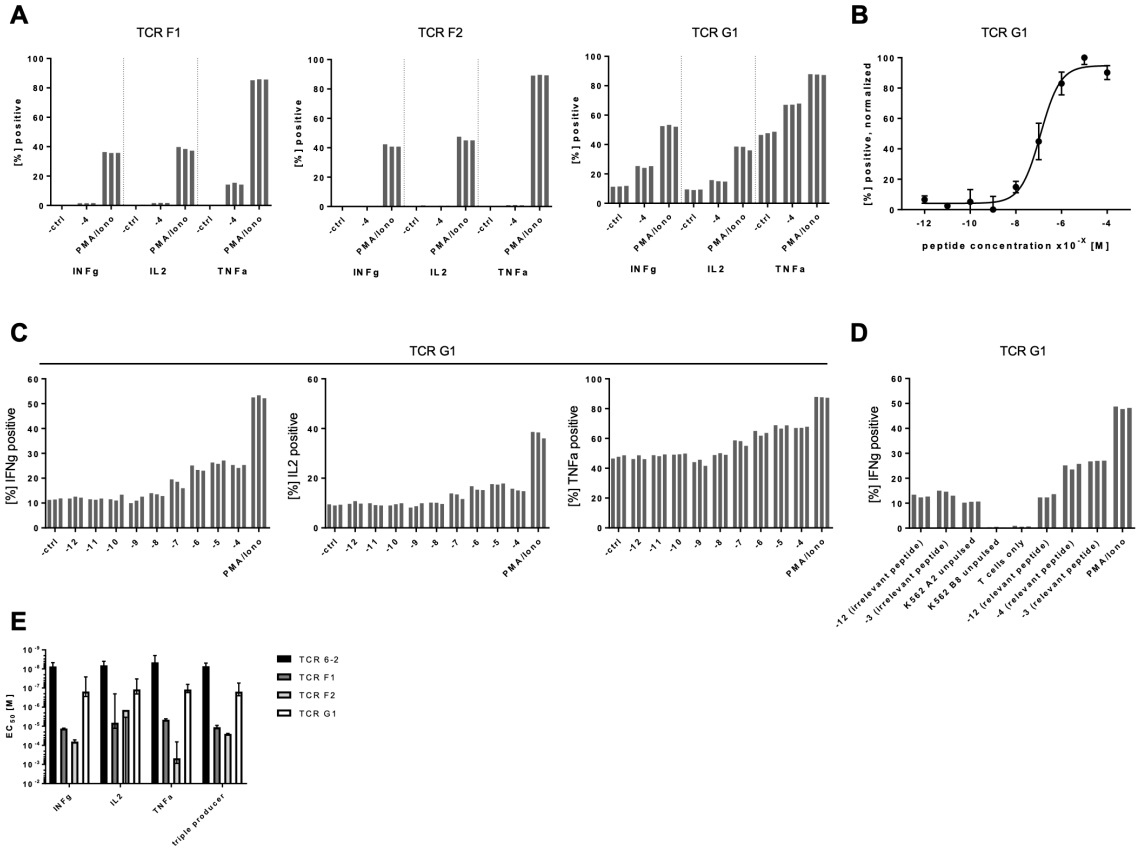

Figure 4. 28: Intracellular cytokine staining of T cells transduced with A2/RNF43-specific TCRs. A) Summary bar-graph for IFNg, TNFa and IL-2 production. T cells transduced with the indicated RNF43 specific TCRs were co-cultured for 4 h with K562 target cells presenting either 10^{-4} M irrelevant peptide ($pp65_{495-503}$) or RNF43 peptide. PMA/Ionomycin served as positive control. **B**) Peptide concentration dependent IFNg production of T cells transduced with RNF43 specific TCR G1. Values are normalized according to IFNg production upon stimulation with highest and lowest peptide concentration. **C**) Peptide concentration dependent production of IFNg, TNFa and IL-2 of T cells transduced with RNF43 specific TCR G1 shown in A) and B). T cells were co-cultured with K562 target cells presenting increasing amounts of peptide 10^{-12}- 10^{-4} M) or 10^{-4} M irrelevant peptide ($pp65_{495-503}$). PMA/Ionomycin served as positive control. **D**) Comparison of IFNg production after TCR G1-transgenic T cells were co-cultured with HLA-A*02:01+ K562 target cells presenting either no or the relevant or the irrelevant peptide epitope. Unpulsed B*08:01+ K562 target cells or T cell only served as additional negative control. PMA/Ionomycin served as positive control. **E**) Half-maximal IFNg, TNFa and IL-2 production (EC_{50}) of T cells transduced with the indicated RNF43 specific TCRs.

4.2.5.4 Killing capacity of A2/RNF43 pMHC multimer-reactive TCRs

Next, we set out to evaluate cytotoxicity of the RNF43 pMHC multimer-reactive TCRs in a killing assay. Therefore, RNF43 TCR-transduced T cells were co-cultured in varying effector to target ratios (E:T) with A*02:01^{+} K562 target cells pulsed with 10^{-6} M relevant or irrelevant peptide epitope. Unpulsed A*02:01^{+} K562 and B*08:01^{+} target cells served as additional negative controls. Again, the in-depth characterized A2/pp65-specific TCR 6-2 served as biological positive control. T cells transduced with the RNF43 pMHC multimer-reactive TCRs F1 and F2 did not show cytotoxicity against any of the K562 target cell samples (Fig 4.29 A+B). Interestingly, T cells transduced with TCR G1 mediated minor reduction of RNF43 peptide pulsed K562 target cells when co-cultured in 1:1 ratio, although this reduction is considerably smaller in comparison to TCR 6-2 (Fig 4.29 A). This slight reduction in surviving K562 target cells could also be seen when TCR G1-transgenic T cells were co-cultured with A*02:01^{+} K562 target cells pulsed with irrelevant peptide as well as unpulsed A*02:01^{+} K562 target cells, but not when co-cultured with unpulsed B*08:01^{+} target cells (Fig 4.29 B+C+D). This reduction gets clearer when normalizing cell death of target cells over the target cell number in the 1:5 ratio (Fig 4.29 D). TCR G1-transgenic T cells lead to a reduction of A*02:01^{+} K562 target cells pulsed with relevant, irrelevant or no peptide, while unpulsed B*08:01^{+} target cells remain un-attacked (Fig 4.29 D). TCR 6-2-transgenic T cells mediate cytotoxicity solely when co-cultured with A*02:01^{+} K562 target cells pulsed with relevant peptide (Fig 4.29 D).

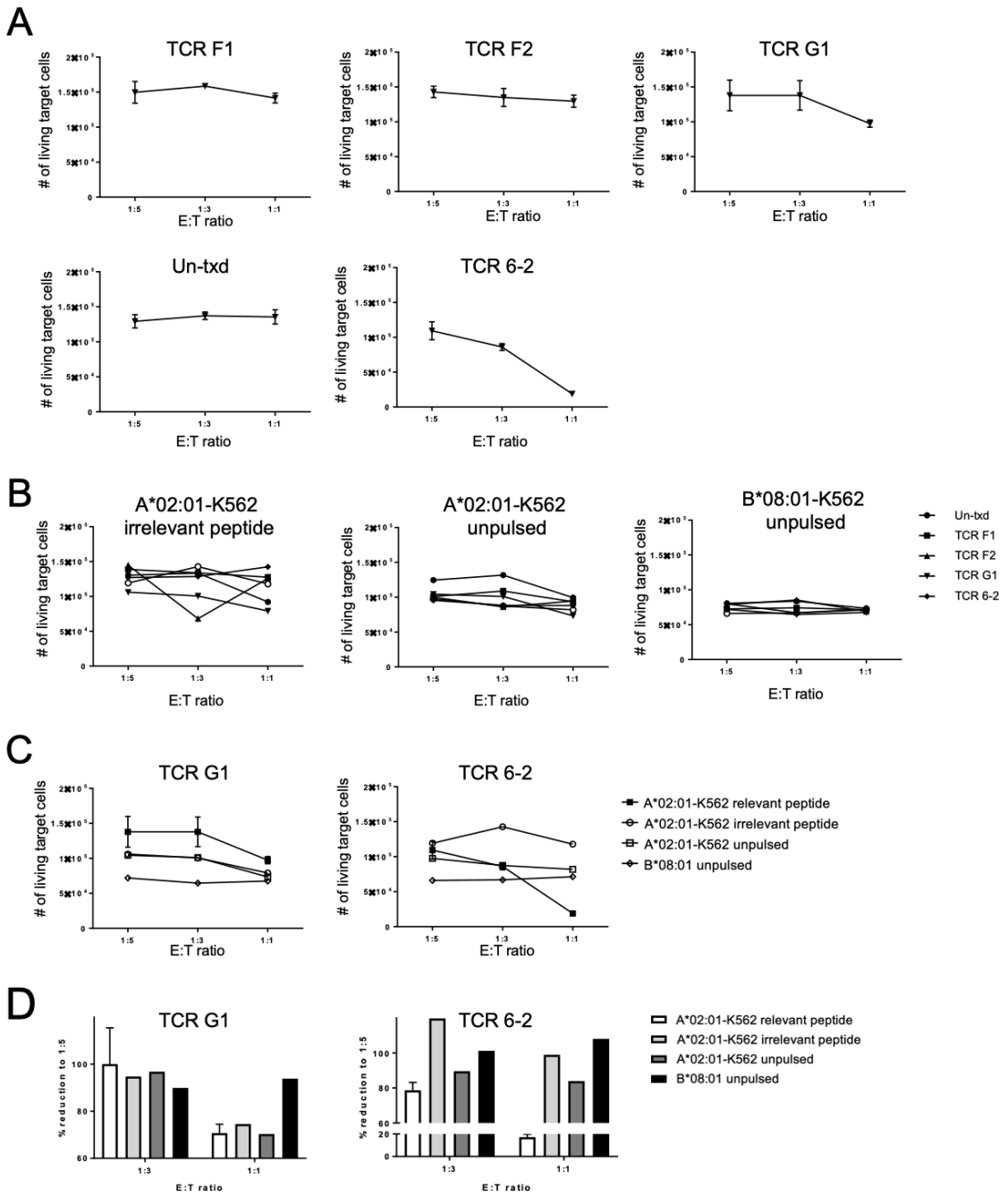

Figure 4. 29: Cytotoxicity of T cells transduced with RNF43 pMHC multimer-reactive TCRs. **A**) T cells transduced with the indicated RNF43 pMHC multimer-reactive TCRs were co-cultured for 18h with A*02:01+ K562 target cells pulsed with 10^{-6} M RNF43 peptide in the effector: target ratio (E:T) 1:5, 1:3, 1:1. Untransduced T cells (Un-txd) served as negative control, A2/pp65$_{593\text{-}503}$ specific TCR 6-2 served as biological positive control. Mean with standard deviation of technical triplicates. **B**) T cells transduced with the indicated RNF43 pMHC multimer-reactive TCR co-cultured with negative controls. **C**) Overview of cytotoxicity for T cells transduced with RNF43 specific TCR G1 or A2/pp65 specific TCR 6-2. **D**) Relative reduction of K562 target cells comparedto E:T ration 1:5 shown in C. Samples using A*02:01+ K562 target pulsed with relevant peptide in triplicates with standard deviation, all negative controls one data point.

Our data demonstrate the potency of our TCR characterization and isolation platform for the identification of functional TCR candidates from the naïve repertoire of antigen-inexperienced donors. Our feeder cell-free single cell

expansion protocol allowed robust generation of T cell clones which could be screened for pMHC multimer reactivity as well as structural TCR avidity. TCRs of pMHC multimer-reactive T cell clones were efficiently extracted using in-house NGS. All identified TCRs were successfully re-expressed in primary human PBMCs and showed a broad range of functional and structural avidity. By screening the naïve T cell repertoire for RNF43-specific TCRs, we generated proof-of-concept data that our platform can be used to identified TCRs with therapeutic value for immunotherapy.

4.2.5.5 Correlating structural and functional avidity of A2/RNF43 pMHC multimer-reactive TCRs

Subsequently, we checked the acquired dataset for potential links between pMHC multimer binding prior and post TCR isolation with functional and structural avidity (Fig 4.30). We saw that the functional TCR G1 had displayed the brightest pMHC multimer signal after feeder-cell free single cell expansion as well as upon TCR transduction (Fig 4.30 A+B). However, the dataset is too small to give conclusive information.

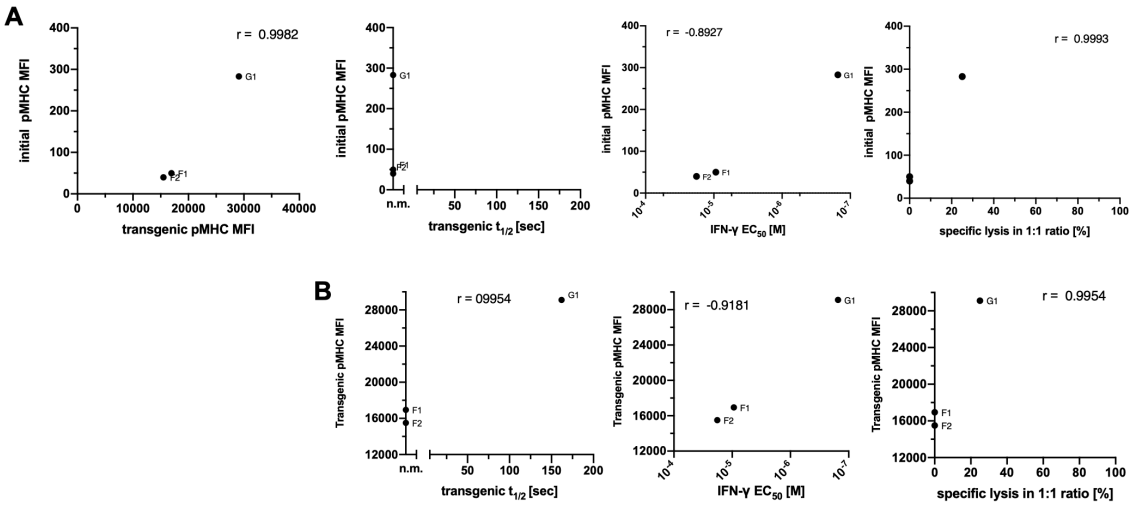

Figure 4. 30: Correlation of initial and transgenic pMHC multimer MFI with functional and structural avidity of A2/RNF43 pMHC multimer-reactive TCRs. A) Correlation of pMHC multimer MFI after feeder-cell free single cell expansion (initial pMHC MFI) versus k_{off}-rate of transgenically re-expressed TCRs, their IFNg EC_{50} and cytotoxicity against K562 target cells. **B**) Correlation of pMHC multimer MFI after TCR gene-transfer into primary human PBMCs versus their k_{off}-rate, their IFNg EC_{50} and cytotoxicity against K562 target cells. Each dot represents the mean of technical replicates, except for pMHC multimer MFI.

Correlating the functional and structural avidity data of the A2/RNF43 pMHC multimer-reactive TCRs reflects the tendency observed for YFV, MART1 and

Her2neu TCRs previously; the k_{off}-rate coincided with functionality (Fig 4.31 B). However, the dataset is too small to compare the predictive power of pMHC multimer binding against the k_{off}-rate.

.

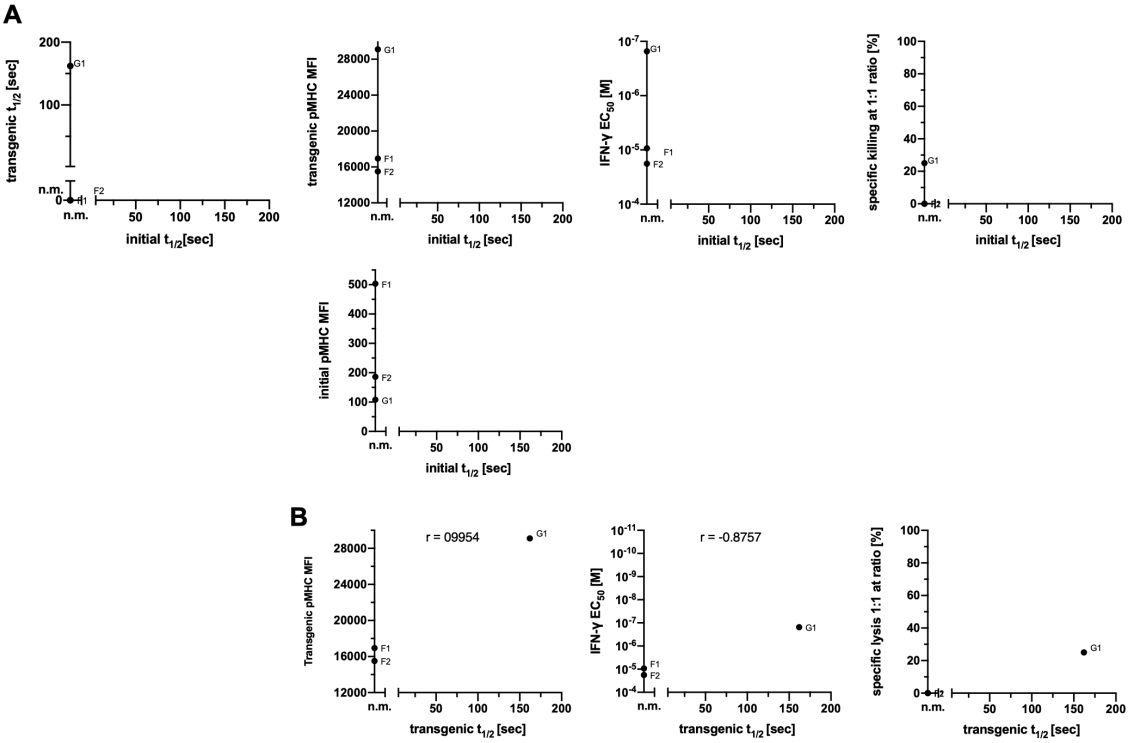

Figure 4. 31: Correlation of structural TCR avidity after feeder-cell free single cell expansion and after transgenic re-expression versus pMHC multimer MFI and functional avidity of A2/RNF43 pMHC multimer reactive TCRs. A) Correlation of k_{off}-rate after feeder-cell free single cell expansion (initial k_{off}-rate) versus k_{off}-rate of transgenically re-expressed TCRs, their pMHC multimer MFI, thei IFNg EC_{50} and cytotoxicity against K562 target cells. **B**) Correlation of k_{off}-rate after TCR gene-transfer into primary human PBMCs versus their pMHC multimer MFI, their IFNg EC_{50}, maximal cytokine secretion and cytotoxicity against K562 target cells. Each dot represents the mean of technical replicates, except for pMHC multimer MFI.

4.3. Correlating structural and functional avidity of all identified multimer-reactive TCRs

We summarized all data that were generated analyzing twelve A2/$YFV_{212-222}$ pMHC multimer-reactive TCRs derived from an antigen-experienced donor as well as the data derived from the six A2/$MART1_{(A27L)26-35}$, seven A2/$Her2neu_{369-377}$ and three A2/RNF43 pMHC multimer-reactive TCRs derived from the naïve repertoire of an antigen-inexperienced donor. Plotting these 29 TCRs revealed the a high initial pMHC MFI (prior TCR isolation) did not correlate with a slow k_{off}-rate or strong IFNg secretion upon TCR transfer (4.32 A). Same hold true for pMHC multimer MFI measured for TCR transduced T cells (4.32 B).

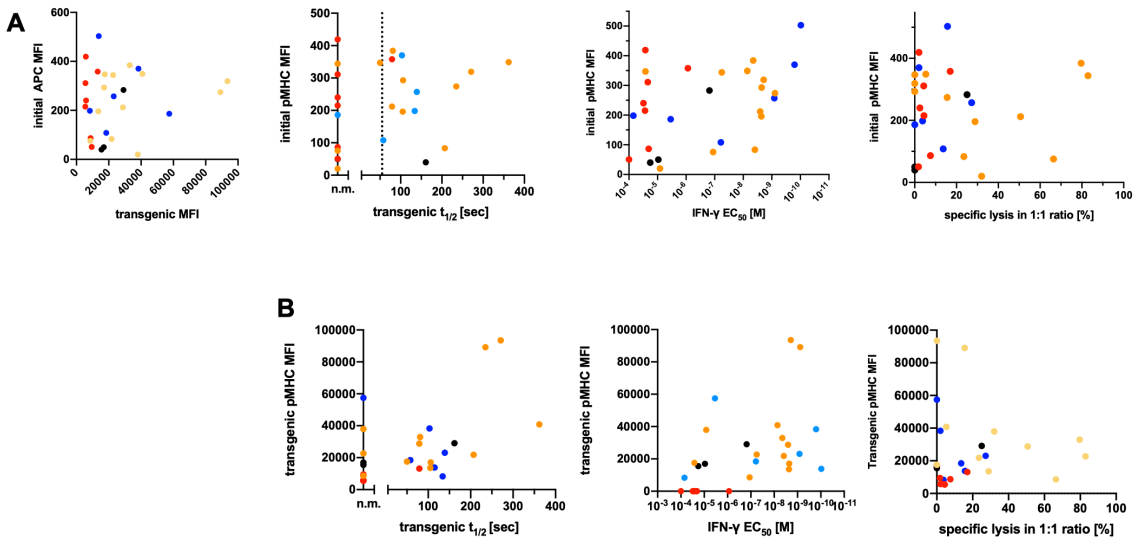

Figure 4. 32: Correlation of initial and transgenic pMHC multimer MFI with functional and structural avidity of all identified pMHC multimer-reactive TCRs. A) Correlation of pMHC multimer MFI after feeder-cell free single cell expansion (initial pMHC MFI) versus k_{off}-rate of transgenically re-expressed TCRs, their IFNg EC_{50} and cytotoxicity against K562 target cells. **B**) Correlation of pMHC multimer MFI after TCR gene-transfer into primary human PBMCs versus their k_{off}-rate, their IFNg EC_{50} and cytotoxicity against K562 target cells. Each dot represents the mean of technical replicates, except for pMHC multimer MFI. Black circle: A2/RNF43; yellow circles: A2/$YFV_{212-222}$; red circles: A2/$Her2neu_{369-377}$; blue circles: A2/$MART1_{(A27L)26-35}$ pMHC multimer-reactive TCRs.

Aligning the k_{off}-rate values that could be already measured directly after feeder cell-free single cell expansion versus IFNg secretion indicated a threshold of $t_{1/2}$ ~60 sec for functional TCRs (Fig 4.33 A). The same tendency was detected for transgenically-expressed TCRs with a cut-off around the same value (Fig 4.33 B). Of note, repetition experiments need to prove whether this tendency also directly translates into superior target cell killing as our data were not conclusive (Fig 4.33).

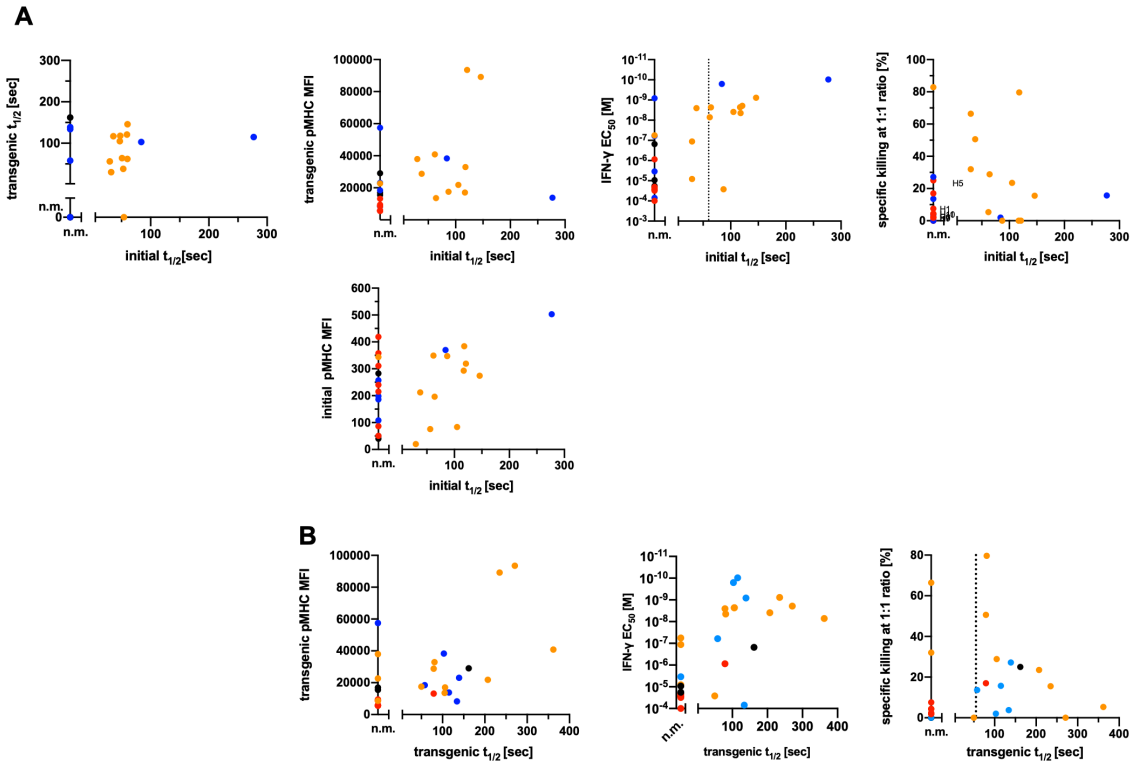

Figure 4. 33: Correlation of structural TCR avidity after feeder-cell free single cell expansion and after transgenic re-expression versus pMHC multimer MFI and functional avidity of all identified pMHC multimer-reactive TCRs. A) Correlation of k_{off}-rate after feeder-cell free single cell expansion (initial k_{off}-rate) versus k_{off}-rate of transgenically re-expressed TCRs, their pMHC multimer MFI, thei IFNg EC_{50} and cytotoxicity against K562 target cells. **B**) Correlation of k_{off}-rate after TCR gene-transfer into primary human PBMCs versus their pMHC multimer MFI, their IFNg EC_{50}, maximal cytokine secretion and cytotoxicity against K562 target cells. Each dot represents the mean of technical replicates, except for pMHC multimer MFI. Dotted line at 60 sec in A) and B). Black circle: A2/RNF43; yellow circles: A2/$YFV_{212-222}$; red circles: A2/$Her2neu_{369-377}$; blue circles: A2/$MART1_{(A27L)26-35}$ pMHC multimer-reactive TCRs.

4.3.1 Double tagged pMHC monomers to streamline pMHC multimer generation

We proved that direct conjunction of feeder cell-free single cell expansion, screening of pMHC multimer reactivity and NGS TCR extraction allows identification of functional TCRs in a high-throughput compatible manner. However, our platform makes extensive use of various pMHC multimer reagents. Consequently, the pMHC multimer generation process developed to a significant rate limiting step within our TCR characterization and isolation platform. We therefore set out to investigate whether it is possible to streamline the generation process for pMHC multimers.

pMHC multimers have become a valuable tool in basic research, clinical immune monitoring and translational immunotherapy. Biotinylated tetramers, reversible Streptamers or dye-conjugated reversible pMHC multimers are distinct pMHC reagents tailored for T cell identification[69], traceless T cell isolation[75] or TCR characterization[56,160]. The respective specific applicability of each pMHC-based reagent is mediated through conjugation of probes and/or (non-)reversible multimerization in separate production processes, which is laborious, time-consuming and prone to variability between the different types of pMHC reagents (Fig 1.5).

We hypothesized that combining a site-specific functionalization tag[129] with a reversible multimerization tag[72] to a double-tagged pMHC (“FLEXamer”) could unite reversibility with the opportunity to equip the pMHC with any desired additional functionality. This could allow the generation of distinct pMHC constructs from one common pMHC precursor, thus streamlining the production process for pMHC multimer reagents (Fig. 4.34).

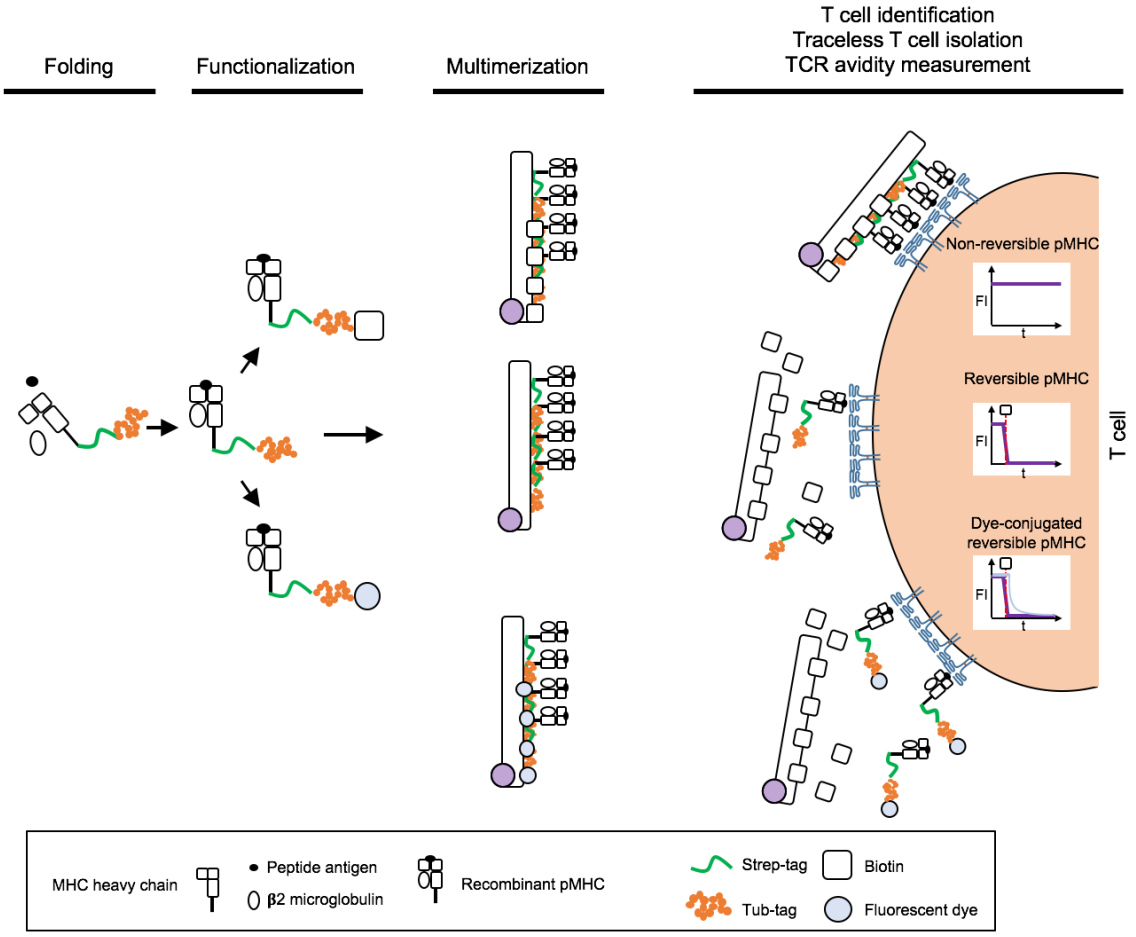

Figure 4. 34: Schematic depiction of double-tagged pMHC monomers for streamlined generation of distinct pMHC reagents. pMHC FLEXamer complexes are assembled from combinations of double-tagged heavy chains, peptide antigens and ß2 microglobulin. The double-tag consists of a reversible multimerization tag and a site-specific functionalization tag. This allows functionalization and multimerization of nonreversible, reversible or dye-conjugated reversible pMHCs from the same precursor molecule for T cell identification, traceless T cell isolation or TCR avidity measurement respectively.

4.3.2 Cloning of Tub-tag functionalization sequence to Streptamers and refolding of double tagged pMHC monomers

For site-specific conjugation, we first chose a new chemo-enzymatic system, termed Tub-tag[129], which is based on a short hydrophilic, unstructured sequence recognized by tubulin tyrosine ligase (TTL)[161]. It was previously published that TTL-catalyzed attachment of tyrosine derivatives, such as 3-azido-L-tyrosine (Y-N_3), allows subsequent addition of functional groups by highly efficient and mild click chemistry[129]. As shown in Fig. 4.35 A), the Tub-tag sequence was successfully cloned seamless to the 3´-end of the Strep-tagged B*07:02 MHC heavy chain (HC). Double tagged B*07:02 MHC HC was recombinantly expressed and subsequently used to refold B*07:02/pp65$_{417-426}$ pMHC monomers. The chromatogram of the SEC indicated stable refolding of the

double tagged B*07:02 MHC HC into the B*07:02/pp65$_{417-426}$ complex (Fig. 4.35 B).

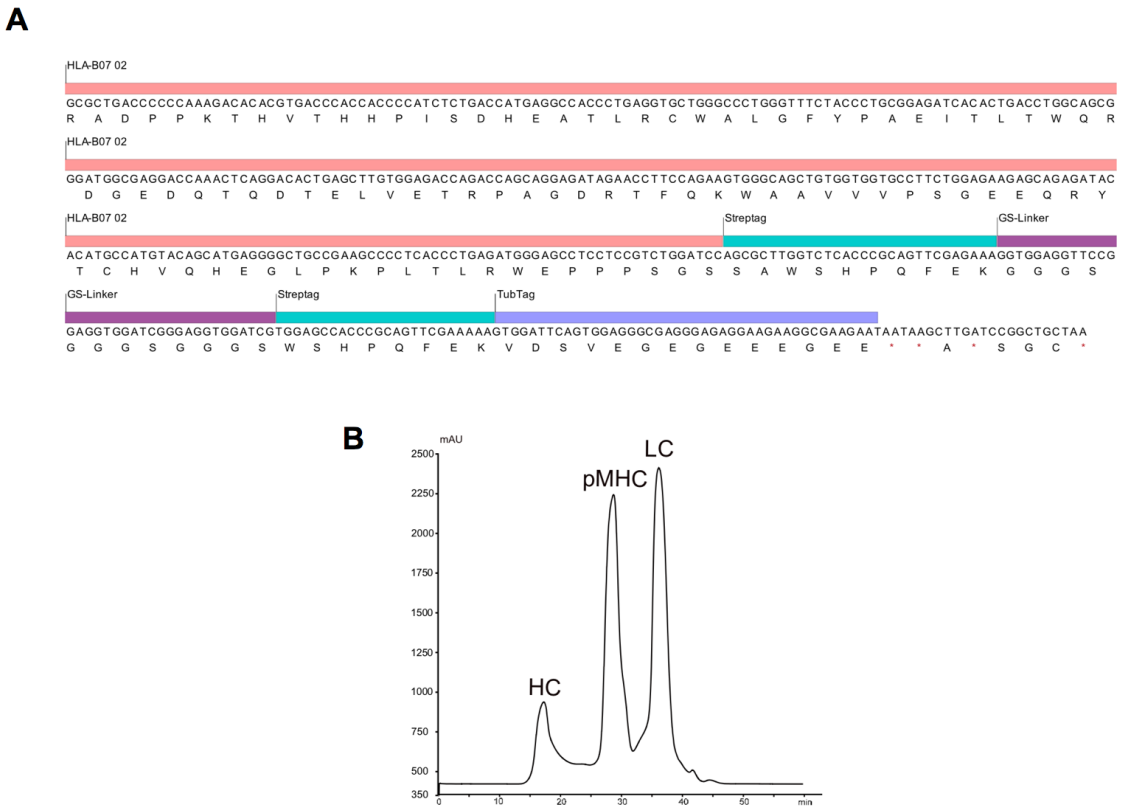

Figure 4. 35: Tub- and Strep-tagged MHC heavy chains can be efficiently assembled into pMHC complexes. A) Coding sequence of B*07:02 fused at the C-terminus to Strep-tag followed by Tub-tag sequence. **B**) Representative size exclusion chromatography profile of B*07:02/pp65$_{417-426}$ pMHC FLEXamer refolding. Fractions of 2nd peak containing double-tagged, monomeric pMHC FLEXamer were collected and pooled. HC: soluble heavy chain aggregates, pMHC: native folded pMHC peak; LC: light chain.

4.3.3 Tub-tagged Streptamers are fully reversible pMHC reagents

To test whether the functionalization-tag interferes with reversibility, we stained and flow-sorted B*07:02/pp65$_{417-426}$-specific CD8$^+$ T cells from peripheral blood of a CMV-seropositive heathy donor either with conventional Streptamers or FLEXamers (Fig. 4.36 A). FLEXamers could stain B*07:02/pp65$_{417-426}$-specific T cells and allowed high purity flow cytometric sorting like conventional Streptamers (Fig. 4.36 B). Upon addition of D-biotin, the pMHC label could be detached. Complete removal of pMHC monomers from the cells is demonstrated by the inability to re-stain the cells by solely adding the Strep-Tactin backbone, whereas addition of the multimerized FLEXamer resulted in efficient re-staining (Fig. 4.36 B).

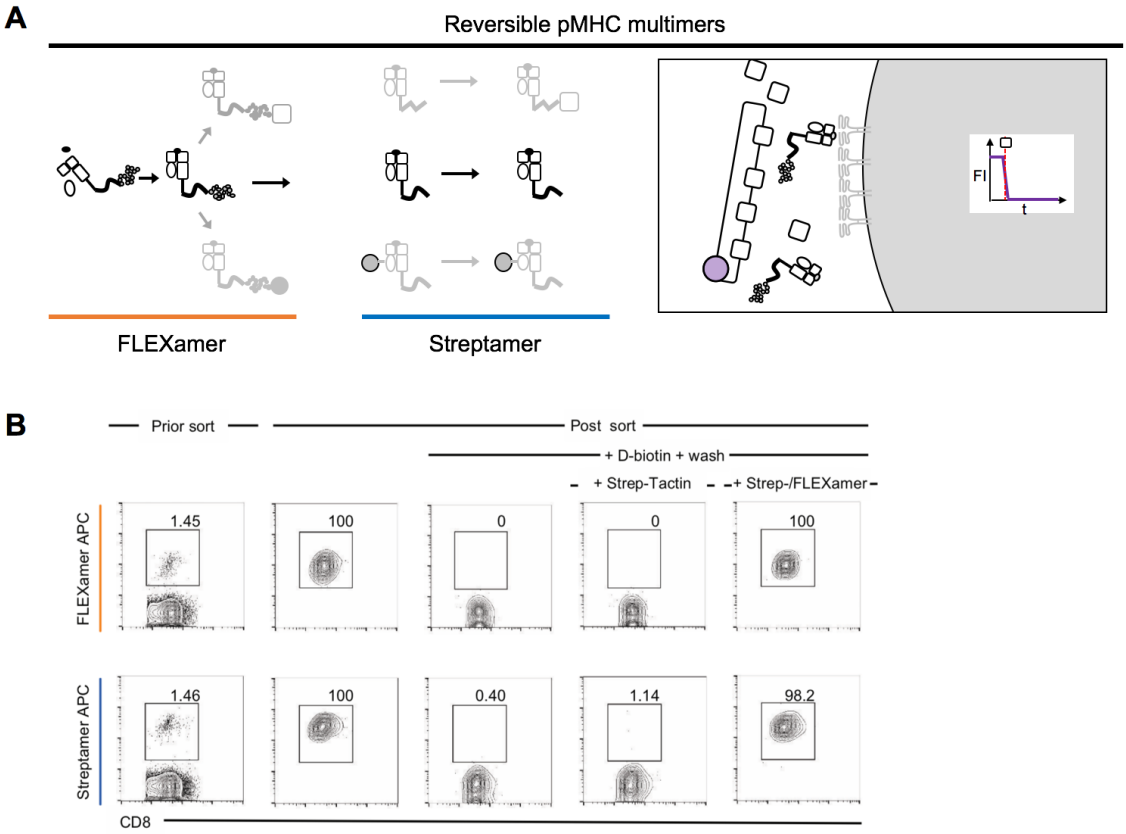

Figure 4. 36 Functionality of unmodified reversible double-tagged FLEXamers compared to Streptamers in traceless T cell isolation. A) Schematic depiction comparing generation of reversible pMHC monomers using FLEXamer or Streptamer technique. **B**) Flow-sort purification and re-staining of B7/pp65$_{417-426}$-specific CD8^{+} T cells from peripheral blood of a CMV-seropositive donor with FLEXamers or conventional Streptamers. Pre-gated on single, living lymphocytes.

4.3.4 Tub-tagged Streptamers can be efficiently functionalized

After validating the functionality of the double tagged FLEXamer precursor pMHC, we performed proof-of-concept experiments to test if we could use the Tub-tag technology[129] to conjugate biotin or dyes to the FLEXamers. We generated two different FLEXamers for the HLA class I heavy chains B*07:02 and B*08:01, which present peptide fragments of the CMV-derived pp65 and IE1, respectively. Tub-tag technology uses a two-step chemo-enzymatic reaction. First, enzymatic activation of the common precursor FLEXamer by TTL with Y-N_3. Second, functionalization of Y-N_3-FLEXamer with dibenzocyclooctyne (DBCO) conjugated probes via click-chemistry. Shift assay and Western Blot of functionalized FLEXamers showed that Tub-tag mediated conjugation of FLEXamerx with biotin (Bio), Atto488 (A488) or sulfo-cyanine5 (sCy5) was highly efficient (Fig. 4.37 A+B).

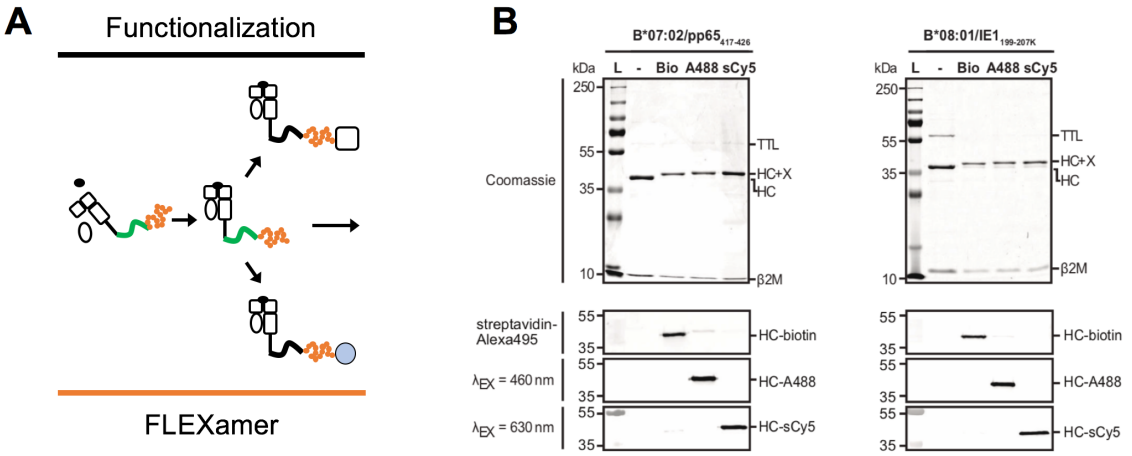

Figure 4. 37: Efficient functionalization of double-tagged FLEXamers with biotin or fluorophores. A) Schematic depiction of FLEXamer-mediated functionalization into distinct pMHC reagents. **B**) SDS-PAGE, followed by Coomassie and Western blot analysis of site-specific labeling of B*07:02/pp65$_{417-426}$ and B*08:01/IE1$_{199-207K}$ heavy chains by TTL-mediated incorporation of 3-azido-L-tyrosine (lane '-') and subsequent click conjugation of DBCO-PEG4-biotin (Bio), DBCO-PEG4-Atto488 (A488) or DBCO-sulfoCy5 (sCy5). 'HC+X' indicates the molecular weight after conjugation of heavy chains (HC). Presence of the respective functional group is shown by streptavidin-Alexa495 based detection of biotin or in-gel fluorescence of A488 and sCy5. Lane 'L' represents the molecular weight marker.

4.3.5 Biotin functionalized FLEXamers are highly functional non-reversible pMHC reagents

Next, we tested the functionality of the biotin-conjugated FLEXamers in comparison to conventionally – via BirA – biotinylated pMHCs (Fig. 4.38 A). To this end, both biotinylated pMHC reagents were multimerized to differently labeled streptavidin backbone and subsequently used to stain Ag-specific cells from peripheral blood of a CMV-seropositive donor. Biotinylated FLEXamers stained B*07:02/pp65$_{417-426}$-specific T cells with high sensitivity and no difference to conventionally biotinylated tetramers (Fig. 4.38 B). An irrelevant epitope/MHC combination (A*02:01/Her2neu$_{369-377}$) served as control for un-specific staining.

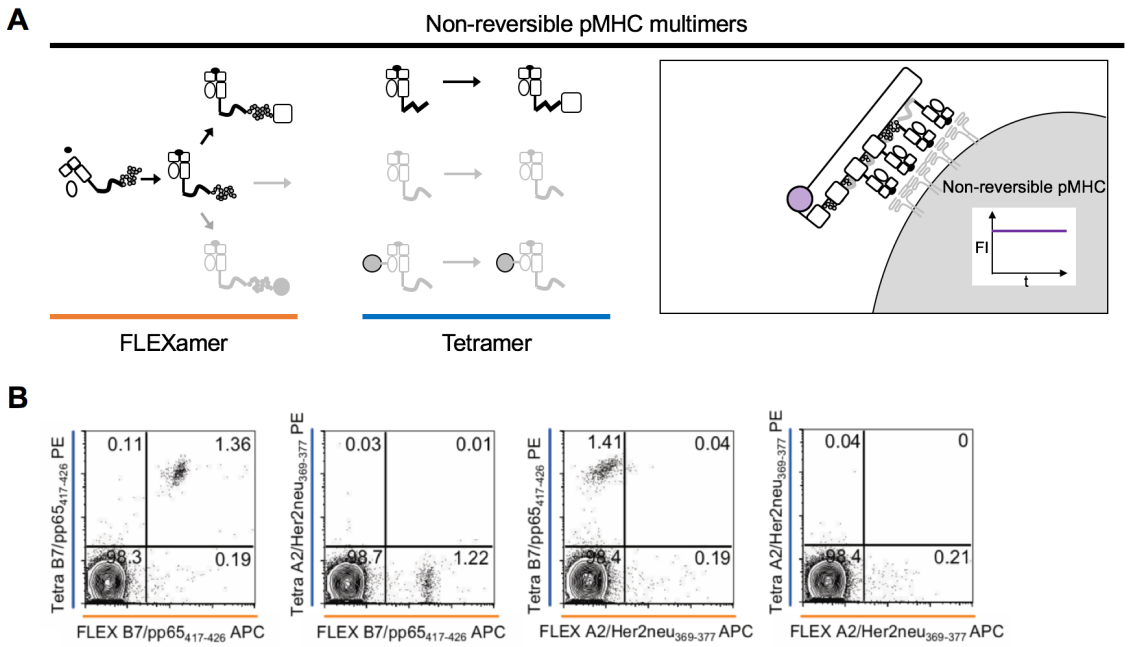

Figure 4. 38 Functionality of non-reversible biotinylated double-tagged FLEXamers compared to conventional tetramers in T cell identification. A) Schematic depiction comparing generation of non-reversible pMHC monomers using FLEXamer or conventional BirA mediated biotinylation. **B**) pMHC multimer staining of B7/pp65$_{417-426}$-specific CD8^{+} T cells from peripheral blood of a CMV-seropositive donor. pMHCs were conventionally biotinylated (Tetra) and multimerized on streptavidin-PE or biotinylated via Tub-tag technique (FLEX) and multimerized on streptavidin-APC. Relevant epitope B7/pp65$_{417-426}$, irrelevant control epitope A2/Her2neu$_{369-377}$. Pregated on single, living CD8+ T cells.

4.3.6 Dye-conjugated FLEXamers allow highly sensitive k_{off}-rate measurement

Conjugation of dyes to Streptamer pMHCs allows direct tracing of pMHC monomer dissociation kinetics on the single-cell level after addition of D-biotin, in order to measure TCR:pMHC k_{off}-rates for TCR structural avidity estimation[53,56](Fig. 4.39 A). When a B*07:02/pp65$_{417-426}$ T cell line was stained with dye-conjugated Streptamers or FLEXamers, the dye-conjugated pMHC monomers showed monomeric pMHC dissociation after initial dye dequenching as previously described[56] (Fig. 4.39 B). Fitting of exponential decay curves yielded defined k_{off}-rates for the TCR:pMHC interaction that were identical for dye-conjugated Streptamers and FLEXamers (Fig. 4.39 D).

Using a double staining with a non-reversible biotinylated pMHC multimer and a reversible dye-conjugated pMHC Streptamer, dissociation kinetics can be tracked without previous purification on a flow cytometer through continuous gating on the non-reversible pMHC multimer+ T cell population[53]. We stained a heterogeneous B*07:02/pp65$_{417-426}$-specific T cell population directly *ex vivo* from

peripheral blood of a CMV-seropositive donor with both non-reversible pMHC conjugated to biotin (multimerized to streptavidin-PE) and reversible pMHC conjugated to A488 (multimerized to Strep-Tactin-APC) (Fig. 4.39 C). Non-reversible pMHC multimers allowed continuous gating on the antigen-specific T cell population after the addition of D-biotin, while the reversible fluorophore-conjugated pMHC monomers dissociated over time (Fig. 4.39 C).

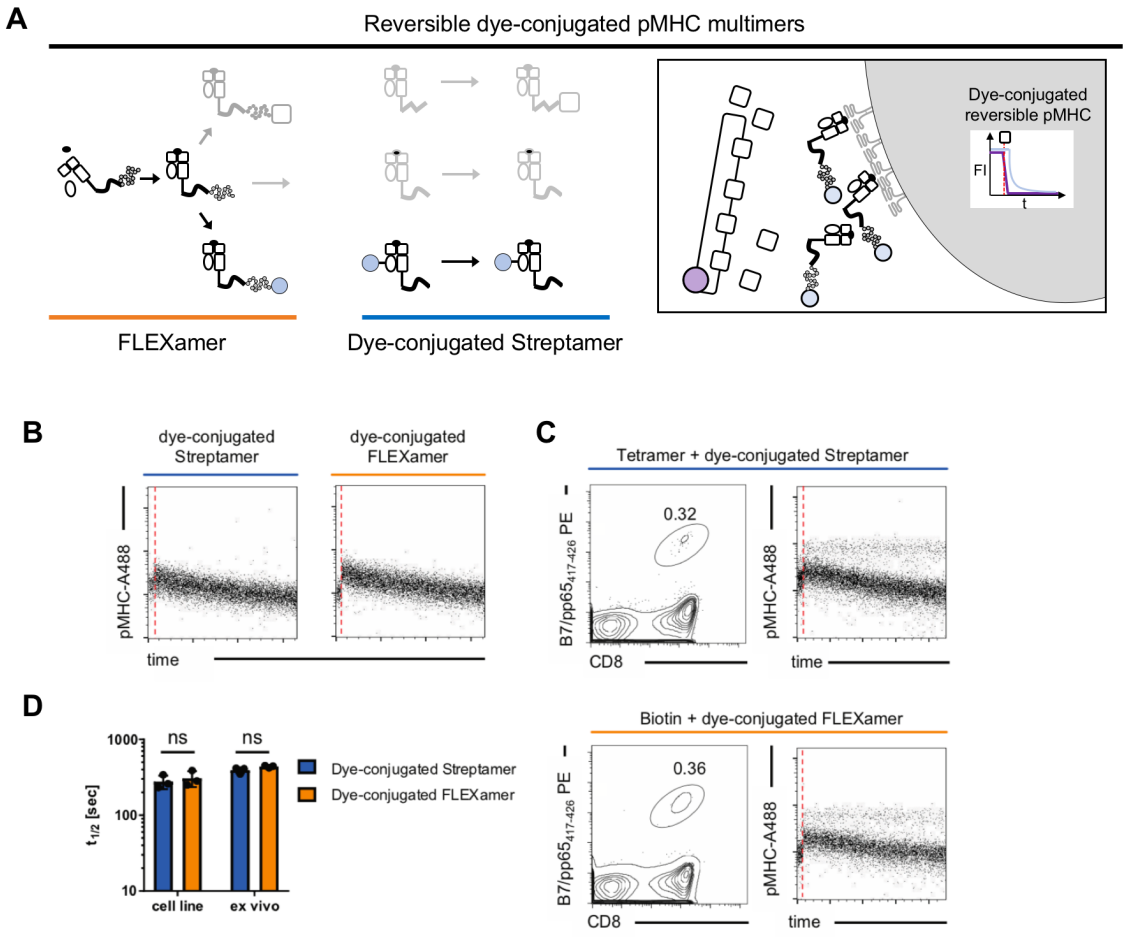

Figure 4. 39 Functionality of dye-conjugated double-tagged FLEXamers compared to dye-conjugated Streptamers in TCR avidity measurement. A) Schematic depiction comparing generation of dye-conjugated reversible pMHC monomers using FLEXamer technique or Maleimide dye-chemistry on Streptamers. **B**) Dissociation kinetics of a B7/pp65$_{417-426}$-specific CD8^{+} T cell line measured with dye-conjugated Streptamers or dye-conjugated FLEXamers. Red dotted line indicates D-biotin addition. **C**) Dissociation kinetics of B7/pp65$_{417-426}$-specific CD8^{+} T cells from peripheral blood of a CMV-seropositive donor, stained with a combination of non-reversible biotinylated pMHCs and reversible dye-conjugated pMHCs. Non-reversible pMHC multimer+ CD8+ T cells are gated for dissociation kinetic of dye-coupled pMHCs after D-biotin addition (red dotted line). **D**) Quantification of technical triplicates of representative experiment shown in B) and C). One symbol represents one dissociation. Unpaired, non-parametric Kolmogorov-Smirnov test. Pre-gated on single, living CD8+ T cells in B) and pre-gated on single, living lymphocytes in C).

4.3.7 Double-tagging of pMHC monomers allows highly efficient and flexible functionalization independent of HLA-allotype and antigen peptide

Encouraged by the much simpler generation process of different pMHC multimer reagents from a single double-tagged FLEXamer precursor, we generated FLEXamers also for other epitope-HLA combinations. We folded in total 26 FLEXamers covering nine HLA class I heavy chains as well as the murine heavy chain H2-Kb (Fig. 4.40 A). The conjugation efficacy with fluorophore or biotin was consistently high for all FLEXamers (Fig. 4.40 B). Due to the skewed frequency distribution of HLA class I alleles, the nine human HLA heavy chains together cover 76,5 % of the EURCAU population (Fig. 4.40 C-D).

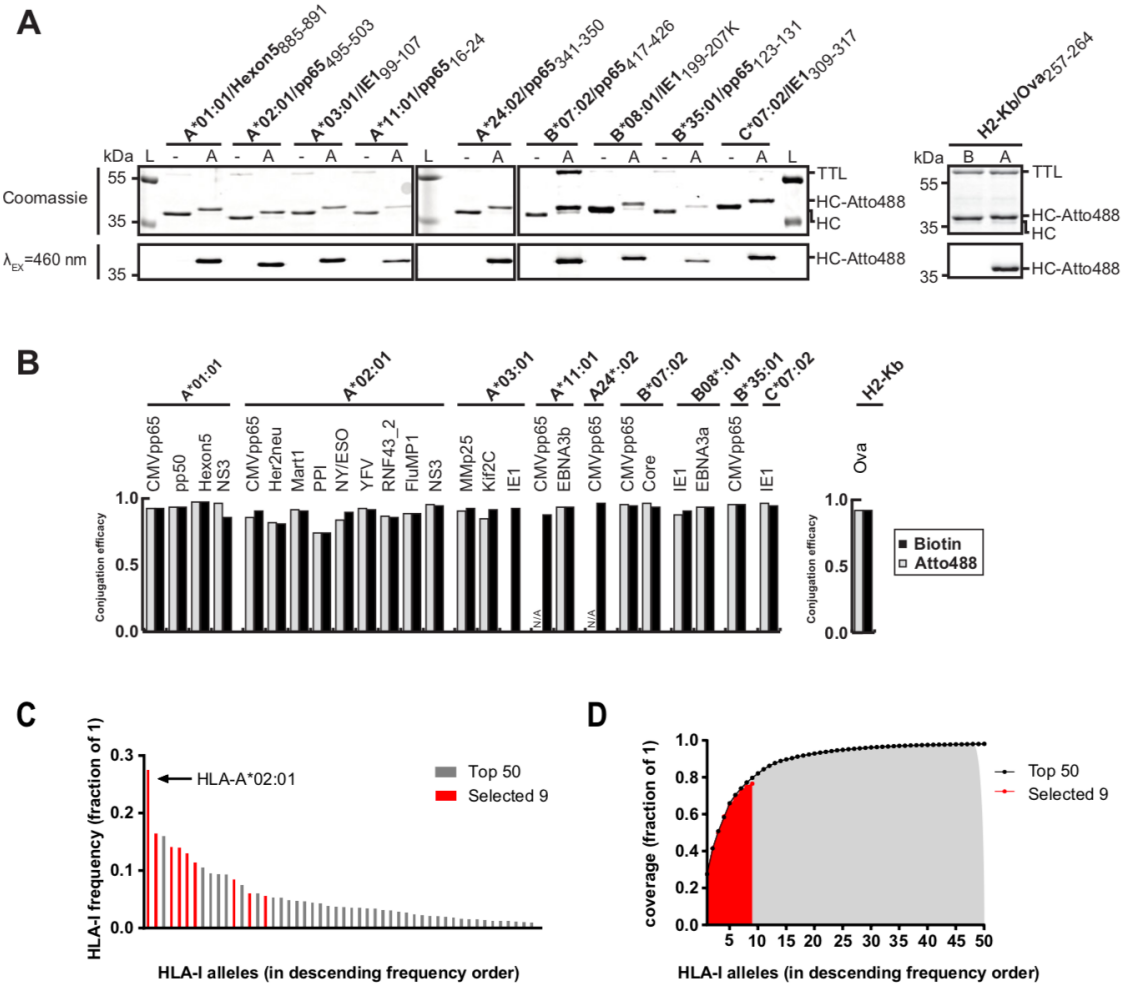

Figure 4. 40: Double-tagged FLEXamers allow highly efficient functionalization irrespective of HLA allotype and presented peptide epitope and can also be transferred to murine MHC. A) SDS-PAGE analysis of site-specific labeling of HLA and MHC monomers by TTL. Incorporation of 3-azido-L-tyrosine ('-') and subsequent click conjugation of DBCO-PEG4-Atto488. 'HC+Atto488' indicates the molecular weight after conjugation of heavy chains (HC). Presence of Atto488 was proven by in-gel fluorescence. 'L' indicates the molecular weight marker. **B**) Conjugation efficacy of all 26 HLA-FLEXamers and murine FLEXamer H2- Kb/OVA coupled to Biotin or Atto488. **C**) 50 most frequent HLA- class I alleles of EURCAU population in descending order with HC used for FLEXamer generation shown in red. **D**) Cumulative coverage

of 50 most frequent HLA- class I alleles (area under the curve in grey) or selected nine FLEXamer HC in red.

4.3.8 FLEXamers can be conjugated to DNA oligonucleotides

Various techniques were developed to tackle the inherent complexity of epitope diversity in pMHC multimer-based immune monitoring. Besides combinatorial fluorophore matrix-based pMHC staining[78,79], DNA barcoding of pMHC reagents[162] has massively enhanced throughput of screening antigen-specific T cell populations and their respective TCR repertoires. Consequently, we set out to test whether Tub-tagged FLEXamers can be conjugated to DNA barcodes.
Fig. 4.41 shows proof-of-concept that single-stranded oligonucleotides can be conjugated to FLEXamers. Oligonucleotide1 (Oligo1) was conjugated using a 4x molar excess over A2/pp65$_{495\text{-}503}$ FLEXamer, additionally A2/ HPV16-E6$_{29–38}$ and A2/HPV16-E7$_{11\text{-}19}$ were labeled with Oligo1 and Oligo2 using an 8x molar excess. Conjugation was analyzed by SDS-PAGE and Coomassie staining, revealing an additional band at approximately 60 kDa representing the MHC HC-oligonucleotide conjugate. A2/pp65$_{495\text{-}503}$ FLEXamer was conjugated with Biotin and Atto488 as control reactions. No conjugation was observed when omitting either azido-tyrosine (wo Y-N3) or the DBCO-containing click reagent (contr) (Fig. 4.41).

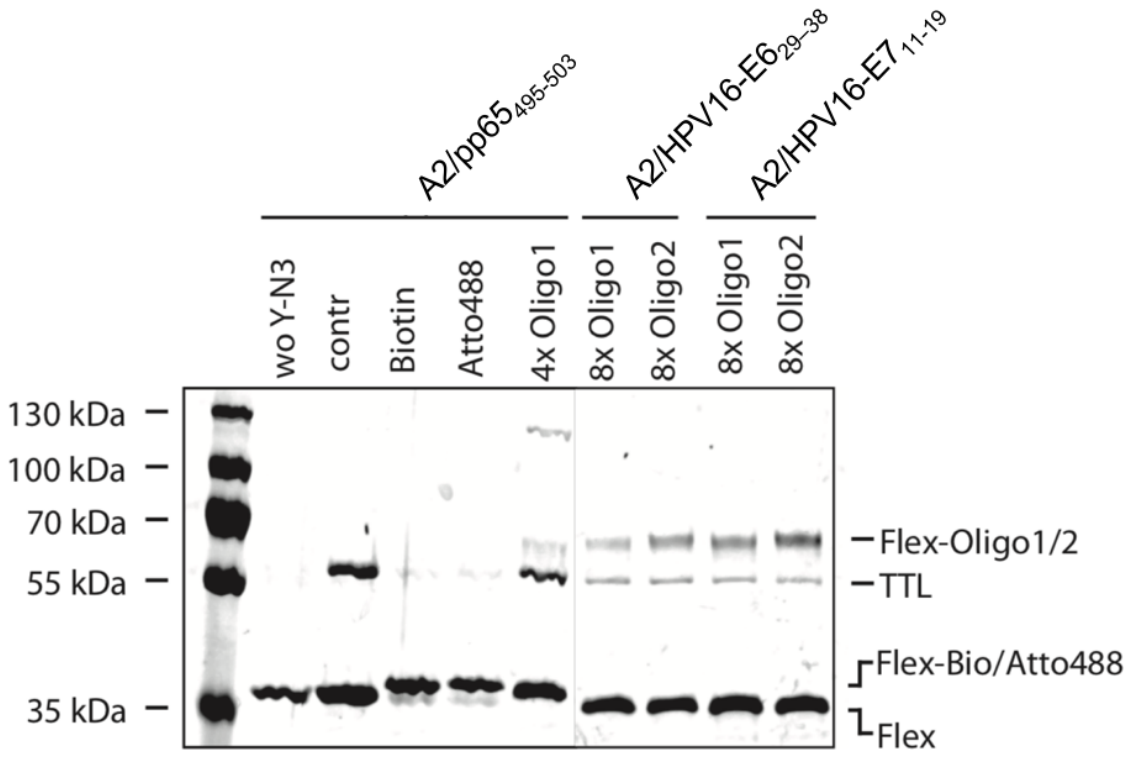

Figure 4. 41: Double-tagged FLEXamers can be functionalized with DNA oligonucleotides. SDS-PAGE analysis of site-specific labeling of HLA by TTL. Incorporation of 3-azido-L-tyrosine ('contr') and subsequent click conjugation of DBCO-PEG4- Atto488, DBCO-PEG4- biotin or DBCO-TEG-oligonucleotides. 'Flex-Bio/Atto488' and 'Flex-Oligo1/2' indicates the molecular weight after conjugation of heavy chains. 'wo- Y-N3' indicates Tub-tag functionalization without addition of 3-azido-L-tyrosine as negative control. Left lane shows the molecular weight marker.

4.3.9 FLEXamers can be armed with toxin and allow killing of Ag-specific T cells

To further test the versatility of the FLEXamer technique, we equipped pMHC FLEXamers with monomethylauristatin F (MMAF), a frequently used antibody drug conjugate (ADC)[163]. Functionality of toxin-armed pMHC reagents has been published previously and was implicated as potential tool to specifically eliminate autoreactive T cells *in vivo*[164,165].

TCR-transgenic T cells specific for A2/pp65$_{495\text{-}503}$ were cultured for 5 d in presence of either MMAF-functionalized relevant pMHC (A2/pp65$_{495\text{-}503}$), MMAF-functionalized irrelevant pMHC (A1/pp65$_{363\text{-}373}$) or MMAF-un-functionalized relevant pMHC (A2/pp65$_{495\text{-}503}$) as control. 0.25 µg or 0.5 µg pMHC monomers were multimerized on Strep-Tactin backbone (SAM2). Fig 4.42 shows proof-of-concept that MMAF functionalized FLEXamers allowed TCR:pMHC-restricted killing of Ag-specific CD8$^+$T cells *in vitro*. Specificity is demonstrated by the fact, that 0.25 µg MMAF coupled A2/pp65$_{495\text{-}503}$ FLEXamers reduced the Ag-specific

CD8$^+$ T cell population down to 15.2 % in comparison to 64.5 % when cells were cultured with un-functionalized A2/pp65$_{495\text{-}503}$ FLEXamers or 60.7 % when cultured with the irrelevant A1/pp65$_{363\text{-}373}$ FLEXamers. Increasing the amount of toxin-armed FLEXamer to 0.5 µg reduced the population of Ag-specific CD8$^+$ T cells down to 4.9 %. However, 0.5 µg un-functionalized relevant FLEXamers does also reduced the size of the Ag-specific population by about 20 % to 43.7 %, which might be explained by activation-induced cell death mediated by excess of pMHC reagent[72]. Increasing the amount of irrelevant toxin-armed A1/pp65$_{363\text{-}373}$ FLEXamer did not affect the size of the Ag-specific CD8$^+$T cell population (Fig 4.42).

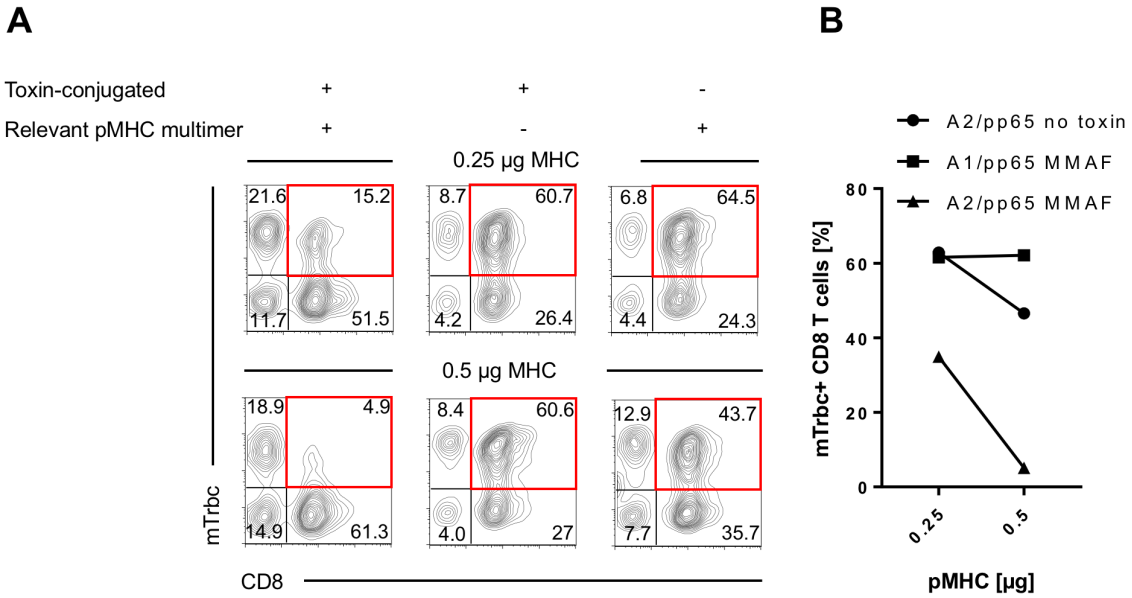

Figure 4. 42: Epitope-driven killing of antigen-specific CD8$^+$T cells using toxin armed double tagged FLEXamers. A) PBMCs transduced with an A2/pp65$_{495\text{-}503}$ specific TCR were cultured as indicated with either relevant or irrelevant pMHCs functionalized with MMAF. MMAF un-functionalized specific pMHC served as additional negative control. After 5d culture, cells were stained with mAbs directed against CD8 and the murine constant region of the T cell receptor beta chain (mTrbc), which is only expressed on the TCR-transgenic T cells. Relevant pMHC: A2/pp65$_{495\text{-}503}$, irrelevant pMHC: A1/pp65$_{363\text{-}373}$. pMHCs were multimerized on Strep-Tactin backbone (SAM2). Pre-gated on single living T cells. A2/pp65$_{495\text{-}503}$ specific TCR 4-2. **B**) Quantification of plots shown in A). Mean of biological duplicates.

4.3.10 FLEXamers can also be generated with Sortase A tag

We wondered whether the advantage of the double tag combining reversibility with versatile functionalization is limited to the specific combination of a Strep-tag and a Tub-tag. To test if this “tag-synergism” is restricted to these to tags, we exchanged the Tub-tag with a sortase A (SrtA) recognition tag. We cloned and refolded an HLA-A*02:01 FLEXamer harboring a SrtA-tag for versatile protein conjugation via transpeptidation[166]. This “SrtA-FLEXamer” construct was

additionally equipped with a His_6-tag for fast and efficient protein purification after transpeptidation (Fig. 4.43 A+B).

Triple (Strep, SrtA, His_6) tagged A*02:01 MHC HC were successfully cloned and refolded into pMHC complex to form A2/$pp65_{495-503}$-SrtA-FLEXamer (Fig 4.43 B+C). Sortase A-mediated transpeptidation allowed efficient functionalization of SrtA-FLEXamers indicated by the faint band at the height of approx. 35 kDa in the column bound fraction (B) compared to the considerable band at the same height in the column unbound fraction (UB) (Fig 4.43 D). Separation of unreacted pMHC educts via the remaining His_6-tag could be verified by the negative control (no addition of SrtA enzyme to SrtA-tagged FLEXamer (Fig 4.43 D).

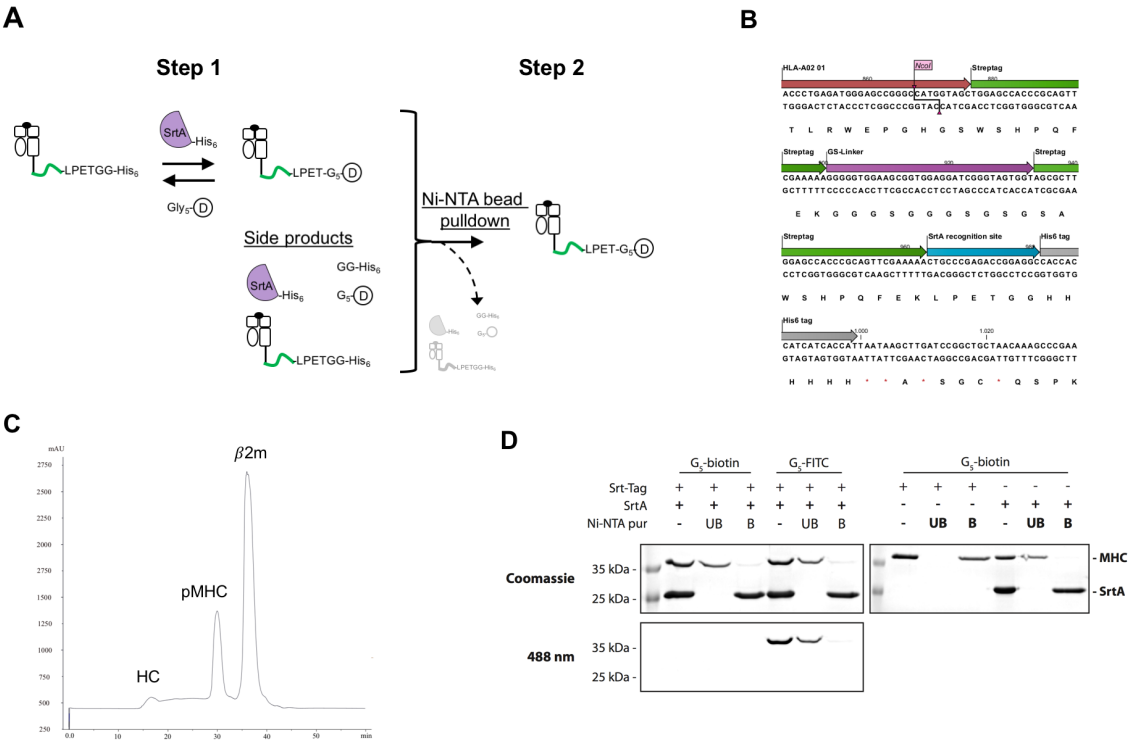

Figure 4. 43 Poly-functionality of double-tagged pMHCs can also be achieved by transpeptidation using a Sortase A recognition tag (SrtA-tag). A) Sketch illustrating the principal of SrtA-/His_6-tagged FLEXamers. **B**) Coding sequence of A*02:01 fused at the C-terminus to Strep-tag followed by SrtA-/His_6-tag sequence. **C**) Representative profile of size exclusion chromatogram. Fractions of 2nd peak containing triple-tagged pMHC monomers were collected and pooled. **D**) SDS-PAGE of SrtA-mediated functionalization of SrtA-tagged FLEXamer (MHC) with biotin or FITC. Transpeptidase reaction components are shown before (-) and after Ni-NTA purification (UB and B). The FLEXamers C-terminal His-tag is replaced with either G_5-biotin or G_5-FITC by the transpeptidation reaction. Labeled FLEXamers remain unbound to Ni-NTA-sepharose beads (UB) whereas the His-tagged SrtA is efficiently captured on the beads (B). Absence of FLEXamer in the bound fraction indicates efficient transpeptidation. Conjugation of FITC is further validated by in-gel fluorescence. Control reactions omitting either SrtA or the Srt- tag show no unspecific coupling.

To test the functionality of the SrtA-FLEXamers, we stained PBMCs transduced with a TCR specific for A*02:01/pp65$_{495-503}$ (TCR 6-2, Thomas R. Müller) with Tub-tag- or SrtA-biotinylated tetramers (Fig. 4.44 A) and also tested reversibility of the SrtA-tag carrying FLEXamer precursor (Fig. 4.44 B). Furthermore, Tub- or SrtA-tag dye-conjugated reversible FLEXamers were tested for characterization of TCR:pMHC k_{off}-rates (Fig. 4.44 C). In each case, SrtA FLEXamers, Tub-tag FLEXamers, and their biotin- or dye-conjugated downstream pMHC products performed equally well (Fig. 4.44 A-D) independent of the respective functionalization strategy. However, compared to Tub-tag, SrtA-mediated pMHC functionalization is overall less efficient which had to be compensated by significantly increased educt consumption. We therefore focused on Tub-tag technology to generate FLEXamers.

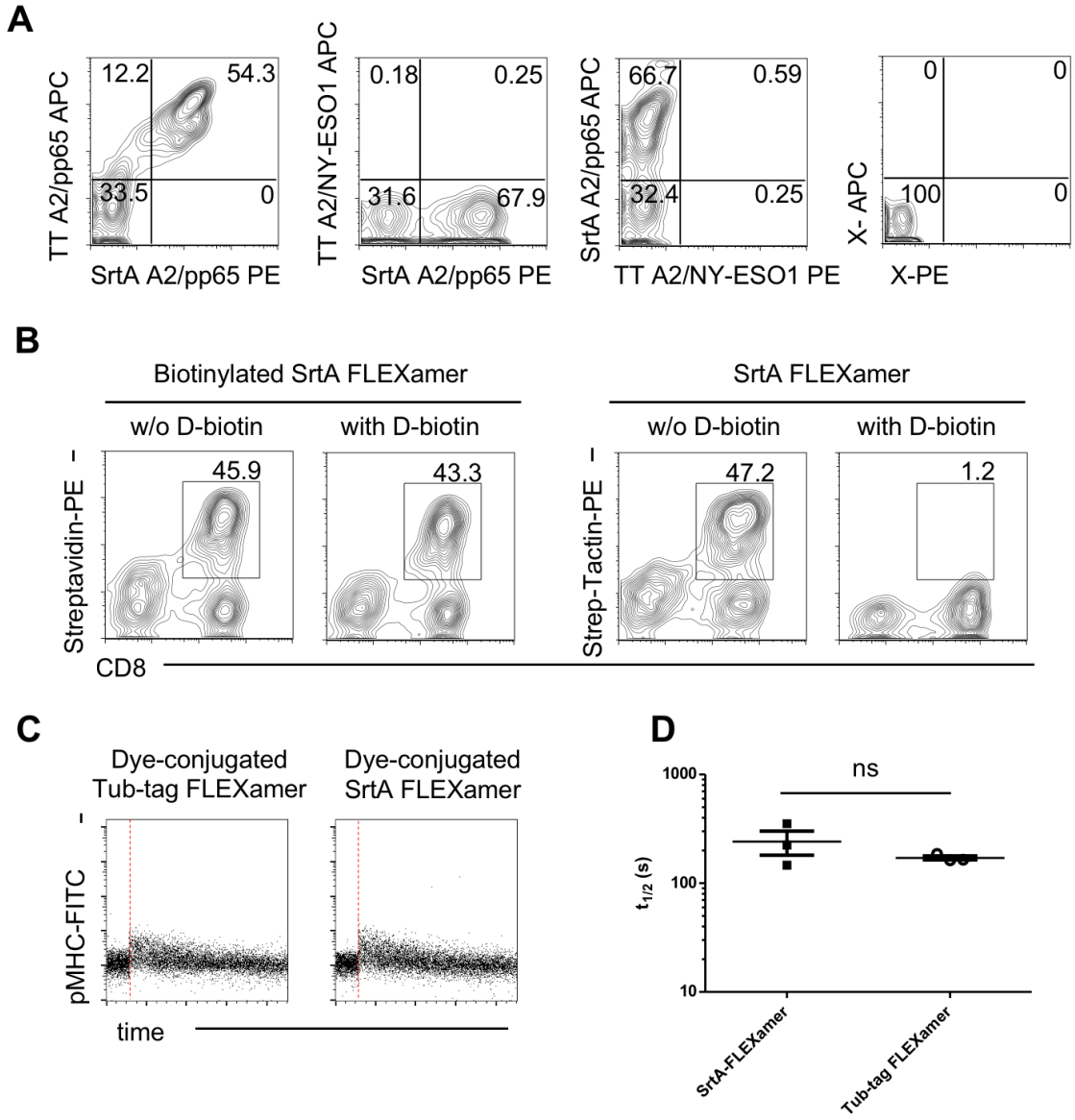

Figure 4. 44: SrtA-FLEXamers perform similar to Tub-tag FLEXamers. A) Staining of PBMCs transduced with an A2/pp65$_{495\text{-}503}$-specific TCR. pMHC reagents were multimerized from pMHC monomers either biotin-functionalized via Tub-tag technique or via SrtA-tag. Staining was performed with a combination of both pMHC reagents. Control stainings were performed with an irrelevant peptide epitope (A2/NY-ESO$_{157\text{-}165}$). **B**) PBMCs transduced with an A2/pp65$_{495\text{-}}$503-specific TCR were stained with either biotin-functionalized SrtA FLEXamers multimerized on streptavidin-PE or with their reversible SrtA FLEXamer precursor multimerized on Strep-Tactin-PE. Samples were incubated with or without D-biotin before acquisition. **C**) Dissociation kinetic of PBMCs transduced with an A2/pp65$_{495\text{-}503}$-specific TCR. Dye-conjugated pMHCs were generated either via Tub-tag technique or via SrtA- tag. Red dotted line indicates injection of D-biotin. **D**) Quantification of technical triplicates of representative experiment shown in C). One symbol represents one dissociation. Unpaired, non-parametric Kolmogorov-Smirnov test. Pre-gated on single, living CD8+ T cells in A), pre-gated on single, living T cells in B) and pre-gated on single, living CD8+ mTrbc+ T cells in C).

4.3.11 Di-peptides allow stable refolding of FLEXamer pMHCs

Various approaches to tackle the complexity resulting from epitope diversity in pMHC based immune monitoring were published recently. UV-cleavable

peptides allow fast peptide exchange for a growing panel of HLA-allotypes[167–169]. However, this technique cannot be used for dye-conjugated pMHCs as dyes get bleached by UV-exposure. Another approach uses low affinity di-peptides that allow stable refolding of pMHC monomers. These “place-holders” can be easily exchanged by incubating di-peptide loaded MHCs with a full length peptide of interest at room temperature[77,132]. We set out to refold A*02:01 with the di-peptide Glycylmethionine (GM) and B*07:02 and B*08:01 with Glycyl-L-leucine (GL), respectively. GM and GL allowed stable folding of pMHC monomers in all three cases (Fig 4.45 A). Relative refolding efficiency was similar for all three di-peptide:MHC monomers with an average absolute yield of about 1 mg pMHC resulting from a standard 200 ml refolding. Of note, di-peptide refoldings yielded comparable results as full-length peptide refoldings (Fig 4.45 B).

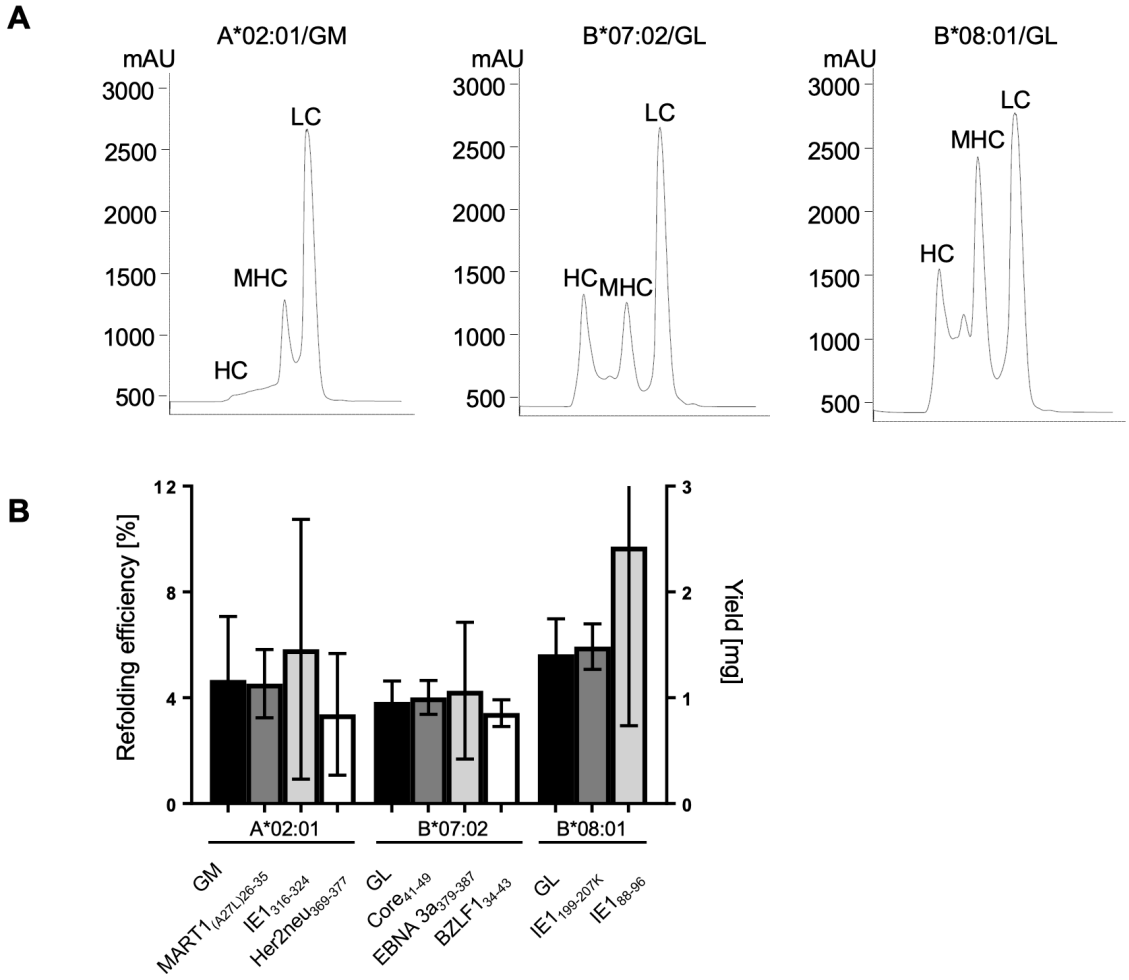

Figure 4. 45: Di-peptides allow efficient refolding of FLEXamer pMHCs. A) Representative size exclusion chromatograms of refoldings using A*02:01/Glycylmethionine (GM) and B*07:02 as well as B*08:01/Glycyl-L-leucine (GL). 2nd peak containing the native pMHC monomers were collected and pooled. **B**) Relative efficiency and yield of di-peptide and standard full-length peptide refoldings. Error bars indicate the standard deviation from the mean average of 4 refoldings.

4.3.12 A*02:01 /GM FLEXamers can be exchanged to full length peptide before or after multimerization of Strep-Tactin

Next, we set out to test whether the di-peptide refolded MHCs can be efficiently loaded with full-length peptides of interest. While the di-peptide exchange technique alone drastically reduces time and labor related to refolding of different full-length peptide/MHC complexes, this technique could also allow screening of antigen-specific T cell populations with a diverse pMHC library, when peptide exchange is performed after multimerization of the MHCs as published recently[170]. Di-peptide loaded MHCs are only stable in the presence of at least 10 mM di-peptide. Below this concentration, the MHCs rapidly degrade (internal communication AG Springer, Jacoby University, Bremen). We used A*02:01/GM FLEXamer and performed the exchange to the $pp65_{495-503}$ full-length peptide either before (+) or after (-) multimerization to Strep-Tactin-APC. A full-length peptide refolded A*02:01/ $pp65_{495-503}$ FLEXamer served as positive control (Fig. 4.46). A*02:01/GM FLEXamer could be efficiently loaded with full-length peptide in their monomeric as well as multimeric form and retained the characteristic reversibility upon incubation with D-biotin (Fig. 4.46).

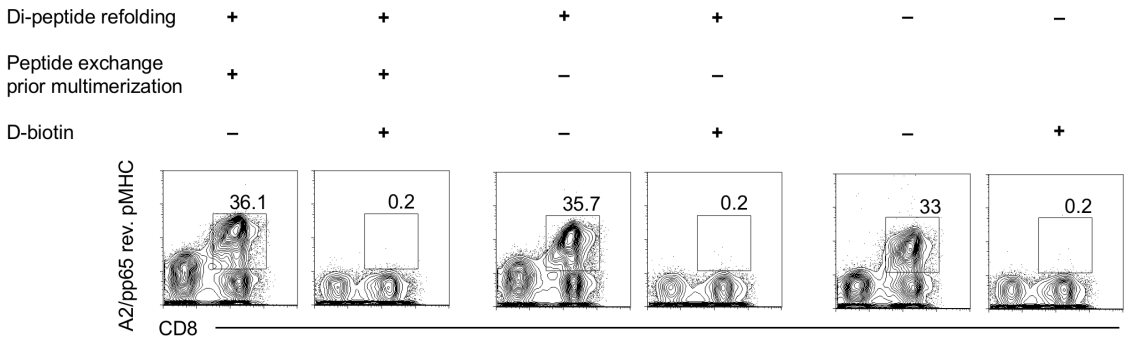

Figure 4. 46: A*02:01/GM FLEXamers can be efficiently loaded with full length peptides prior and post multimerization to Strep-Tactin. PBMCs transduced with an A2/$pp65_{495-503}$-specific TCR were stained with the indicated pMHC reagents. A*02:01/GM FLEXamers were loaded with full length peptide either prior (+) or post (-) multimerization to Strep-Tactin. Full length peptide refolded A2/$pp65_{495-503}$-FLEXamer served as positive control. Samples were incubated with (+) or without (-) D-biotin before acquisition. Pre-gated on single living T cells.

4.3.13 Di-peptide loaded FLEXamers can be functionalized

Following, we tested whether the di-peptide loaded FLEXamers are stable enough to be functionalized before doing the exchange to a full-length peptide of interest. To do so, we supplemented all buffers needed during Tub-tag

functionalization with the corresponding di-peptide to achieve at least a 10mM di-peptide concentration in the final buffer. We performed proof-of-concept experiments using A*02:01/GM as well as B*07:02/GL and B*08:01/GL FLEXamer. Peptide exchange was either performed before or after functionalization (GM/GL or pp65/IE1, respectively) Fig. 4.47 A). Functionalization was efficient with both biotin (Bio) and fluorophore (A488). However, dye conjugation appeared less efficient for B*07:02/GL and B*08:01/GL FLEXamers indicated by the lower band representing un-functionalized MHC HC (Fig. 4.47 A). The resulting biotin functionalized B*07:02/GL FLEXamer performed as well as a full-length peptide refolded B*07:02/pp65$_{417-426}$ FLEXamer when tested on a B*07:02/pp65$_{417-426}$-specific cell line. A*02:01/Her2neu$_{369-377}$ was used as irrelevant pMHC control (Fig. 4.47 B). Also, the resulting dye-conjugated B*07:02/GL FLEXamer showed comparable dissociation kinetics to the full-length peptide refolded dye-conjugated B*07:02/pp65$_{417-426}$-FLEXamer in a k_{off}-rate measurement using a B*07:02/pp65$_{417-426}$-specific cell line (Fig. 4.47 C).

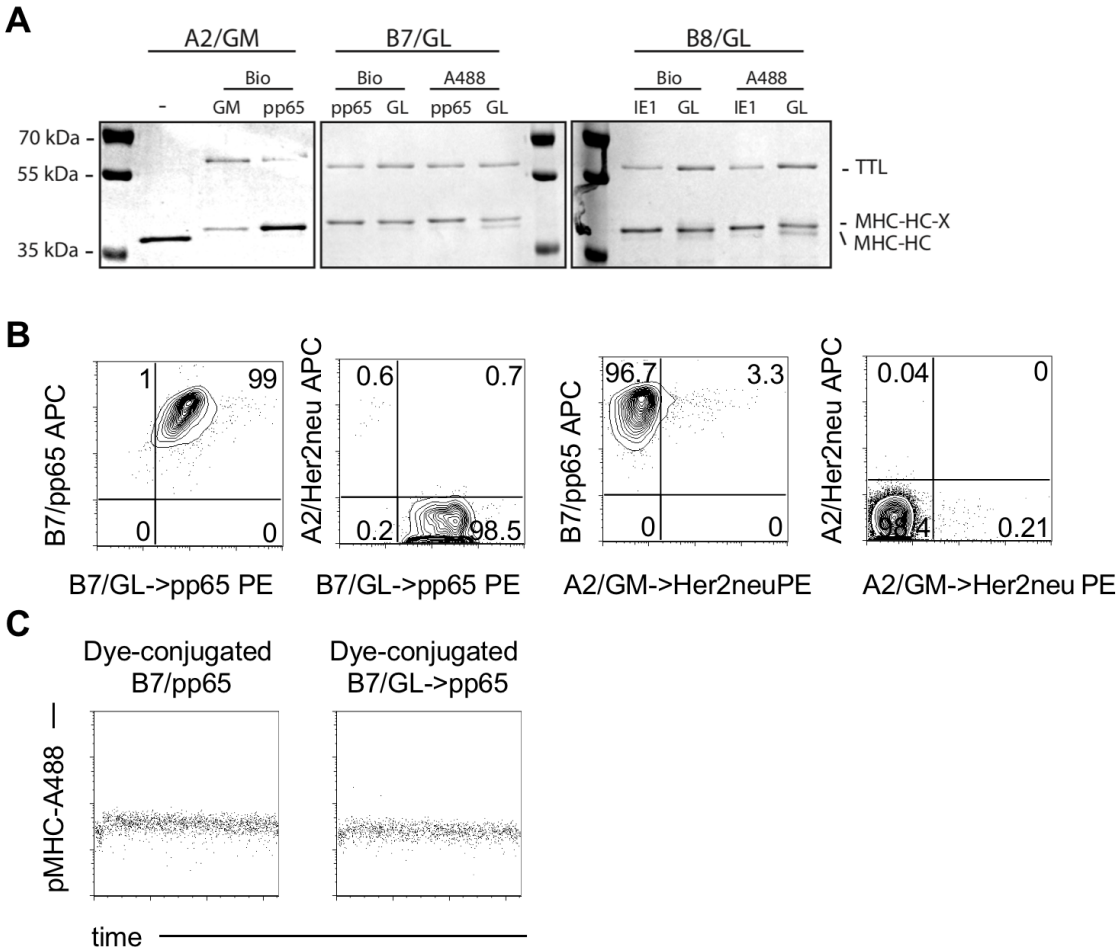

Figure 4. 47: Di-peptide loaded FLEXamers can be functionalized using Tub-tag technique. **A**) SDS-PAGE analysis of site-specific labeling of di-peptide (GM/GL) or full-length peptide (pp65/IE1) loaded FLEXamers. Incorporation of 3-azido-L-tyrosine ('-') and subsequent click conjugation of DBCO-PEG4- Atto488 and DBCO-PEG4- biotin. 'MHC-HC-X' indicates the molecular weight after conjugation of heavy chains. 'MHC-HC' indicates remaining un-functionalized HC. Molecular weight marker with the corresponding size. **B**) Staining of a B*07:02/pp65$_{417-426}$-specific cell line using di-peptide- or full-length peptide loaded, biotin-functionalized pMHC Multimers. pMHC monomers were biotin-functionalized as shown in A), (exchanged to full length peptide) and multimerized to streptavidin PE or streptavidin APC. Control staining was performed with an irrelevant peptide epitope (A*02:01/Her2neu$_{369-377}$). **C**) k_{off}-rate measurement of a B*07:02/pp65$_{417-426}$-specific cell line using di-peptide- or full-length peptide loaded, dye-functionalized pMHC monomers (as shown in A). Dissociation of A488-pMHC monomers over time. Pre-gated on single living CD8+ T cells in B) and C).

5 Discussion

Adoptive T cell transfer against viral infection and cancer has led to outstanding clinical results. T cells within a certain window of high-avidity (optimal avidity) to their target epitope are considered to be most effective for immunotherapy. Mounting evidence suggests that large parts of a T cell's avidity is imprinted within the structure of the TCR. Consequently, immunotherapy using T cells engineered to express optimal avidity TCRs has moved into the focus of current research. Still, *de novo* identification of 'optimal avidity' TCRs poses a significant bottleneck within current TCRs isolation workflows. Although the development of single cell TCR PCR protocols in combination with NGS significantly accelerated identification of new TCR candidates, determination of a T cell's antigen-specificity or avidity upon TCR re-expression is laborious and time consuming. Hence, this thesis aimed at developing a short and robust *in vitro* propagation step that allows clonal expansion of single $CD8^+$ T cells for subsequent validation of pMHC multimer reactivity by pMHC multimer restaining as well as determination of structural TCR avidity by flow cytometry based k_{off}-rate assay *before* identification of the TCR via PCR. This work provides a feeder cell-free single $CD8^+$T cell expansion protocol as well as a multiplex color code staining panel to analyze up to 16 single cell derived clones for pMHC multimer reactivity or structural avidity in parallel. Direct conjunction of feeder cell-free single cell expansion, pMHC multimer reactivity screening and NGS TCR identification allowed the extraction of a large TCR set. Retroviral transfer of TCR candidates validated extraction of functional TCRs from antigen-experienced as well as naïve $CD8^+$T cell repertoires of heathy donors. Furthermore, this thesis describes a novel double tag-based pMHC reagent (FLEXamer) that allows fast and versatile functionalization to streamline the generation process for reversible, non-reversible as well as dye-conjugated reversible pMHC reagents. Implementation of FLEXamers into our pMHC multimer-based TCR isolation and characterization platform further accelerated the identification of new TCR candidates. By combining FLEXamer and dipeptide exchange techniques, we united versatile probe conjugation with fast peptide epitope exchange.

5.1 Short term feeder cell-free single cell expansion

In vitro expansion of primary human PBMCs is subject to inherent natural variation in survival and proliferation of T cells. This variability increases with decreasing cell number per sample and is maximal when looking at single cell level[97]. To minimize variability upon *in vitro* expansion, we set out to establish a feeder cell-free short-term single $CD8^+$ T cell expansion protocol (Fig 4.1, Fig 4.2, and Marten Plambeck, unpublished data). Double pMHC multimer staining of naïve $CD8^+$ T cells enabled identification of rare pMHC multimer-reactive T cells (Fig 4.2 A). Flow cytometry-based single cell sort into 384 well plate filled with CD3/CD28 Expamer and Il-2 as expansion stimuli allowed clonal expansion (Fig 4.2 B) to sufficient size to validate pMHC multimer reactivity by pMHC multimer restaining as well as determination of structural avidity using flow-cytometry based k_{off}-rate assay (Fig 4.2 C+D). T cell clones respond to strong stimulation with decrease in functional avidity by downregulation of TCR and CD8 co-receptor. We therefore used more gently stimulating CD3/CD28 Expamers instead of plate bound CD3/CD28 mAbs. Resting of T cells clones prior to analysis did not increase pMHC reagent stainability (data not shown). Still, TCR and CD8 co-receptor downregulation induced by the stressful feeder cell-free expansion may reduce stainability with pMHC multimers as well as dye-labeled Streptamers for k_{off}-rate measurement in our assay. Accepting this, structural TCR avidity data of T cell clones derived prior to TCR isolation was only used to rank TCR candidates into low and high-avidity. Worth mentioning, the described feeder cell-free single cell expansion protocol was optimized for naïve $CD8^+$ T cells. For expansion of antigen-experienced T cell subsets, adoptions are necessary (Thomas R. Müller, unpublished data). Improvements, such as cytokine cocktails leading to faster or prolonged proliferation (e.g. Il-7; Il-12, Il-15) may be tested in future. However, the current version convinces by its simplicity and reduction of Il-2 and CD3/CD28 Expamer as single stimulation reagent.

5.2 Multiplex analysis of pMHC multimer reactivity and structural TCR avidity from single cell-derived T cell clones

Depending on the size of the antigen-specific target population as well as the amount of starting material, we were able to sort several hundred pMHC

multimer-reactive $CD8^+$ T cells. To reduce the time needed to validate pMHC multimer reactivity and/or structural avidity of the resulting T cell clones, we established a CD45 mAb based multiplex color code (Fig 4.3 A). We chose PB, PO, PC7 and ECD as they were easy to implement in existing staining panels. These 4 colors allowed simultaneous processing and analyzing of up to 16 samples (e.g. single cell derived clones) and thereby screening of more than 120 single cell derived clones per day (chapter 4.2.3). In case of single cell-derived clones, very low cell numbers had to be processed. Additionally, clones needed to be transferred in new wells before pooling to avoid mAb carry over during color coding. Although multiplex color coding significantly reduced time needed for analysis, sample processing remained a rate limiting factor. New sample processing techniques allow thorough sample washing with minimal cell loss (e.g. DA-Cell Technology, Curiox Biosystems). Implementing these techniques into staining routine could further accelerate T cell analysis. Although, we did not see any sign that the of CD45 mAbs influence/alter the k_{off}-rate (data not shown), careful testing of new mAb clones appears mandatory. Alternatively, intracellular dyes, such as cell trace violet (CTV) could replace mAbs completely and avoided any potential interference in TCR:pMHC interaction. However, CTV is toxic and could therefore lead to serious cell loss when processing few hundred cells such as in case of single cell expanded clones.

5.3 Identification, Characterization and Isolation of rare pMHC multimer-reactive T cell populations

To validate our TCR characterization and isolation platform we used 4 different epitope specific T cell populations derived from vaccination induced antigen-experienced (A2/$YFV_{212-222}$) as well as naïve T cell repertoires (A2/$MART1_{(A27L)26-35}$, A2/$Her2neu_{369-377}$, A2/RNF43). We first took advantage of the abundant medium to high-avidity T cells in peripheral blood after YFV vaccination. $CD8^+$ T cell clones generated via feeder cell-free single cell expansion protocol could be analyzed for their structural TCR avidity using flow based k_{off}-rate assay (Fig 4.4 A). Our data mirrored the diverse structural avidity distribution of the A2/$YVF_{212-222}$ specific T cells described previously (Fig 4.4 B). These results verified that we were able to identify T cells above a certain structural TCR avidity by direct conjunction of feeder cell-free single cell expansion and k_{off}-rate measurement.

Determined half-lives allowed to categorize TCRs into low and high structural TCR avidity. TCR PCR and NGS (Thomas R. Müller) allowed robust identification of full paired TCR sequences in all described experiments (Fig. 4.5, 4.11, 4.17, 4.23). The TCR retrieval efficiency of the single clone PCR is limited by the recovery efficiency of the single cell expansion. In our hands, recovery efficiency for the naïve $CD8^+$ T cell repertoire was robustly above 80 %. However, for "hard to expand" (e.g. terminally differentiated) T cell subsets, single cell PCR might be the more efficient option.

Screening the naïve T cell repertoire for $MART1_{(A27)26-35}$-specific T cells using our TCR characterization and isolation platform confirmed the described unusually high precursor frequency of antigen-specific $CD8^+$ T cells. Again, we could validate the pMHC multimer reactivity of sort-purified feeder cell-free single cell-expanded $CD8^+$ T cells (Fig 4.11 A). Interestingly, out of 179 analyzed T cell clones we found only two $MART1_{(A27)26-35}$ pMHC multimer-reactive T cell clone with an k_{off}-rate above detection limit after single cell expansion (Fig 4.11 B). Moreover, none of the A2/$Her2neu_{369-377}$ and A2/RNF43 pMHC multimer-reactive T cell clones possessed a TCR with measureable structural TCR avidity after feeder free single cell expansion (Fig 4.17 A + Fig 4.25 A). This observation may reflect the avidity distribution within the naïve T cell repertoire. It is believed that most antigen-specific T cells within the naïve repertoire possess a low-avidity TCR. Only upon antigen encounter (i.e. infection) functional T cell clones preferentially expand and transit into the memory compartment of the T cell repertoire. However, this finding has to be substantiated by screening further TCRs specific for various epitopes. Still, our platform provides the means to evaluate the avidity distribution within the naïve T cell repertoire.

5.4 In-depth characterization of identified TCR candidates

We successfully re-expressed all identified TCRs in primary human PBMCs (Fig 4.6 A, 4.12 A, 4.18 A, 4.26 A and data not shown). Furthermore, we analyzed pMHC multimer reactivity as well as pMHC multimer specificity of the TCRs by staining TCR transduced T cells either with relevant or irrelevant pMHC multimers (Fig 4.6 B, 4.12 B, 4.18 B, 4.26 B and data not shown). Here, all re-expressed TCRs showed pMHC multimer reactivity – although to varying degree – with exception of the $Her2neu_{369-377}$ TCR H1 and TCR H9 (4.18 B). Of note, these

TCRs also showed the lowest initial APC pMHC MFI in the pMHC multimer re-staining after single cell expansion prior to TCR extraction (Fig 4.17). Our data additionally inform about CD8 dependence in pMHC multimer binding, when looking on TCR-transgenic $CD4^+$ T cells (Fig 4.6 B, 4.12 B, 4.18 B, 4.26 B). We grouped our TCRs binary into CD8-dependent and CD8-independent pMHC multimer binder. However, a more detailed analysis of the degree of CD8-(in-) dependence of the TCRs might reveal interesting information about structural TCR avidity.

None of the listed TCRs showed cross-reactivity against the irrelevant pMHC multimer control (Fig 4.6 A, 4.12 A, 4.18 A, 4.26 A and data not shown).

Analyzing the structural avidity of the TCR-transduced T cells revealed that the 29 TCRs cover a broad k_{off}-rate spectrum ranging from below 30 sec (limit of detection) to above 300 sec of half-life (Fig 4.7 B, 4.13 B, 4.19 B, 4.27 B). Interestingly, a minimal half-life of ~60 sec after feeder-cell-free single cell expansion seemed to predict whether a TCR possessed a measurable k_{off}-rate when transgenically re-expressed (Fig 4.7 C). Still, this tendency has to be validated with further experiments. 4 out of 6 A2/MART1 pMHC multimer-reactive TCRs showed an k_{off}-rate of ~100 sec after transgenic re-expression (Fig 4.13). Two of these TCRs (TCR M2 and M11) were derived from clones that already showed measurable k_{off}-rate before TCR extraction (Fig 4.11 A+B)). This high degree of medium-avidity TCRs among the transgenically re-expressed TCRs against a self-epitope was somehow surprising. However, several reasons may explain this observation. First, the MART1 epitope is likely insufficiently presented in the thymus. Thus, MART1-specific TCRs might undergo no (or less stringent) negative selection, explaining the unusually high number of MART1-specific T cells in the periphery[145]. Additionally, we used the commonly used heteroclitic peptide variant of the A*02:01-restricted MART1 epitope (ELAGIGILTV)[150,151]. Although, it has been proposed that the A27L aa exchange does not influence the peptide presentation to T cells, the aa exchange leads ultimately to the self-epitope “**A**AGIGILTV” turning into the non-self-epitope “E**L**AGIGILTV”. Still, all observations have to be seen with the limitation that we can only judge the avidity of T cells that recover to clone after single cell sort. This technical limitation might bias the avidity distribution of pMHC multimer-reactive TCRs that we are able to identify and isolate.

One out of five A2/Her2neu$_{369-377}$ (Fig 4.19) and one out of three A2/RNF43 (Fig 4.27) pMHC multimer-reactive TCRs showed a measurable k_{off}-rate, respectively. Further validation of functional avidity looking at cytokine secretion after co-culture with peptide-pulsed K562 target cells revealed that the 29 TCRs cover a broad spectrum of peptide sensitivity (Fig 4.8, 4.14, 4.20, 4.28). Preliminary data derived from killing assays indicate that the broad diversity in cytokine secretion is also reflected in the TCRs ability to execute cytotoxicity (Fig 4.8, 4.14, 4.20, 4.29). Summarizing, the identified set of 29 TCRs could all be re-expressed and pMHC multimer reactivity could be confirmed. Furthermore, they cover a broad range of structural and functional avidities. This set of TCRs might help to further analyze the relationship between a TCR's structural avidity and how the TCR inherent binding strength influences functional avidity.

5.5 Correlating functional and structural avidity of identified TCRs

Our platform allowed to gather information about pMHC multimer reactivity and structural TCR avidity of short-term feeder cell-free expanded T cell clones before TCR extraction. Correlating this information to their performance upon transgenic re-expression might help to identify parameters that predict functional TCR avidity. Several groups use pMHC multimer staining intensity as selection criteria for TCR isolation. Although this selection criteria might help to enrich for functional TCRs, this strategy poses the risk to exclude fully functional TCRs with inferior pMHC multimer staining[149,171]. Measuring monomeric TCR:pMHC dissociation rates might allow more robust identification of functional TCRs[52,124]. Our data indicate that both, koff-rate obtained directly after feeder cell-free single cell expansion as well as koff rates of TCR-transuced T cells coincided with functional avidity measured by IFNγ secretion (Fig 4.32+ 4.33). However, these data need to be substantiated with more TCRs to enhance their statistical power. A new innovative approach that enable to determine the half-live of each and every pMHC multimer-reactive T cell already during (index) sorting might help to close this lack of data rapidly (Elvira D´Ippolito, unpublished data). In our hands, pMHC multimer staining intensity of transgenically re-expressed TCRs correlates poorly with IFNγ EC_{50} values Fig 4.32+ 4.33), which is in line with published

findings[172,173]. Correlating the half-lives measured from transgenically-expressed TCRs with their IFNγ EC_{50} values indicates a $t_{1/2}$ cut-off around ~60 sec. Above 60 sec most TCRs possess functional avidity, although to varying degree (Fig 4.39 D), again validating that large parts of the structural avidity is imprinted in the TCR itself[56]. This cut-off value can also be seen when looking at the correlation between initial $t_{1/2}$ (measured before TCR extraction) and transgenic $t_{1/2}$ (upon TCR transfer into primary human PBMCs) (Fig 4.32+ 4.33). Still, half-lives acquired after feeder cell-free single cell expansion have to be seen as guidance for broad avidity categories rather than exact values, as they were derived from a context of strong T cell activation. Therefore, acquired values might note reflect the “true” half-life. However, our data indicate that TCRs with a half-life above 60 sec are with high likelihood also functional when transgenically re-expressed. This data is in line with observations seen for human virus-specific TCRs (Thomas R. Müller, unpublished data) as well as in murine CMV infection models (Kilian Schober, unpublished data). Again, these data set needs to be substantiated with more TCRs for further validation. However, our TCR characterization and isolation platform provides the means to extract fully functional TCRs and gather important information about the relation of structural and functional avidity.

5.6 FLEXamers as basis for versatile pMHC monomer functionalization

Reversible, non-reversible and dye-conjugated reversible pMHC multimers are indispensable tools for in-depth characterization of T cells. However, their conventional generation is a time- and labor-intensive process, as the reagents are made up from three distinct pMHC monomers (Fig 1.5). Consequently, pMHC reagent generation developed to be a significant bottleneck within our pMHC multimer-based TCR characterization and isolation platform. We tested whether the combination of a functionalization-tag and a reversible multimerization-tag fused to pMHC monomers allows to merge the strength of conventionally distinct pMHCs in one common precursor complex (Fig 4.34).

The Tub-tag allows highly efficient and versatile protein functionalization while Strep-tagged pMHCs mediate reversible multimerization to StrepTactin. Both

tags were cloned seamlessly 5´ to the coding sequence (CDS) of HLA-B*07:02 (Fig 4.35 A). *In vitro* refolding of double tagged HLA-B*07:02 formed stable pMHC monomers (Fig 4.35 B) and indicated that the double tag does not sterically impair the tertiary structure of the complex.

5.7 FLEXamers are highly functional pMHC reagents

Direct comparison of double tagged B7/pp65$_{417-426}$-Flexamers and Streptamers in flow cytometry-based purification of a CMV-specific CD8$^+$ T cell population revealed that FLEXamers stained even small antigen-specific T cell populations as sensitively and specifically as Streptamers. We also confirmed that the FLEXamer complex can be disrupted upon addition of D-biotin (Fig 4.36). Consequently, the Tub-tag did not impair the multimerization of the pMHC monomers via the Strep-tag and did not alter the reversible nature of the Strep-tag:Strep-Tactin interaction.

Tub-tag technology allowed site-directed protein functionalization in a chemo-enzymatic reaction (Fig 4.37 A). TTL mediates attachment of Y-N_3 which serves as a handle to covalently link DBCO-functionalized groups via click chemistry. Conjugation experiments indicated that the TTL mediated highly efficient ligation of Y-N_3 to FLEXamers as coupling of Y-N_3-FLEXamers with DBCO-biotin/A488/sCy5 resulted in almost complete turnover into functionalized pMHC monomers (Fig 4.37 B). These data confirmed that Tub- and Strep-tagged FLEXamers are fully functional reversible pMHC monomers which additionally serve as a precursor to add biotin and fluorophores with high efficiency.

Functional tests compared biotin functionalized FLEXamers to conventionally generated tetramers (Fig 4.38) and fluorophore-conjugated FLEXamers with conventionally generated fluorophore-conjugated Streptamers (Fig 4.39). Both, biotin-conjugated and fluorophore-conjugated FLEXamers performed equally good as conventionally generated pMHC reagents (Fig 4.38 B and Fig 4.39 B-D). These data demonstrated that FLEXamers represent a mean to generate functionalized pMHC monomers significantly faster compared to conventional pMHC functionalization while simultaneously ensuring high quality of the generated pMHC reagents. As all reagents are produced from a single precursor construct, the FLEXamer technique also allows to reduce batch to batch variability between different pMHC reagents.

5.8 FLEXamer technique can be applied to a broad set of HLA-allotypes

We cloned and refolded 26 FLEXamers covering nine human HLA class I heavy chains as well as the murine heavy chain H2-Kb, which is frequently used in pre-clinical mouse models (Fig 4.40). In all cases, conjugation efficacy was consistently high, indicating that the FLEXamer technique can be presumably applied for all MHC class I complexes of interest (Fig 4.40 A+B). We chose a set of nine HLA-allotypes which cover – due to the skewed frequency distribution of the HLA class I alleles – together 76,5 % of the EUROCAU population and also entail two allotypes (A*24:02 and A*11:01) which are highly prevalent in Asian populations (Fig 4.40 C+D). The ligation efficacy of TTL to the protein of interest (and consequently the conjugation efficacy via click chemistry) is significantly influenced by the steric accessibility of the Tub-tag. We fused the Tub-tag to the C-terminus of the MHC HC, which poses the most solvent exposed site of the heterotrimeric complex as it – in the native protein – anchors the complex into the membrane of the antigen presenting cell. Additionally, this site of the protein is spatially most distant to the TCR:pMHC interface and has therefore minimal risk to interfere with proper antigen recognition by cognate T cells.

5.9 FLEXamers can be equipped with a variety of functional groups

DNA barcoding of pMHC multimers allows parallel detection and subsequent sequencing of various different antigen-specific T cells and opened new avenues for in-depth TCR repertoire analysis. However, current methods to generated DNA-barcoded pMHC multimers add biotinylated pMHC monomers and biotinylated DNA-barcode to fluorophore labeled streptavidin, which then competes for biding to the same scaffold. Although added in a defined ratio, the amount of DNA-barcode and pMHC monomer per backbone is hard to control, leading to varying staining and sequencing quality of the resulting pMHC multimer. The FLEXamer technique could allow to tackle this issue as it i) allows equimolar pMHC:oligomer conjugation and ii) multimerization is mediated by the (DNA-barcoded) FLEXamer via the Strep-tag. Thus, no competition effects in multimerization should occur. Proof-of-concept conjugation experiments showed that DNA-barcodes can be conjugated to FLEXamers (Fig. 4.41). However,

conjugation efficacy was considerably lower than for all other tested functional groups. This might be explained be the fact that DNA strands are about 30x heavier than dyes or biotin. Additionally, DNA can form bulky tertiary structures which could sterically hinder close orientation of the N3 and DBCO group to react with each other. Future experiments need to determine whether the achieved conjugation is sufficient to achieve satisfactory sequencing results. To further improve conjugation efficacy, organic solvents such as DMSO should be tested that might support the click chemistry reaction of bulky functional groups.

pMHC multimers were developed and are primarily used to label antigen-specific T cells. Although reversible, non-reversible and dye-conjugated reversible pMHC monomers form three distinct pMHC multimers with unique properties, their main purpose is the identification and characterization of antigen-specific $CD8^+$ T cells mediated by the highly specific TCR:pMHC interaction. However, it was recently shown that this TCR:pMHC interaction can also be used to specifically eliminate autoreactive $CD8^+$ T cells *in vivo.* Here, pMHC multimers were equipped with an alpha-emitting radiopharmaceutical which selectively depleted defined $CD8^+$ T cell population while the general immune function remained uneffected[164]. However, a weakness of the described “suicide pMHC tetramers” results from their production process. For multimerization, biotinylated pMHC monomers and biotinylated radiolabel is added to a streptavidin backbone. Although done in a defined ratio, this leads to a barely controllable arming of pMHC tetramers with the radiopharmaceutical, which might result in dramatic shifts of the therapeutic window of such reagents. We conjugated FLEXamers to the toxin MMAF as this allows a controlled 1:1 molar ratio of toxin:pMHC monomer, which should result in a more defined suicide pMHC multimer. *In vitro* proof-of-concept experiments with MMAF armed FLEXamers demonstrated selective killing of antigen-specific $CD8^+$ T cells, while toxin-armed irrelevant FLEXamers did not reduce the frequency of the target population (Fig 4.42). However, we also detected toxin-independent killing induced by the unarmed relevant FLEXamers likely resulting from activation induced cell death (Fig 4.42). This finding underlines that toxin-armed pMHC multimers have a small therapeutic window. Therefore, strict control of arming efficiency of suicide pMHC multimers is essential, which can be achieved by the FLEXamer technique. Still, most autoimmune diseases are $CD4^+$

T cell-mediated. Consequently, for therapeutic applications toxin-armed FLEXamers have to be generated from MHC class II complexes.

5.10 FLEXamers can be generated with different functionalization tags

We could prove that the Tub- and Strep-tag can be combined to allow versatile probe conjugation with reversible multimerization of pMHC monomers. To test, whether this “tag-synergism” is restricted to the Tub-and Strep-tag combination, we generated SrtA-FLEXamers that should allow probe conjugation via transpeptidation. Additionally, this construct harbored an His_6-tag, to enable simple depletion of educts during downstream processing using Ni-NTA columns (Fig 4.43 A+B).

Strep-SrtA-His_6-tagged A*02:01 was recombinantly expressed and used to refold A*02:01/$pp65_{495-503}$ pMHC monomers. The chromatogram of the SEC indicated stable refolding of the triple tagged A*02:01 MHC HC into the A*02:01/$pp65_{495-503}$ complex Fig. 4.43 C). Sortase A mediated efficient functionalization of SrtA-FLEXamers while the His-tag allowed depletion of residual His-tagged educts and His-tagged Sortase A enzyme in downstream purification (Fig. 4.43 D).

Unconjugated as well as biotin- and fluorophore- conjugated SrtA-FLEXamer was subsequently compared against Tub-tag-FLEXamers. Reversible, non-reversible as well as reversible dye-conjugated FLEXamer reagents performed equally well in staining experiments, independent of the respective functionalization strategy (Fig 4.44 A-D). We conclude that the tag-synergism combining one functionalization tag with one reversible multimerization tag can be transferred to any tags mediating these characteristics.

5.11 Combining di-peptide exchange and FLEXamer technique

Our data demonstrate that the FLEXamer technique allows fast and efficient probe conjugation of pMHC monomers. Consequently, for each allotype of interest only one plasmid and its corresponding protein has to be generated to produce a large set of differentially functionalized pMHC monomers. This streamlines the production of pMHC reagents significantly. Still, for each epitope a new refolding has to performed. Therefore, we set out to combine the

FLEXamer technique with the di-peptide exchange technique, which allows rapid epitope loading of MHCs. We successfully tested the di-peptides GM and GL for refolding of A*02:01, B*07:02 and B*08:01 FLEXamers, respectively (Fig 4.45 A). Interestingly, refolding efficiency as well as total yield of di-peptide refoldings was comparable to standard full-length peptide refoldings (Fig 4.45 B).

In principle, the di-peptide exchange technique allows pMHC multimer based screening of a diverse TCR repertoire in a microtiter plate. To achieve this miniaturization, yet unexchanged dipeptide MHCs are multimerized to a backbone as the first step. Following, the peptide exchange is performed as the second step leaving in each well a different pMHC reagent. To prove this concept, we exchanged A*02:01/GM FLEXamers with full-length peptide prior or post multimerization to Strep-Tactin backbone. Both pMHC reagents stained A2/pp65-specific T cells as good as full-length peptide refolded pMHC reagents (Fig 4.46). These data indicate, that i) FLEXamers can be easily combined with di-peptide exchange technique and ii) that this combination allows rapid generation of a diverse pMHC multimer library in microtiter plates. If this finding can be generalized to other di-peptide/allotype combinations remains to be tested. Each allotype has a unique peptide binding grove and therefore a characteristic ability to bind a certain peptide repertoire. If a given allotype binds a di-peptide with sufficient affinity to allow stable refolding and efficient peptide exchange remains to be tested empirically for each di-peptide/MHC combination.

To further merge the FLEXamer and di-peptide exchange technique, we evaluated if di-peptide-loaded pMHC monomers can be functionalized with biotin or A488. Di-peptide loaded FLEXamers remain stable over the course of the two-step chemo-enzymatic reaction and can be functionalized with the same high efficiency as full-length peptide refolded pMHCs (Fig 4.47 A). Resulting biotin and A488 functionalized FLEXamers proved to be as functional as their full-length peptide loaded counterparts (Fig 4.47 B+C).

6 Summary

Immunotherapy using naturally occurring pathogen- or tumor-specific T cells as well as receptor-transgenic T cells showed outstanding results in several clinical studies. Recently, CAR-transgenic T cells were FDA-approved for the treatment of lymphomas. Intensive research focuses on the optimization of TCR-transgenic T cells for the use in immunotherapy, which will further broaden the spectrum of treatable cancer and other disease entities. Still, *de novo* identification of TCRs providing optimal functionality remains a bottleneck in current TCR characterization and isolation workflows. We developed a short-term feeder cell-free single $CD8^+$ T cell expansion protocol that allows the validation of pMHC multimer reactivity by pMHC multimer restaining as well as structural TCR avidity measurement by flow cytometry-based k_{off}-rate measurement *before TCR identification*. Direct conjunction of the screening for pMHC multimer binding with TCR sequencing allowed the identification of 28 TCRs. All TCRs could be transgenically re-expressed in primary human PBMCs and showed a broad range of structural and functional avidities. This set of TCRs will help to further study the relationship between structural and functional avidity. Consequently, these first results point towards the urgent need to establish more versatile technologies for fast and efficient characterization and isolation of TCRs for immunotherapy. Therefore, we developed a novel double-tagged pMHC monomer (FLEXamer), which allows versatile probe conjugation to generate distinct pMHC reagents from a single precursor. FLEXamers performed in all functional tests as well as conventionally generated pMHC multimers, while being produced considerably faster and in a more standardized manner. We successfully combined FLEXamer reagents with the di-peptide exchange technique for rapid peptide loading. Merging the FLEXamer and di-peptide exchange technique allows to generate a diverse set of functionalized pMHC reagents from a single precursor protein and additionally fast and efficient peptide loading to generate a large pMHC multimer library. Combining the FLEXamer and di-peptide exchange technique with our TCR characterization and isolation platform will accelerate the *de novo* identification of TCR for the use in immunotherapy.

7 References

1. Davis, M. M. & Bjorkman, P. J. T-cell antigen receptor genes and T-cell recognition. *Nature* **334,** 395–402 (1988).
2. Swain, S. L., Mckinstry, K. K. & Strutt, T. M. Expanding roles for CD4+ T cells in immunity to viruses. *Nat Rev Immunol* **12,** 136–148 (2013).
3. Bridgeman, J. S., Sewell, A. K., Miles, J. J., Price, D. A. & Cole, D. K. Structural and biophysical determinants of αβ T-cell antigen recognition. *Immunology* **135,** 9–18 (2012).
4. Garcia, K. C. *et al.* An αβ T Cell Receptor Structure at 2 . 5 Å and Its Orientation in the TCR-MHC Complex. *Adv. Sci.* **274,** 209–219 (2009).
5. Garboczi, D. N. *et al.* Pillars Article : Structure of the Complex Between Human T-Cell Receptor , Viral. (2015).
6. Zarnitsyna, V. I., Evavold, B. D., Schoettle, L. N., Blattman, J. N. & Antia, R. Estimating the diversity, completeness, and cross-reactivity of the T cell repertoire. *Front. Immunol.* **4,** 1–11 (2013).
7. Qi, Q. *et al.* Diversity and clonal selection in the human T-cell repertoire. *Proc. Natl. Acad. Sci.* **111,** 13139–13144 (2014).
8. Venturi, V. *et al.* Sharing of T cell receptors in antigen-specific responses is driven by convergent recombination. *Proc. Natl. Acad. Sci.* **103,** 18691–18696 (2006).
9. Elhanati, Y., Murugan, A., Callan, C. G., Mora, T. & Walczak, A. M. Quantifying selection in immune receptor repertoires. *Proc. Natl. Acad. Sci.* **111,** 9875–9880 (2014).
10. Alam, S. M. *et al.* T-cell-receptor affinity and thymocyte positive selection. *Nature* **381,** 616–620 (1996).
11. Jameson, S. C. & Hoquist, Kristin A and Bevan, M. B. Positive Selection of Thymocytes. 2–5 (1995).
12. Schober, K., Buchholz, V. R. & Busch, D. H. TCR repertoire evolution during maintenance of CMV-specific T-cell populations. *Immunol. Rev.* **283,** 113–128 (2018).
13. Moon, J. J. *et al.* Naive CD4+ T cell frequency varies for different epitopes and predicts repertoire diversity and response magnitude. *Immunity* **27,** 612–625 (2007).
14. Blattman, J. N. *et al.* Estimating the Precursor Frequency of Naive Antigen-specific CD8 T Cells. *J. Exp. Med.* **195,** 657–664 (2002).
15. Alanio, C., Lemaitre, F., Law, H. K. W., Hasan, M. & Albert, M. L. Enumeration of human antigen – specific naive CD8+ T cells reveals conserved precursor frequencies. *Blood* **115,** 3718–25 (2010).
16. Langman, R. E. & Cohn, M. The E-T (Elephant-Tadpole) paradox necessitates the concept of a unit of b-cell function: The protecton. *Mol. Immunol.* **24,** 675–697 (1987).
17. Rammensee, H. G., Falk, K. & Rötzschke, O. Peptides naturally presented by MHC class I molecules. *Annu. Rev. Immunol.* **11,** 213–44 (1993).
18. Schumacher, T. N. M. & Ploegh, H. L. Are MHC-bound peptides a

nuisance for positive selection? *Immunity* **1,** 721–723 (1994).
19. Bjorkman, P. J. *et al.* Structure of the human class I histocompatibility antigen, HLA-A2. *Nature* **329,** 506–12 (1987).
20. Klein, J., Sato, A. & Rosen, F. The HLA System First of Two Parts. *New Engl. J. Med. Rev.* **343,** 702–709 (2000).
21. Falk, K., Rötzschke, O., Stevanović, S., Jung, G. & Rammensee, H. G. Allele-specific motifs revealed by sequencing of self-peptides eluted from MHC molecules. *Nature* **351,** 290–296 (1991).
22. Gragert, L., Madbouly, A., Freeman, J. & Maiers, M. Six-locus high resolution HLA haplotype frequencies derived from mixed-resolution DNA typing for the entire US donor registry. *Hum. Immunol.* **74,** 1313–1320 (2013).
23. Neefjes, J. & Ploegh, H. surface expression and the association of HLA class I heavy chain with β2-microglobulin: differential effects of inhibition of glycosylation on class I subunit association. *Eur. J. Immunol.* 801–810 (1988).
24. Carrington, M. & O'Brien, S. J. The Influence of *HLA* Genotype on AIDS. *Annu. Rev. Med.* **54,** 535–551 (2003).
25. Hedrick, P. W. & Thomson, G. A two-locus neutrality test: Applications to humans, E. coli and lodgepole pine. *Genetics* **112,** 135–156 (1986).
26. Schmidt, A. H. *et al.* Estimation of high-resolution HLA-A, -B, -C, -DRB1 allele and haplotype frequencies based on 8862 German stem cell donors and implications for strategic donor registry planning. *Hum. Immunol.* **70,** 895–902 (2009).
27. Del Val, M., Schlicht, H. J., Ruppert, T., Reddehase, M. J. & Koszinowski, U. H. Efficient processing of an antigenic sequence for presentation by MHC class I molecules depends on its neighboring residues in the protein. *Cell* **66,** 1145–1153 (1991).
28. Kloetzel, P. M. Antigen processing by the proteasome. *Nat. Rev. Mol. Cell Biol.* **2,** 179–187 (2001).
29. Cohn, M. Dissecting the two models of TCR structure–function relationships. *Immunol. Res.* **64,** 795–803 (2016).
30. Evavold, B. D. & Allen, P. M. Separation of IL-4 production from Th cell proliferation by an altered T cell receptor ligand. *Science (80-.).* **252,** 1308–1310 (1991).
31. Evavold, B. D., Sloan-Lancaster, J. & Allen, P. M. Tickling the TCR: selective T-cell functions stimulated by altered peptide ligands. *Immunol. Today* **14,** 602–609 (1993).
32. Irvine, D. J., Purbhoo, M. A., Krogsgaard, M. & Davis, M. M. Direct observation of ligand recognition by T cells. *Nature* **419,** 845–849 (2002).
33. Valitutti, S., Miller, S., Cella, M., Padovan, E. & Lanzavecchia, A. Serial triggering of many T-cell receptors by a few peptide-MHC complexes. *Nature* **375,** 148–151 (1995).
34. Jiang, N. *et al.* Two-stage cooperative T Cell Receptor-peptide Major Histocompatibility Complex-CD8 trimolecular interactions amplify antigen discrimination. *Immunity* **28,** 13–23 (2011).
35. Mason, D. A very high level of crossreactivity is an essential feature of the T- cell receptor. *Immunol. Today* **19,** 395–404 (1998).
36. Zehn, D., King, C., Bevan, M. J. & Palmer, E. TCR signaling requirements for activating T cells and for generating memory. *Cell. Mol. Life Sci.* **69,** 1565–1575 (2012).

37. Schmid, D. A. *et al.* Evidence for a TCR Affinity Threshold Delimiting Maximal CD8 T Cell Function. *J. Immunol.* **184,** 4936–4946 (2010).
38. Stone, J. D., Chervin, A. S. & Kranz, D. M. T-cell receptor binding affinities and kinetics: impact on T-cell activity and specificity. *Immunology* **126,** 165–176 (2009).
39. Gao, G. F. *et al.* Crystal structure of the complex between human CD8alpha(alpha) and HLA-A2. *Nature* **387,** 630–634 (1997).
40. Kern, P. S. *et al.* Structural basis of CD8 coreceptor function revealed by crystallographic analysis of a murine CD8αα ectodomain fragment in complex with H-2K. *Immunity* **9,** 519–530 (1998).
41. Luescher, I. F. *et al.* Cd8 modulation of t-cell antigen receptor–ligand interactions on living cytotoxic t lymphocytes. *Nature* **373,** 353–356 (1995).
42. Garcia, K. C. *et al.* CD8 enhances formation of stable T-cell receptor/MHC class I molecule complexes. *Nature* **384,** 577–581 (1996).
43. Alexander-Miller, M. A., Leggatt, G. R. & Berzofsky, J. A. Selective expansion of high- or low-avidity cytotoxic T lymphocytes and efficacy for adoptive immunotherapy. *Proc. Natl. Acad. Sci. U. S. A.* **93,** 4102–7 (1996).
44. Harari, A. *et al.* Functional signatures of protective antiviral T-cell immunity in human virus infections. *Immunol. Rev.* **211,** 236–254 (2006).
45. Hersperger, A. R. *et al.* Perforin expression directly ex vivo by HIV-specific CD8+T-cells is a correlate of HIV elite control. *PLoS Pathog.* **6,** 1–13 (2010).
46. Almeida, J. R. *et al.* Superior control of HIV-1 replication by CD8 $^{+}$ T cells is reflected by their avidity, polyfunctionality, and clonal turnover. *J. Exp. Med.* **204,** 2473–2485 (2007).
47. Barth, R. J., Mulé, J. J., Spiess, P. J. & Rosenberg, S. a. Interferon gamma and tumor necrosis factor have a role in tumor regressions mediated by murine CD8+ tumor-infiltrating lymphocytes. *J. Exp. Med.* **173,** 647–658 (1991).
48. Viganò, S. *et al.* Functional avidity: A measure to predict the efficacy of effector T cells? *Clin. Dev. Immunol.* **2012,** (2012).
49. Puech, P. H. *et al.* Force measurements of TCR/pMHC recognition at T cell surface. *PLoS One* **6,** (2011).
50. Huang, J. *et al.* The kinetics of two dimensional TCR and pMHC interactions determine T cell responsiveness. *Nature* **464,** 932–936 (2010).
51. Zhang, S.-Q. *et al.* Direct measurement of T cell receptor affinity and sequence from naive antiviral T cells. *Sci. Transl. Med.* **8,** 341ra77-341ra77 (2016).
52. Nauerth, M. *et al.* TCR-ligand koff rate correlates with the protective capacity of antigen-specific CD8+ T cells for adoptive transfer. *Sci. Transl. Med.* **5,** 192ra87 (2013).
53. Nauerth, M. *et al.* Flow cytometry-based TCR-ligand Koff-rate assay for fast avidity screening of even very small antigen-specific T cell populations ex vivo. *Cytom. Part A* **89,** 816–825 (2016).
54. Hebeisen, M. *et al.* Identification of rare high avidity, tumor reactive CD8+ T cells by monomeric TCR-ligand off-rates measurements on living cells. *Cancer Res.* (2015). doi:10.1158/0008-5472.CAN-14-3516
55. Lever, M., Maini, P. K., Van Der Merwe, P. A. & Dushek, O. Phenotypic

models of T cell activation. *Nat. Rev. Immunol.* **14,** 619–629 (2014).
56. Nauerth, M. *et al.* TCR-ligand koff-rate predicts protective capacity of antigen- specific CD8+ T cells for adoptive transfer. **5,** (2013).
57. Klein, L., Kyewski, B., Allen, P. M. & Hogquist, K. A. Positive and negative selection of the T cell repertoire: what thymocytes see and don't see. *Nat. Rev. Immunol.* **14,** 377–391 (2016).
58. Ozga, A. J. *et al.* pMHC affinity controls duration of CD8 $^{+}$ T cell–DC interactions and imprints timing of effector differentiation versus expansion. *J. Exp. Med.* **213,** 2811–2829 (2016).
59. Butz, E. A. & Bevan, M. J. Massive Expansion of Antigen-Specific CD8+ T Cells during an Acute Virus Infection. *Immunity* **8,** 167–175 (1998).
60. Malherbe, L., Hausl, C., Teyton, L. & McHeyzer-Williams, M. G. Clonal selection of helper T cells is determined by an affinity threshold with no further skewing of TCR binding properties. *Immunity* **21,** 669–679 (2004).
61. Zehn, D., Lee, S. Y. & Bevan, M. J. Complete but curtailed T-cell response to very low-affinity antigen. *Nature* **458,** 211–214 (2009).
62. Busch, D. H. & Pamer, E. G. T Cell Affinity Maturation by Selective Expansion during Infection. *J. Exp. Med.* **189,** 701–710 (1999).
63. Savage, P. A., Boniface, J. J. & Davis, M. M. A kinetic basis for T cell receptor repertoire selection during an immune response. *Immunity* **10,** 485–492 (1999).
64. van Heijst, J. W. J. *et al.* Recruitment of Antigen-Specific CD8+ T Cells in Response to Infection Is Markedly Efficient. *Science (80-.).* **325,** 1265–1270 (2009).
65. Derby, M. A., Alexander-Miller, M. A., Tse, R. & Berzofsky, J. A. High-Avidity CTL Exploit Two Complementary Mechanisms to Provide Better Protection Against Viral Infection Than Low-Avidity CTL. *J. Immunol.* **166,** 1690–1697 (2001).
66. Zeh, Herbert J, I. *et al.* High Avidity CTLs for Two Self-Antigens Demonstrate Superior In Vitro and In Vivo Antitumor Efficacy. *J. Immunol.* **162,** 989–994 (1999).
67. Zhong, S. *et al.* T-cell receptor affinity and avidity defines antitumor response and autoimmunity in T-cell immunotherapy. *Proc. Natl. Acad. Sci.* **110,** 6973–6978 (2013).
68. Restifo, N. P., Dudley, M. E. & Rosenberg, S. A. Adoptive immunotherapy for cancer: Harnessing the T cell response. *Nat. Rev. Immunol.* **12,** 269–281 (2012).
69. Altman, J. *et al.* Phenotypic analysis of antigen-specific T lymphocytes. *Science (80-.).* **274,** 94–96 (1996).
70. O'Herrin, S. M. *et al.* Antigen-Specific Blockade of T Cells In Vivo Using Dimeric MHC Peptide. *J. Immunol.* **167,** 2555–2560 (2001).
71. Maile, R. *et al.* Antigen-specific modulation of an immune response by in vivo administration of soluble MHC class I tetramers. *J. Immunol.* **167,** 3708–14 (2001).
72. Knabel, M. *et al.* Reversible MHC multimer staining for functional isolation of T-cell populations and effective adoptive transfer. *Nat. Med.* **8,** 631–637 (2002).
73. Voss, S. & Skerra, A. Mutagenesis of a flexible loop in streptavidin leads to higher affinity for the Strep-tag II peptide and improved performance in recombinant protein purification. *Protein Eng.* **10,** 975–982 (1997).
74. Schmidt, T. G. M. & Skerra, A. The Strep-tag system for one-step

purification and high-affinity detection or capturing of proteins. *Nat. Protoc.* **2,** 1528–1535 (2007).
75. Neuenhahn, M. *et al.* Transfer of minimally manipulated CMV-specific T cells from stem cell or third-party donors to treat CMV infection after allo-HSCT. *Leukemia* **31,** 2161–2171 (2017).
76. Toebes, M. *et al.* Design and use of conditional MHC class I ligands. *Nat. Med.* **12,** 246–251 (2006).
77. Saini, S. K. *et al.* Dipeptides catalyze rapid peptide exchange on MHC class I molecules. *Proc. Natl. Acad. Sci.* **112,** 202–207 (2015).
78. Hadrup, S. R. *et al.* Parallel detection of antigen-specific T-cell responses by multidimensional encoding of MHC multimers. *Nat. Methods* **6,** 520–526 (2009).
79. Newell, E. W., Klein, L. O., Yu, W. & Davis, M. M. Simultaneous detection of many T-cell specificities using combinatorial tetramer staining. *Nat. Methods* **6,** 497–499 (2009).
80. Bentzen, A. K. *et al.* Large-scale detection of antigen-specific T cells using peptide-MHC-I multimers labeled with DNA barcodes. *Nat. Biotechnol.* **34,** 1037–1045 (2016).
81. Kochenderfer, J. N. *et al.* Eradication of B-lineage cells and regression of lymphoma in a patient treated with autologous T cells genetically engineered to recognize Brief report Eradication of B-lineage cells and regression of lymphoma in a patient treated with autologous T cells. **116,** 4099–4102 (2010).
82. Kochenderfer, J. N. *et al.* Chemotherapy-refractory diffuse large B-cell lymphoma and indolent B-cell malignancies can be effectively treated with autologous T cells expressing an anti-CD19 chimeric antigen receptor. *J. Clin. Oncol.* **33,** 540–549 (2015).
83. Maude, S. L. *et al.* Tisagenlecleucel in Children and Young Adults with B-Cell Lymphoblastic Leukemia. *N. Engl. J. Med.* **378,** 439–448 (2018).
84. Kolb, H. J. *et al.* Donor leukocyte transfusions for treatment of recurrent chronic myelogenous leukemia in marrow transplant patients. *Blood* **76,** 2462–2465 (1990).
85. Author, L., Rosenberg, S. A., Spiess, P. & Lafreniere, R. A New Approach to the Adoptive Immunotherapy of Cancer with Tumor-Infiltrating. *Source Sci. New Ser.* **233,** 1318–1321 (1986).
86. Riddell, S. R. *et al.* Restoration of Viral Immunity in Immunodeficient Humans by the Adoptive Transferof T cell Clones. **257,** 3209–3217 (1992).
87. Schreiber, R. D. Cancer Immunoediting : Integrating Suppression and Promotion. **1565,** 1565–1571 (2014).
88. Price, D. A. *et al.* T cell receptor recognition motifs govern immune escape patterns in acute SIV infection. *Immunity* **21,** 793–803 (2004).
89. Levine, A. G., Arvey, A., Jin, W. & Rudensky, A. Y. Continuous requirement for the TCR in regulatory T cell function. *Nat. Immunol.* **15,** 1070–1078 (2014).
90. Hinrichs, C. S. & Rosenberg, S. A. Exploiting the curative potential of adoptive T-cell therapy for cancer. *Immunol. Rev.* **257,** 56–71 (2014).
91. Tran, K. Q. *et al.* Minimally cultured tumor-infiltrating lymphocytes display optimal characteristics for adoptive cell therapy. *J. Immunother.* **31,** 742–751 (2008).
92. Gattinoni, L., Klebanoff, C. A. & Restifo, N. P. Paths to stemness: Building

the ultimate antitumour T cell. *Nat. Rev. Cancer* **12,** 671–684 (2012).
93. Graef, P. *et al.* Serial Transfer of Single-Cell-Derived Immunocompetence Reveals Stemness of CD8+Central Memory T Cells. *Immunity* **41,** 116–126 (2014).
94. Gattinoni, L. *et al.* A human memory T cell subset with stem cell-like properties. *Nat. Med.* **17,** 1290–1297 (2011).
95. Kaneko, S. *et al.* IL-7 and IL-15 allow the generation of suicide genemodified alloreactive self-renewing central memory human T lymphocytes IL-7 and IL-15 allow the generation of suicide gene – modified alloreactive self-renewing central memory human T lymphocytes. *Blood* **113,** 1006–1015 (2009).
96. Stemberger, C. *et al.* A Single Naive CD8+ T Cell Precursor Can Develop into Diverse Effector and Memory Subsets. *Immunity* **27,** 985–997 (2007).
97. Buchholz, V. R. *et al.* Disparate Individual Fates Compose Robust CD8+ T Cell Immunity. *Science (80-.).* **340,** 630–635 (2013).
98. Morgan, R. A. *et al.* Cancer Regression in Patients After Transfer of Genetically Engineered Lymphocyte. *Science (80-.).* **314,** 126–130 (2006).
99. Rosenberg, S. A. *et al.* Durable complete responses in heavily pretreated patients with metastatic melanoma using T-cell transfer immunotherapy. *Clin. Cancer Res.* **17,** 4550–4557 (2011).
100. Schrum, A. G., Turka, L. A. & Palmer, E. Surface T-cell antigen receptor expression and availability for long-term antigenic signaling. *Immunol. Rev.* **196,** 7–24 (2003).
101. Gallegos, A. M. *et al.* Control of T cell antigen reactivity via programmed TCR downregulation. *Nat. Immunol.* **17,** 379–386 (2016).
102. Dembić, Z. *et al.* Transfer of specificity by murine α and β T-cell receptor genes. *Nature* **320,** 232–238 (1986).
103. Baum, C. *et al.* Chance or necessity? Insertional mutagenesis in gene therapy and its consequences. *Mol. Ther.* **9,** 5–13 (2004).
104. Roth, T. L. *et al.* Reprogramming human T cell function and specificity with non-viral genome targeting. *Nature* **559,** 405–409 (2018).
105. Overwijk, W. W. & Restifo, N. P. Autoimmunity and the immunotherapy of cancer: targeting the ‘self’ to destroy the ‘other’. *Crit. Rev. Immunol.* **20,** 433–50 (2000).
106. Parkhurst, M. R. *et al.* T cells targeting carcinoembryonic antigen can mediate regression of metastatic colorectal cancer but induce severe transient colitis. *Mol. Ther.* **19,** 620–626 (2011).
107. Robbins, P. F. *et al.* Tumor regression in patients with metastatic synovial cell sarcoma and melanoma using genetically engineered lymphocytes reactive with NY-ESO-1. *J. Clin. Oncol.* **29,** 917–924 (2011).
108. Hinrichs, C. & Restifo, N. P. Reassessing target antigens for adoptive T cell therapy. *Nat. Biotechnol.* **33,** 999–1008 (2013).
109. Linnemann, C. *et al.* High-throughput epitope discovery reveals frequent recognition of neo-antigens by CD4+T cells in human melanoma. *Nat. Med.* **21,** 81–85 (2015).
110. Robbins, P. F. *et al.* Mining Exomic Sequencing Data to Identify Mutaded Antigens Recognized by Adoptively Transferred Tumor-reactive cells. *Nat. Med.* **19,** 747–752 (2013).
111. Gros, A. *et al.* PD-1 identifies the patient-specific CD8+ tumor-reactive repertoire filtrating human tumors. *J. Clin. Invest.* **124,** 2246–59 (2014).

112. Cohen, C. J. *et al.* Isolation of neoantigen-specific T cells from tumor and peripheral lymphocytes. *J. Clin. Invest.* **125,** 3981–3991 (2015).
113. Gros, A. *et al.* Prospective identification of neoantigen-specific lymphocytes in the peripheral blood of melanoma patients. *Nat. Med.* **22,** 433–438 (2016).
114. Topalian, S. L., Drake, C. G. & Pardoll, D. M. Immune checkpoint blockade: A common denominator approach to cancer therapy. *Cancer Cell* **27,** 451–461 (2015).
115. Pauken, K. E. *et al.* Epigenetic stability of exhausted T cells limits durability of reinvigoration by PD-1 blockade. *Science (80-.).* **354,** 1160–1165 (2016).
116. Philip, M. *et al.* Chromatin states define tumor-specific T cell dysfunction and reprogramming. *Nature* **545,** 452–456 (2017).
117. Buchholz, V. R., Neuenhahn, M. & Busch, D. H. CD8+ T cell differentiation in the aging immune system: Until the last clone standing. *Curr. Opin. Immunol.* **23,** 549–554 (2011).
118. Strønen, E. *et al.* Targeting of cancer neoantigens with donor-derived T cell receptor repertoires. *Science (80-.).* **352,** 1337–1341 (2016).
119. Clement, M. *et al.* Anti-CD8 antibodies can trigger CD8 + T-cell effector function in the absence of TCR engagement and improve pMHCI tetramer staining. *J Immunol* **187,** 654–663 (2012).
120. Lissina, A. *et al.* Protein kinase inhibitors substantially improve the physical detection of T-cells with peptide-MHC tetramers. *J. Immunol. Methods* **340,** 11–24 (2009).
121. Huang, J. *et al.* Detection, phenotyping, and quantification of antigen-specific T cells using a peptide-MHC dodecamer. *Proc. Natl. Acad. Sci.* **113,** E1890–E1897 (2016).
122. Stemberger, C. *et al.* Novel Serial Positive Enrichment Technology Enables Clinical Multiparameter Cell Sorting. *PLoS One* **7,** e35798 (2012).
123. Dössinger, G. *et al.* MHC Multimer-Guided and Cell Culture-Independent Isolation of Functional T Cell Receptors from Single Cells Facilitates TCR Identification for Immunotherapy. *PLoS One* **8,** (2013).
124. Hebeisen, M. *et al.* Identification of rare high-avidity, tumor-reactive CD8+T Cells by Monomeric TCR-ligand off-rates measurements on living cells. *Cancer Res.* **75,** 1983–1991 (2015).
125. Allard, M. *et al.* TCR-ligand dissociation rate is a robust and stable biomarker of CD8+ T cell potency. *JCI Insight* **2,** (2017).
126. Kim, S. M. *et al.* Analysis of the paired TCR α- and β-chains of single human T cells. *PLoS One* **7,** (2012).
127. Sun, X. *et al.* Unbiased analysis of TCRα/β chains at the single-cell level in human CD8+T-cell subsets. *PLoS One* **7,** 1–11 (2012).
128. Redmond, D., Poran, A. & Elemento, O. Single-cell TCRseq: Paired recovery of entire T-cell alpha and beta chain transcripts in T-cell receptors from single-cell RNAseq. *Genome Med.* **8,** 1 (2016).
129. Schumacher, D. *et al.* Versatile and Efficient Site-Specific Protein Functionalization by Tubulin Tyrosine Ligase. *Angew. Chemie - Int. Ed.* **54,** 13787–13791 (2015).
130. Busch, D. H. & Pamer, E. G. MHC class I/peptide stability: implications for immunodominance, in vitro proliferation, and diversity of responding CTL. *J. Immunol.* **160,** 4441–4448 (1998).

131. Garboczi, D. N., Hung, D. T. & Wiley, D. C. HLA-A2-peptide complexes: refolding and crystallization of molecules expressed in Escherichia coli and complexed with single antigenic peptides. *Proc. Natl. Acad. Sci. U. S. A.* **89,** 3429–3433 (1992).
132. Saini, S. K. *et al.* Dipeptides promote folding and peptide binding of MHC class I molecules. *Proc. Natl. Acad. Sci.* **110,** 15383–15388 (2013).
133. Gerhard, M., Busch, D. H., Doessinger, G., Schumacher, A. & Linnemann, C. T cell receptors and peptides derived by mutations for the treatment of cancer. **1,** 1–58 (2016).
134. Lundegaard, C. *et al.* NetMHC-3.0: accurate web accessible predictions of human, mouse and monkey MHC class I affinities for peptides of length 8-11. *Nucleic Acids Res.* **36,** 509–512 (2008).
135. Mishto, M. *et al.* Modeling the in Vitro 20S Proteasome Activity: The Effect of PA28-αβ and of the Sequence and Length of Polypeptides on the Degradation Kinetics. *J. Mol. Biol.* **377,** 1607–1617 (2008).
136. Yang, S. *et al.* Development of optimal bicistronic lentiviral vectors facilitates high-level TCR gene expression and robust tumor cell recognition. *Gene Ther.* **15,** 1411–1423 (2008).
137. Cohen, C. J., Zhao, Y., Zheng, Z., Rosenberg, S. A. & Morgan, R. A. Enhanced antitumor activity of murine-human hybrid T-cell receptor (TCR) in human lymphocytes is associated with improved pairing and TCR/CD3 stability. *Cancer Res.* **66,** 8878–8886 (2006).
138. Dietrich, P. Y. *et al.* TCR analysis reveals significant repertoire selection during in vitro lymphocyte culture. *Int. Immunol.* **9,** 1073–1083 (1997).
139. Sharma, S. K. & Alexander-Miller, M. A. Increased sensitivity to antigen in high avidity CD8+ T cells results from augmented membrane proximal T-cell receptor signal transduction. *Immunology* **133,** 307–317 (2011).
140. Wooldridge, L. *et al.* Tricks with tetramers: how to get the most from multimeric peptide-MHC. *Immunology* **126,** 147–164 (2009).
141. Dolton, G. *et al.* More tricks with tetramers: A practical guide to staining T cells with peptide-MHC multimers. *Immunology* **146,** 11–22 (2015).
142. Johnson, K. G., Bromley, S. K., Dustin, M. L. & Thomas, M. L. A supramolecular basis for CD45 tyrosine phosphatase regulation in sustained T cell activation. *Proc. Natl. Acad. Sci. U. S. A.* **97,** 10138–10143 (2000).
143. Fuertes Marraco, S. A. *et al.* Long-lasting stem cell-like memory $CD8^+$ T cells with a naïve-like profile upon yellow fever vaccination. *Sci. Transl. Med.* **7,** (2015).
144. Cole, D. K. *et al.* Germ line-governed recognition of a cancer epitope by an immunodominant human T-cell receptor. *J. Biol. Chem.* **284,** 27281–27289 (2009).
145. Pinto, S. *et al.* Misinitiation of intrathymic MART-1 transcription and biased TCR usage explain the high frequency of MART-1-specific T cells. *Eur. J. Immunol.* **44,** 2811–2821 (2014).
146. Devine, L., Sun, J., Barr, M. R. & Kavathas, P. B. Orientation of the Ig domains of CD8 alpha beta relative to MHC class I. *J. Immunol.* **162,** 846–851 (1999).
147. Wooldridge, L. *et al.* Enhanced immunogenicity of CTL antigens through mutation of the CD8 binding MHC class I invariant region. *Eur. J. Immunol.* **37,** 1323–1333 (2007).
148. Laugel, B. *et al.* Different T Cell Receptor Affinity Thresholds and CD8

Coreceptor Dependence Govern Cytotoxic T Lymphocyte Activation and Tetramer Binding Properties. *J. Biol. Chem.* **282,** 23799–23810 (2007).
149. Derby, M. A., Wang, J., Margulies, D. H. & Berzofsky, J. A. Two intermediate-avidity cytotoxic T lymphocyte clones with a disparity between functional avidity and MHC tetramer staining. *Int. Immunol.* **13,** 817–824 (2001).
150. Kawakami, Y. *et al.* Identification of the immunodominant peptides of the MART-1 human melanoma antigen recognized by the majority of HLA-A2-restricted tumor infiltrating lymphocytes. *J. Exp. Med.* **180,** 347–52 (1994).
151. Romero, P. *et al.* Antigenicity and immunogenicity of Melan-A/MART-1 derived peptides as targets for tumor reactive CTL in human melanoma. *Immunol. Rev.* **188,** 81–96 (2002).
152. Sotiropoulou, P. A. *et al.* Cytotoxic T-cell precursor frequencies to HER-2 (369-377) in patients with HER-2/neu-positive epithelial tumours. *Br. J. Cancer* **89,** 1055–1061 (2003).
153. Allard, M., Hebeisen, M. & Rufer, N. Assessing T Cell Receptor Affinity and Avidity Against Tumor Antigens. *Oncoimmunology* 665–679 (2018). doi:10.1007/978-3-319-62431-0
154. Ilyas, S. & Yang, J. C. Landscape of Tumor Antigens in T Cell Immunotherapy. *J. Immunol.* **195,** 5117–5122 (2015).
155. Saeterdal, I. *et al.* Frameshift-mutation-derived peptides as tumor-specific antigens in inherited and spontaneous colorectal cancer. *Proc. Natl. Acad. Sci.* **98,** 13255–13260 (2001).
156. Giannakis, M. *et al.* RNF43 is frequently mutated in colorectal and endometrial cancers. *Nat. Genet.* **46,** 1264–1266 (2014).
157. Engels, B. *et al.* Relapse or eradication of cancer is predicted by peptide-major histocompatibility complex affinity. *Cancer Cell* **23,** 516–526 (2013).
158. Kammertoens, T. & Blankenstein, T. It's the peptide-mhc affinity, stupid. *Cancer Cell* **23,** 429–431 (2013).
159. Karpanen, T. & Olweus, J. The potential of donor T-cell repertoires in neoantigen-targeted cancer immunotherapy. *Front. Immunol.* **8,** 1–8 (2017).
160. Hebeisen, M. *et al.* Identifying individual T cell receptors of optimal avidity for tumor antigens. *Front. Immunol.* **6,** (2015).
161. Prota, A. E. *et al.* Structural basis of tubulin tyrosination by tubulin tyrosine ligase. *J. Cell Biol.* **200,** 259–270 (2013).
162. Bentzen, A. K. & Hadrup, S. R. Evolution of MHC-based technologies used for detection of antigen-responsive T cells. *Cancer Immunol. Immunother.* **66,** 657–666 (2017).
163. Doronina, S. O. *et al.* Enhanced activity of monomethylauristatin F through monoclonal antibody delivery: Effects of linker technology on efficacy and toxicity. *Bioconjug. Chem.* **17,** 114–124 (2006).
164. Yuan, R. R. *et al.* Targeted deletion of T-cell clones using alpha-emitting suicide MHC tetramers. *Blood* **104,** 2397–2402 (2004).
165. Vincent, B. G. *et al.* Toxin-Coupled MHC Class I Tetramers Can Specifically Ablate Autoreactive CD8+ T Cells and Delay Diabetes in Nonobese Diabetic Mice. *J. Immunol.* **184,** 4196–4204 (2010).
166. Popp, M. W., Antos, J. M., Grotenbreg, G. M., Spooner, E. & Ploegh, H. L. Sortagging: A versatile method for protein labeling. *Nat. Chem. Biol.* **3,** 707–708 (2007).

167. Rodenko, B. *et al.* Generation of peptide-MHC class I complexes through UV-mediated ligand exchange. *Nat. Protoc.* **1,** 1120–1132 (2006).
168. Frøsig, T. M. *et al.* Design and validation of conditional ligands for HLA-B*08:01, HLA-B*15:01, HLA-B*35:01, and HLA-B*44:05. *Cytom. Part A* **87,** 967–975 (2015).
169. Chang, C. X. L. *et al.* Conditional ligands for Asian HLA variants facilitate the definition of CD8+T-cell responses in acute and chronic viral diseases. *Eur. J. Immunol.* **43,** 1109–1120 (2013).
170. Luimstra, J. J. *et al.* A flexible MHC class I multimer loading system for large-scale detection of antigen-specific T cells. *J. Exp. Med.* **215,** 1493–1504 (2018).
171. Rius, C. *et al.* Peptide–MHC Class I Tetramers Can Fail To Detect Relevant Functional T Cell Clonotypes and Underestimate Antigen-Reactive T Cell Populations. *J. Immunol.* **7637,** ji1700242 (2018).
172. Sommermeyer, D. *et al.* NY-ESO-1 antigen-reactive T cell receptors exhibit diverse therapeutic capability. *Int. J. Cancer* **132,** 1360–1367 (2013).
173. Lyons, G. E. *et al.* T-cell receptor tetramer binding or the lack there of does not necessitate antigen reactivity in T-cell receptor transduced T cells. *Cancer Immunol. Immunother.* **55,** 1142–1150 (2006).

Acknowledgements

An dieser Stelle danke ich allen Arbeitskollegen, Freunden und sowie meiner Familie die durch ihre Unterstützung maßgeblich zum Erfolg dieser Doktorarbeit beigetragen haben.

Ein besonderer Dank gilt meinem Doktorvater Prof. Dirk Busch, der mir dieses spannende und anspruchsvolle Projekt anvertraut hat und mich mit weitgehenden Freiheiten und seiner ganzen Erfahrung in der Bewältigung zahlreicher Herausforderungen unterstützte. Gleicher Dank gilt Dr. Kilian Schober, der mir als betreuender Postdoc mit Rat und Tat zur Seite stand. Unvergessen bleibt seine detailverliebte Korrektur von Vorträgen und Manuskripten. Eine Eigenheit die mir mittlerweile selbst ins Blut übergegangen scheint. Zusammen mit Prof. Dirk Haller bildeten sie mein Thesis Komitee und haben als solches meine Doktorarbeit betreut, wofür ich mich herzlich bedanke.

Des Weiteren möchte ich mich bei meinen Arbeitskollegen bedanken, die immer bereitwillig ihr Wissen mit mir geteilt haben. Speziell möchte ich Andreas Stengl nennen, durch dessen außerordentliches Engagement und Fachwissen die Realisierung der FLEXamere erst möglich wurde. An dieser Stelle danke ich auch Prof. Heinrich Leonhardt für die Unterstützung bei dem FLEXamer Projekt sowie Prof. Sebastian Springer für die fruchtvolle Kooperation über den Di-Peptid Austausch.

Ebenfalls sind hier meine Kooperationspartner und Arbeitskollegen Lothar Germeroth, Christian Stemberger, Mateusz Poltorak, Stefan Dreher, Patricia Gräf und Michaela Wagner bei Juno Therapeutics GmbH zu nennen, die mir mit Reagenzien, Zellen sowie kritischer Diskussion meiner Ergebnisse immer eine große Hilfe waren.

Überdies danke ich Fabian Mohr, Thomas Müller und Marten Plambeck für fachliche – und sportliche – Unterstützung in allen Lebenslagen. Philipp Lückemeier, Kristof Wing und Florian Voit danke ich für Hilfestellungen rund um das Thema k_{off}-rate Assay. Der AG Schiemann, allen voran Immanuel Andrä und Lynette Henkel danke ich für unermüdliches Zellsortieren und Reparieren der Durchfluss-Zytometer auch weit nach Feierabend. Anna Hochholzer, Franziska

Graml und Monika Hammel möchte ich für ihre exzellente technische Assistenz danken.
Ein besonderer Dank gilt ebenfalls all meinen Studenten; Patrick Huppertz, Maria Gerget, Maximilian Kampick, Johannes Groffmann, Jonathan Schwach und Ann-Kristin Triebert, die mit viel Einsatz und Leidenschaft dieser Doktorarbeit immer wieder neuen Vortrieb verliehen.
Auch möchte ich mich bei meinen Freunden in Essen und München sowie meiner Familie ganz herzlich bedanken. Eure Unterstützung galt mir immer als sicherer Hafen, um Laborkrisen zu bewältigen. Der letzte Dank gilt meiner Komplizin Samantha, die mich über 4 Jahre Promotion jederzeit unterstützt, aufgebaut und ertragen hat.